AD-A129 526   IDENTIFICATION AND QUANTIFICATION OF THE WATER SOLUBLE   1/2
               COMPONENTS OF JP-4..(U) NORTH DAKOTA STATE UNIV FARGO
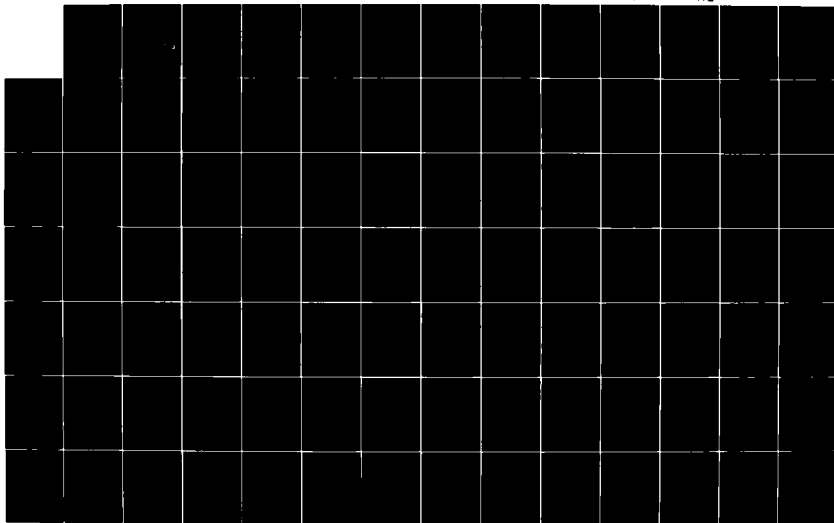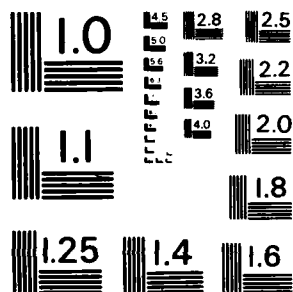   DEPT OF ZOOLOGY   J D BRAMMER ET AL. 23 DEC 82
UNCLASSIFIED   AFOSR-TR-83-0513 AFOSR-78-3709   F/G 21/4   NL

MICROCOPY RESOLUTION TEST CHART
NATIONAL BUREAU OF STANDARDS-1963-A

REPORT DOCUMENTATION PAGE	READ INSTRUCTIONS BEFORE COMPLETING FORM

1. REPORT NUMBER	2. GOVT ACCESSION NO.	3. RECIPIENT'S CATALOG NUMBER
AFOSR-TR- 83-0513	AD A129 526	

4. TITLE (and Subtitle)	5. TYPE OF REPORT & PERIOD COVERED
Identification and Quantification of the Water Soluble Components of JP-4 and a Determination of Their Biological Effects Upon Selected Freshwater Organisms	Annual Technical Report 9/30-81 - 9/29/82
	6. PERFORMING ORG. REPORT NUMBER

7. AUTHOR(s)	8. CONTRACT OR GRANT NUMBER(s)
J.D. Brammer R.L. Puyear	AFOSR-78-3709

9. PERFORMING ORGANIZATION NAME AND ADDRESS	10. PROGRAM ELEMENT, PROJECT, TASK AREA & WORK UNIT NUMBERS
Zoology Department North Dakota State University Fargo, N.D. 58105	2312/A5 61102F

11. CONTROLLING OFFICE NAME AND ADDRESS	12. REPORT DATE
Department of the Air Force Air Force Office of Scientific Research/NL Bolling Air Force Base, D.C. 20332	12/23/82
	13. NUMBER OF PAGES
	159

14. MONITORING AGENCY NAME & ADDRESS(if different from Controlling Office)	15. SECURITY CLASS. (of this report)
	UNCLASSIFIED
	15a. DECLASSIFICATION/DOWNGRADING SCHEDULE

16. DISTRIBUTION STATEMENT (of this Report)

Approved for public release; distribution unlimited.

17. DISTRIBUTION STATEMENT (of the abstract entered in Block 20, if different from Report)

DTIC
SELECTED
JUN 21 1983
H

18. SUPPLEMENTARY NOTES

19. KEY WORDS (Continue on reverse side if necessary and identify by block number)

Toluene Metabolism, Benzene Metabolism, Enzyme Induction, Aniline Hydroxylase, Aminopyrine Demethylase, Liver Cell Fractionation, Fathead Minnow, Bluegill Sunfish, White Rat. Fathead Minnow Development, Fathead Minnow Abnormal Development.

20. ABSTRACT (Continue on reverse side if necessary and identify by block number)

The vial equilibration technique with several modifications was used to evaluate the metabolic rates of benzene and toluene in rat liver. Effect of pH, incubation time, protein concentration and benzene concentration on rates of in vitro benzene metabolism were studied. No induction of hepatic metabolism of benzene was found with the pretreatment of phenobarbital (PB-75 mg/kg/day for 3 days) or 3-methylcholanthrene (3MC-20 mg/kg/day for 3 days) or Aroclor 1254 (PCB- 75 mg/kg/day for 3 days). Increased metabolism of toluene was observed with all three pretreatments. Aminopyrine demethylase (APDM) activity was also induced by the

DD FORM 1473 EDITION OF 1 NOV 65 IS OBSOLETE

83 06 20 143

xenobiotics. Aniline hydroxylase (AH) activity was induced by 3MC and PCB. Studies of metabolic rates of various subcellular fractions of rat liver reveal that toluene and benzene metabolism was lowest in the 104,000 x g microsomal pellet. This rate was restored to that of the 12,000 x g supernatant when the microsomal pellet was resuspended in 104,000 x g supernatant (cytosol). The role that the cytosol plays in the metabolism of benzene and toluene is not known.

The techniques developed in the investigation of various hepatic enzymes systems of the rat were applied to the study of analogous hepatic enzyme systems of the sunfish of the genus Leeomis. In vitro metabolism of aminopyrine, aniline, and toluene was quantified. Aminopyrine demethylase activity was greatest at around 38 C. Aniline hydroxylase activity was greater at lower temperatures in the 25-27 C range. Toluene was metabolized slowly at 37 C. Of the three substrates, aminopyrine was metabolized most readily. Aniline and toluene were metabolized at approximately the same rate.

A closed.static bioassay system was developed for measuring the uptake, bioconcentration and distribution of ^{14}C benzene and toluene in adult fathead minnows. Toluene was more readily bioconcentrated than benzene. Benzene was concentrated in tissues in the following order: bile > spleen > lipid > liver > ovary > muscle. Toluene concentration was measured in the same tissues. The concentrations were bile > liver > ovary > lipid > spleen > muscle. Piperonyl butoxide, an inhibitor of liver mix function oxidases, inhibited the bio-accumulation of ^{14}C toluene in the bile.

The pre-hatching development of the fathead minnow at 25 C was determined using direct observation of live embryos and light and scanning electron microscopy techniques. Development was divided into 32 stages, each representing a point in time in the developmental continuum. Hatching normally occurred after 120 hours.

Fathead minnow embryos were stressed by exposure to different toluene concentrations in a mini-diluter system. Toluene concentrations of 30-50 mg/l produced a premature hatch while 60-80 mg/l toluene resulted in a delayed hatch. Morphological abnormalities observed in live embryos and serial sections included curvature of the notochord, abnormal heart and circulatory system development, hydration and swelling of the pericardial coelom, hemorrhaging, overall stunted appearance, reduced eye size, and a unique movement of the ventrally located periblast layer.

Work Scope (September 30, 1981-September 29, 1982)

This phase of the research entailed:

I. Repeating and completing work on water solubilities of major JP-4 jet fuel alkylbenzenes at five different temperatures and four different salinities. Work is nearly complete for determining the maximal water solubilities of JP-4 derived alkylbenzenes. This research will be submitted to the BULLETIN OF ENVIRONMENTAL CONTAMINATION AND TOXICOLOGY.

II. LC50 and MATC for toluene in fathead minnow embryos, 1-day posthatch protolarvae and 30-day old fish has been published in the BULLETIN OF ENVIRONMENTAL CONTAMINATION AND TOXICOLOGY 29, 12-17, 1982.

III. Metabolism of benzene and toluene, aminopyrine demethylase and aniline hydroxylase activities by liver subcellular fractions from control and induced rats activities.

IV. Toluene metabolism and activities of aminopyrine demethylase and aniline hydroxylase in the liver of Bluegill sunfish Lepomis ssp.

V. Bioaccumulation and tissue distribution of ^{14}C benzene and ^{14}C toluene by fathead minnows in a closed static bioassay system.

VI. The prehatching development of the fathead minnow.

VII. Effects of toluene on the prehatching development of the fathead minnow.

A DETAILED ACCOUNT OF EACH PHASE LISTED ABOVE IS DESCRIBED BELOW.

III. Metabolism of benzene and toluene by various subcellular fractions of rat liver.

Introduction

Xenobiotic compounds, once having entered a living organism are subjected to enzyme attack and undergo biotransformations. The major site of xenobiotic metabolism is in the liver (15). The ability of PB (2,5,8,9), 3MC (2,5), and PCB (4,10) to influence hepatic functions have been reported.

Benzene is known to be a widely spread environmental pollutant since it is a major component of motor fuels (1). Benzene and toluene are organic solvents used mostly in industry (3). Recently, toluene and benzene have been found to be major water soluble components of JP-4 jet fuel (11).

The ability of liver microsomal enzymes to metabolize benzene and toluene has been documented (5,7,8). In most of these studies the rate of metabolism of benzene and toluene was carried out using radiotracer methods (5,7). These methods are rather time consuming and accuracy is dependent upon low background counts. SATO and NAKAJIMA (13) introduced a headspace sampling technique for measuring volatile hydrocarbons using the vial equilibration method. The technique is sensitive and rapid. In this study, the headspace sampling technique with several modifications was used to evaluate the metabolism of benzene and toluene by liver preparations from control rats and rats treated with PB, 3MC, or PCB.

Materials and Methods

Reagents

Benzene and toluene used were Omnisolv (Matheson, Coleman and Bell). Glucose-6-phosphate (G-6-P), glucose-6-phosphate dehydrogenase (from Bakers yeast), NADP and 3-methylcholanthrene were purchased from Sigma Chemical Co (St. Louis, MO). Coomassie brilliant blue G-250 was obtained from Serva, Feinbiochemica, Heidelberg. Aroclor 1254 was purchased from Analabs, Inc. The sodium phenobarbital was a gift from the College of Pharmacy. All other chemicals were analytical or reagent grade.

1. Animals and Pretreatments

Male Sprague-Dawley rats (150-200 gm) were used Baseline rates of benzene and toluene metabolism were determined using control rats. The effect of various xenobiotic enzyme inducers upon benzene and toluene metabolism was determined with rats pretreated with PB, 3MC, or PCB.

1.1 PB pretreatment

Animals were injected intraperitoneally (i.p.) with either 100 mg/kg body weight sodium phenobarbital (PB group) in 0.85% NaCl, or with 0.85% NaCl (control groups) daily for 4 days. In a later study, the rats were injected i.p. with 75 mg/kg body weight sodium phenobarbital in 0.85% NaCl for 3 days,

or 0.85% NaCl for 3 days.

- 3 -

1.2 3MC pretreatment

Rats were pretreated, with i.p. injects of 3MC in peanut oil for 3 days at a dose of 20 mg/kg body weight. Control rats were injected i.p. with peanut oil only.

1.3 PCB pretreatment

PCB (75 mg/kg) injections were administered i.p. for 3 days. Control animals received only comparable volumes of corn oil.

Body weights of rats were measured immediately before sacrificing. PB treated and control rats, or 3 MC treated and controls were killed 24 hours after the last injection. PCB treated and control rats were sacrificed 120 hours after the last injection because only APDM induction was seen at 24 hours. Waiting 120 hours caused the induction of toluene APDM and AH to be observed.

2. Liver Enzyme Preparations

2.1 General Procedures

Rats were decapitated and their livers removed, weighed, and rinsed in ice cold 0.154 M KCl/0.1 M phosphate (K+) buffer, pH 7.4. All subsequent steps were preformed at 0-4 C. The homogenate was prepared using three 3 second pulses, 3500 rpm, delivered by a Tekmar SDT Tissumizer adding 1 gm of liver to 9 ml of 0.154 M KCl/0.1 M phosphate buffer, pH 7.4. For pH enzyme activity studies, 0.154 M KCl was used instead of 0.154 M KCl phosphate buffer, pH 7.4 to prepare the liver homogenate. The homogenate was centrifuged at 12,000 x g for 20 minutes using a Beckman Mod-
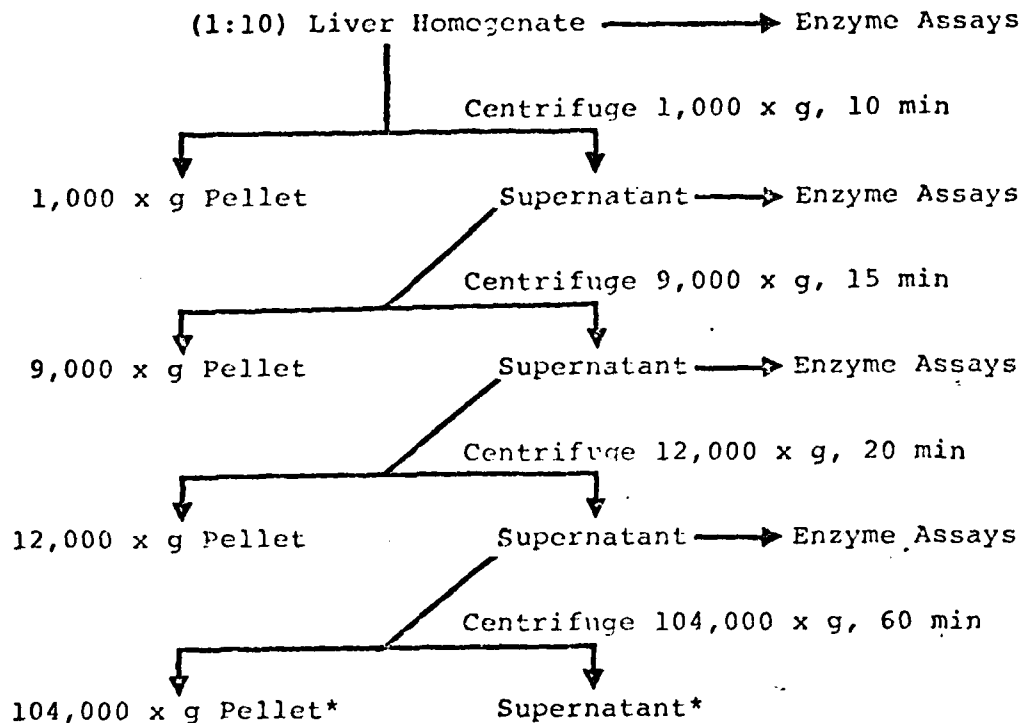
el J-21B high speed centrifuge. This 12,000 x g supernatant fraction was used as a crude microsomal enzyme source for most of the studies.

When microsomes were used the 12,000 x g supernatant was centrifuged again at 104,000 x g for 60 minutes with a Beckman Model L ultracentrifuge. The resulting microsomal pellet was resuspended in 0.154 M KCl/0.1 M phosphate buffer so that the final concentration of microsomes was equivalent to 100 mg liver/ml buffer.

2.2 Scheme Used for the Subcellular Fractionation of Rat Liver Homogenate.

Six untreated male rats (average weight = 150 gm) were used. Livers from two rats were pooled in order to provide sufficient tissue for fractionation. A 10 % liver homogenate was prepared as described above. The crude liver homogenate was fractionated using differential centrifugation described in Figure 1.

Figure 1. Liver Fractionation Scheme

```
(1:10) Liver Homogenate ─────────▶ Enzyme Assays
                 │
                 │        Centrifuge 1,000 x g, 10 min
       ┌─────────┴─────────┐
       ▼                   ▼
1,000 x g Pellet       Supernatant ──▶ Enzyme Assays
                        │
                        │   Centrifuge 9,000 x g, 15 min
       ┌────────────────┘
       ▼                   ▼
9,000 x g Pellet       Supernatant ──▶ Enzyme Assays
                        │
                        │   Centrifuge 12,000 x g, 20 min
       ┌────────────────┘
       ▼                   ▼
12,000 x g Pellet      Supernatant ──▶ Enzyme Assays
                        │
                        │   Centrifuge 104,000 x g, 60 min
       ┌────────────────┘
       ▼                   ▼
104,000 x g Pellet*    Supernatant*
```

* In order to study the enzyme activity in the microsomal frac-
tion the 104,000 x g pellet was resuspended in either 0.154 M
KCl/ 0.1 M posphate buffer or in 104,000 x g supernatant. The re-
suspension allowed 1 ml to be equivalent to 100 mg of liver.

3. Headspace Sampling of Benzene and Toluene Metabolism Using Gas Chromatography.

Substrates were prepared by mixing 10 ul of benzene or toluene in 100 ml of glass distilled water in a closed serum bottle. The temperature of the solution was maintained at 5 C using a cooling magnetic mixer (Stir Kool, Model SK12). Substrate was withdrawn through the stopper using a glass Hamilton syringe of an appropriate volume.

Vials used in the metabolism studies were 17 ml glass vials with screw caps which had a 1 cm opening. Teflon lined rubber septa (2 mm thick) were inserted into the caps to provide airtight closures for the vials. The Teflon lining was used to prevent the adsorption of the substrate to the rubber septa.

Sample vials contained 2.0 ml of cofactor (0.372 mg NADP, 2.60 mg G-6-P, and 2.4 mg $MgCl_2$ in 2.0 ml of 0.1 M phosphate buffer, pH 7.4, unless otherwise stated), 1.0 ml of liver enzyme source and 0.10 ml of benzene or toluene (unless otherwise stated). Final concentrations of the reaction mixture were 0.162 mM NADP, 3.23 mM G-6-P, 8.12 mM Mg^{+2}, 32.26 mg liver wet weight (LWW)/ml, 36.3 uM benzene or 30.3 uM toluene. When microsomal suspensions were used as the enzyme source, 2 units of glucose-6-phosphate dehydrogenase were also added to the sample vials. Reference vials contained the same amount of enzyme and substrate, but 2.0 ml of buffer were substituted for cofactor. In preliminary experiments, it was observed that there was no significant difference in the amount of benzene or toluene in the headspace when the

reference vial was prepared using denatured liver supernatant along with cofacor or using liver supernatant without cofactor. Because it was faster and easier to use liver supernatant without first denaturing, and the results were the same, we chose to use the undenatured enzyme preparation.

Both sample and reference vials were incubated at 37 C for 20 minutes (unless otherwise stated) at 120 oscillations/min in a Dubnoff metabolic water bath. At the end of the incubation period, 0.5 ml of the gaseous phase (headspace) was sampled.

A sample was removed and held to a constant volume using a Valco 6-port valve fitted with a 0.5 ml Teflon sample loop (Figure 2). A Teflon tube (1.6 mm O.D. x 1 mm I.D.) was used to transfer the gas phase sample from the metabolism vial to the injection valve. A 24 gauge Hamilton needle with a number 2 point was cut off at the hub and attached to the free end of the transfer line with a 1/16 inch Swagelok union (U). A 1/16 inch Vespel ferrule with a 0.028 inch hole was used to secure the needle to the Swagelok union and transfer line. The sample was introduced into the loop in the following manner: the toggle valve of line B (TV1) was shut, closing it to the atmosphere. The toggle valve of line E (TV2) was opened, allowing the sample loop to be evacuated to a negative 15 psi using a laboratory vacuum pump. When the evacuation pressure was reached, TV2 was closed, maintaining the vacuum or negative pressure in the sample loop (D). The needle attached to line B was inserted through the septum of a metabolism vial (A); TV1 was opened, allowing a sample of gas from A(b)

- 8 -

to be transfer d to the sample loop (D). The gaseous sample was injected onto ne chromatographic column by rotating the handle of the valve (C) so that the carrier gas (He) was routed through the sample loop to the GC rather than directly to the GC.
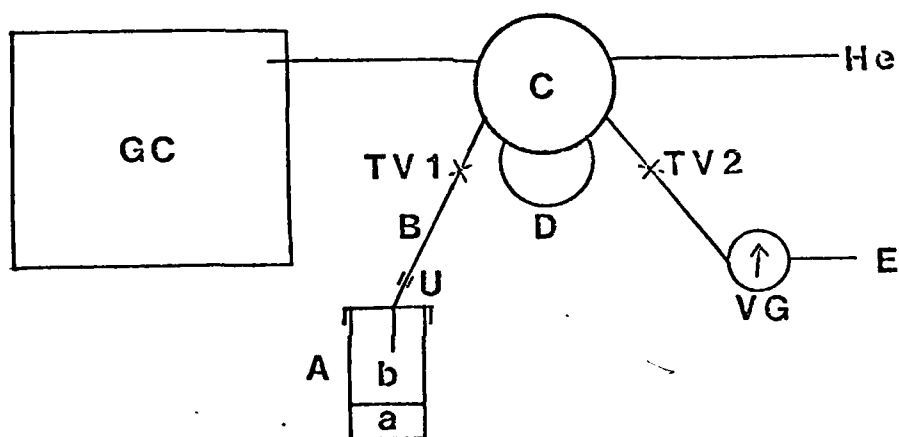
Figure 2. Diagram of Valco 6-port injector valve systems.

A - Metabolism vial with (a) metabolism mixture and (b) head-space, B - Teflon sample transfer line, C - Valco 6-port valve, D - 0.5 ml Teflon sample loop, E - Vacuum line to pump, TV1 & TV2 - Toggle valves 1 & 2, VG - Vacuum gauge, He - Helium carrier gas, GC - Gas chromatograph, U - 1/16" Swagelok union.

The gas chromatograph used to detect the benzene or toluene in the headspace gas sample of the metabolism vial was a Varian Model 3760. It was equiped with a hydrogen flame detector. Chromatographic separations were carried out using a 91.4 cm x 2 mm I.D. stainless steel column packed with 10% 1,2,3 tris (2-cyanoethoxy) propane on 100/120 mesh Chromosorb PAW (Supelco, Inc.) Operating conditions used were: column oven temperature, 85 C; inlet temperature, 150 C; detector temperature 210 C; gas flow rates were adjusted to: helium, 20 ml/min; air, 250 ml/min; and hydrogen, 45 ml/min. Detector sensitivity was adjusted to $2X10^{-10}$ amps/mv. The areas of chromatographic peaks were determined using a Spectra Physics 4000 Data System. The ratios of peak area between blank and reaction vials were used to calculate the amount of metabolism (13).

After the headspace was sampled, protein in the sample vial was precipitated using 1 ml 20% trichloroacetic acid (TCA) (w/v) and saved for protein determination.

4. Aminopyrine Demethylase & Aniline Hydroxylase Enzyme Assays.

4.1 Aminopyrine demethylase assay

Reaction mixtures contained 0.372 mg NADP, 2.60 mg G-6-P, 2.40 mg $MgCl_2$ in 1.5 ml of 0.1 M phosphate buffer, pH 7.4, 1.0 ml of the liver enzyme source, and 0.5 ml of 30.27 mM aminopyrine in glass distilled water. (Final concentrations were 0.167 mM NADP, 3.33 mM G-6-P, 8.39 mM Mg^{+2}, 33.3 mg LWW/ml, and

5.04 mM aminopyrine). Two units of glucose-6-phosphate dehydrogenase were added when 104,000 x g microsomal suspensions were used. Blanks were prepared by substituting buffer for cofactor. All samples and blanks were incubated at 37 C in a Dubnoff metabolic water bath (120 oscillations/min) for 20 minutes. At the end of the incubation period, the reaction was stopped by adding 1.0 ml 10% TCA (w/v). The protein precipitate was removed by centrifugation with a table top centrifuge to obtain a clear supernatant. The clear supernatant was mixed with 1.5 ml Nash's Reagent (15.0 gm ammonium acetate, 0.3 ml acetic acid, 0.2 ml acetyl acetone in 99.5 ml glass distilled water), and was incubated at 58-60 C for 8 minutes. The reaction mixture was allowed to cool to room temperature. The formaldehyde formed was measured at 412 nm by a Perkin-Elmer 124 double beam spectrophotometer. A standard curve was prepared by using a range of formaldehyde from 50 - 250 uM.

4.2 Aniline hydroxylase assay

Blanks and reaction mixtures were the same as in aminopyrine demethylase assay except 0.5 ml of 153.64 mM aniline in 0.1 M phosphate buffer replaced the 0.5 ml aminopyrine. (Final concentration of aniline in the reaction mixture was 25.61 mM). At the end of the 20 minute incubation period, the reactions were stopped using 1.0 ml of 20% TCA (w/v). A clear supernatant was obtained by centrifuging with a table top centrifuge. One ml of 1 M sodium carbonate followed by 1.0 ml of 1% phenol reagent (v/v) (1.1 ml phenol in 100 ml 0.5 M NaOH),

- 11 -

was mixed with 1 ml of clear supernatant. After incubating 20-25 minutes at room temperature, the absorbance was measured at 630 nm. The amount of p-aminophenol (PAP) formed was determined by comparing the absorbance of a series of standards varying in concentration from 10-80 uM.

The precipitated proteins from the two enzyme assays were saved for protein determinations.

4.3 Protein assay with Coomassie brilliant blue G-250.

The protein precipitates were dissolved in 5 ml of 0.5 N KOH. Dissolved proteins were diluted 1:5 with 0.1 N KOH (1.0 ml protein in 0.5 N KOH and 4.0 ml 0.1 N KOH); 100 ul of the diluted protein was mixed with 5.0 ml of Coomassie reagent (12). The absorbance at 595 nm was recorded after 5-10 minutes. Protein concentrations were determined by comparing the absorbance of a series of standards ranging in concentration from 100-500 ug/ml bovine serum albumin (BSA). standards.

Results

5. Effects of selected parameters on rate of benzene metabolism in 12,000 x g liver supernatant.

5.1 Effect of incubation time

The rate of benzene metabolism was measured by varying the incubation time from 5 to 40 minutes (Table 1). The rate of benzene metabolized increased linearly for the first 20 minutes in both experimental groups, but was not linear after this time. Pretreatment of rats with PB caused reduction in

the rate of benzene metabolism. The slope of the metabolism line for the first 20 min in the control group was 0.146 and 0.114 in the PB group. These values represent 0.128 and 0.067 uM of benzene metabolized per min in each group respectively.

TABLE 1. EFFECT OF INCUBATION TIME ON BENZENE METABOLISM
IN 12,000 X G SUPERNATANT

Incubation time (min)	nmoles of benzene metabolized /mg protein*	
	CONTROL	PB INDUCED**
5	0.63(0.14)	0.37(0.07)
10	1.40(0.20)	0.90(0.01)
15	2.06(0.03)	1.40(0.05)
20	2.84(0.50)	2.11(0.23)
30	4.00(0.40)	2.20(0.20)
40	4.58(0.50)	2.40(0.15)

*Mean +/- SEM for 3 rats: number in bracket represents SEM
**PB 100 mg/kg/day in 0.85% NaCl for 4 days.

5.2 Effect of pH

To determine the effect of pH on the rate of benzene metabolism the pH of the incubation medium was varied between 7.0 and 7.8. Table 2 shows that the metabolic rate was highest at a pH between 7.3 and 7.4. There was no difference between control and PB treated rats in pH optimum of metabolic rate.

TABLE 2. EFFECT OF pH ON RATE OF BENZENE METABOLISM
IN 12,000 X G SUPERNATANT

| pH | nmoles of benzene metabolized /20 min/mg protein* | |
	CONTROL	PB INDUCED**
7.0	1.24(0.12)	0.83(0.24)
7.3	1.76(0.03)	1.34(0.04)
7.4	1.75(0.15)	1.35(0.05)
7.5	1.42(0.26)	1.23(0.14)
7.8	0.97(0.24)	0.86(0.23)

*Mean +/- SEM for 3 rats: number in bracket represents SEM
**PB 100 mg/kg/day in 0.85% NaCl for 4 days.

5.3 Effect of liver wet weight concentration

A series of 12,000 x g liver supernatant dilutions (1 g   ver
+ 4 ml buffer) from control liver were used as the enzyme   .rce.
Final concentrations of LWW per assay were 30, 50, 100, 150, and
200 mg. Table 3 shows that the rate of benzene metabolism in-
creased as the protein concentration increased. The metabolic
rate was linear up to 100 mg LWW (9.80 +/- 0.77 mg protein) per
assay.

- 14 -

TABLE 3. EFFECT OF PROTEIN CONCENTRATION ON BENZENE METABOLISM IN 12,000 X G SUPERNATANT

volume of 12,000 x g supernatant (1:5)	mg protein /assay	nmoles of benzene metabolized/20 min
		CONTROL
0.15	3.15 (0.43)	5.93 (1.7)
0.25	4.63 (0.68)	9.27 (2.6)
0.50	9.80 (0.77)	18.68 (5.3)
0.75	14.24 (0.93)	25.58 (6.3)
1.00	19.04 (0.59)	27.86 (7.8)

*Mean +/- SEM for 3 rats: number in bracket represents SEM

- 15 -

5.4 Effect of benzene concentration

Six different benzene concentrations were used. The rate of benzene metabolism increased with increasing benzene concentration in the incubation medium, for both control and PB treated rats (Table 4). By using a double reciprocal plot of the reaction rate versus benzene concentration, the apparent Km (Michaelis constant) was found to be 13.89 uM and 34.48 uM for controls and PB treated respectively. For control and PB treated rats the maximum velocities were found to be 0.170 and 0.120 nmoles/min/mg of protein respectively.

TABLE 4. EFFECT OF SUBSTRATE CONCENTRATION ON BENZENE
METABOLISM IN 12,000 X G SUPERNATANT

concentration of benzene (uM)	nmoles of benzene metabolized /20 min/mg protein*	
	CONTROL	PB TREATED**
8.79	1.54(0.31)	0.58(0.09)
17.58	2.16(0.12)	0.79(0.16)
26.37	2.28(0.24)	1.01(0.12)
35.16	2.57(0.10)	1.25(0.09)
52.73	2.82(0.18)	1.55(0.21)
70.31	3.29(0.23)	1.72(0.14)

*Mean +/- SEM for 3 rats: number in bracket represents SEM
**PB 100 mg/kg/day in 0.85% NaCl for 4 days.

Based upon the results of these studies the final incubation conditions chosen were: pH of 7.4, 20 minute incubation time, 100 mg LWW and 36.30 uM benzene.

5.5 Effect of treating rats with PB, 3MC and PCB on weight and protein content of liver and selected enzyme activities.

Data reported in Tables 5-7 were obtained from the same groups of rats. Table 5 indicates there was an increase in liver weight and protein content of 12,000 x g supernatant and microsomes from livers of animals treated with PB and PCB. Microsomes from the liver of rats treated with 3MC had a protein content similar to the control rats. In all groups of rats it was found that protein content of the 12,000 x g supernatant was about 3 times greater than in the microsomes.

TABLE 5. EFFECT OF PHENOBARBITAL, 3-METHYLCHOLANTHRENE AND AROCLOR 1254 ON LIVER WEIGHT AND LIVER PROTEIN OF RAT*

Treatment[1]	Gm liver weight/ 100 gm body weight	mg of protein/gm of liver	
		12,000 x g supernatant	microsomes
Group 1			
Controls	4.60(0.26)	83.17(1.0)	25.66(0.3)
PB	5.91(0.44)[2]	91.57(3.0)[2]	33.16(2.9)[2]
Group 2			
Controls	4.88(0.22)	84.4(3.8)	25.88(3.0)
3MC	5.44(0.23)[2]	93.80(0.3)[2]	29.10(4.1)
Group 3			
Controls	5.53(0.23)	75.73(1.9)	22.43(0.6)
PCB	7.17(0.60)[2]	88.50(4.2)[2]	32.57(2.3)[2]

*Mean +/- SEM for 3 rats; number in bracket represents SEM.
1. Male rats (150-200 gm) were injected i.p. with PB (75 mg/kg) in saline, 3MC (20 mg/kg) in peanut oil, with PCB (75 mg/kg) in corn oil or with the vehicles alone for 3 days. The rats of group 1 and 2 were sacrificed 24 hours after the last injection. The rats of group 3 were sacrificed 120 hours after the last dose.
2. Significantly higher than paired controls by the Student's t-test, $P < .025$.

Results from the 12,000xg supernatant indicates that benzene metabolism was 10-48% less than toluene metabolism in the control rats (Table 6). It was also found that treatment with PB, 3MC or PCB resulted in a reduction in benzene metabolism by as much as 40%. Toluene metabolism increased by as much as 33% following xenobiotic treatment. Aminopyrine demethylase activity increased after rats were treated with PB, 3MC, or PCB. Aniline hydroxylase activity did not change folowing PB treatment, however it did increase when 3MC or PCB were used as the inducing agent. Hepatic metabolism of toluene was greater than benzene. Xenobiotic treatment resulted in an increased toluene metabolism, but a reduction in benzene metabolism. These same xenobiotics induced aminopyrine demethylase and aniline hydroxylase activity.

The results of liver microsomal enzyme metabolism of benzene and toluene, or aminopyrine demethylase and aniline hydroxylase are presented in Table 7. Benzene metabolism was lower than toluene in the microsomes as noted in Table 6 for the 12,000 x g supernatant. The metabolic rates of toluene and benzene appear to be similar as shown in Tables 6 & 7. It should be noted, however, that the results are expressed on a per mg protein basis. If the data is calculated for nmoles/20 min/assay, values are approximately 3 times higher for the 12,000 x g supernatant. This indicates that toluene and benzene are metabolized by microsomes as well as other components found in 12,000 x g supernatant. To demonstrate this fact, a sample calculation is presented below.

- 18 -

```
12,000 x g (Table 5-6)
Benzene metabolism = 2.83 nmoles/20 min/mg protein
Total protein/assay (100 mg LWW) = 8.32 mg
(2.83 nmoles/20 min)(8.32 mg/assay)=23.55 nmoles/20 min/assay

Microsomes (Tables 5 & 7)
Benzene metabolism = 3.49 nmoles/20 min/mg protein
Total protein/assay (100 mg LWW) = 2.57 mg
(3.49 nmoles/20 min)(2.57 mg/assay)=8.97 nmoles/20 min/assay
```

The aminopyrine demethylase and aniline hydroxylase activities were 3 to 4 times higher in the microsomes than in the 12,000 x g supernatant. Microsomal aminopyrine demethylase was induced by all three xenobiotics while aniline hydroxylase activity was not affected by any of the treatments (Table 7).

TABLE 6. EFFECT OF PHENOBARBITAL, 3-METHYLCHOLANTHRENE
AND AROCLOR 1254 PRETREATMENT ON SOME HEPATIC ENZYME ACTIVITIES
IN 12,000 X G SUPERNATANT

	Enzyme activity[2] nmoles/20 min/mg protein			
Treatment[1]	metabolism of benzene	metabolism of toluene	activity of aminopyrine demethylase	activity of aniline hydroxylase
Group 1				
Control	2.83(0.60)	3.15(0.36)	71.6(14)	5.58(0.61)
PB	1.71(0.40)[4]	4.69(0.08)[3]	136.6(8)[3]	5.22(0.42)
Group 2				
Control	1.73(0.36)	3.33(0.24)	63.2(8)	3.48(0.20)
3MC	1.58(0.22)	4.65(0.44)[3]	101.4(10)[3]	5.02(0.91)[3]
Group 3				
Control	2.32(0.42)	4.10(0.09)	62.84(7.6)	3.38(0.40)
PCB	1.37(0.38)[4]	4.84(0.38)[3]	141.33(7.5)[3]	5.92(0.92)[3]

1. Rats were treated as described in Table 5.
2. Enzyme activities are expressed as nanomoles of benzene or toluene metabolized/20 min/mg protein, and nanomoles of product formed/20 min/mg protein for aminopyrine demethylase and aniline hydroxylase activity. Mean +/- SEM for 3 rats: number in bracket represents SEM.
3. Significantly higher than paired controls by the Student's t-test, P<.05.
4. Significantly different from paired controls by the Student's t-test, P<.05.

TABLE 7. EFFECT OF PHENOBARBITAL, 3-METHYLCHOLANTHRENE AND AROCLOR 1254 PRETREATMENT ON HEPATIC 104,000 X G MICROSOMAL ENZYME ACTIVITIES

	Enzyme activity[2] nmoles/20 min/mg protein			
Treatment[1]	metabolism of benzene	metabolism of toluene	activity of aminopyrine demethylase	activity of aniline hydroxylase
Group 1				
Control	3.49(0.40)	4.26(0.04)	176.6(8)	18.76(0.8)
PB	2.16(0.26)[4]	4.93(0.24)[3]	261.0(12)[3]	17.04(0.4)
Group 2				
Control	3.98(0.90)	4.28(0.20)	164.6(4)	19.01(3)
3MC	1.19(0.58)[4]	4.09(0.30)	191.2(9)[3]	16.20(4)
Group 3				
Control	5.53(1.40)	6.19(0.82)	289.7(30)	20.87(1.5)
PCB	2.61(1.30)	4.65(1.39)	554.6(13)[3]	20.69(0.3)

1. Rats were treated as described in Table 5.
2. Enzyme activities are presented as in Table 6. Mean +/- SEM for 3 rats: number in bracket represents SEM.
3. Significantly higher than paired controls by the Student's t-test, $P < .05$.
4. Significantly different from paired controls by the Student's t-test, $P < .05$.

5.6 Comparison of hepatic xenobiotic metabolizing enzyme activities in various subcellular fractions.

The data presented in Table 8 shows that the rates of metabolism of benzene and toluene were highest in the crude liver homogenate and lowest in the microsomal suspension. The metabolic rate of the microsomal suspension was restored to nearly that of the 12,000 x g supernatant, when the microsomes were resuspended in the 104,000 x g supernatant. Conversely, the activities of aminopyrine demethylase and aniline hydroxylase were higher in the microsomal fraction than in other subcellular fractions. The

APDM and AH activities were lowest in the crude liver homogenate

(Table 9).

TABLE 8. COMPARISON OF BENZENE AND TOLUENE METABOLISM
IN VARIOUS SUBCELLULAR FRACTIONS OF CONTROL RAT LIVER

| Enzyme Source[1] | Benzene metabolism[2] | | Toluene metabolism[2] | |
	nmoles/min /gm liver[3]	nmoles/20min /mg protein	nmoles/min /gm liver[3]	nmoles/20min /mg protein
Crude homogenate	11.31A (1.75)	1.77 (0.21)	23.27A (2.02)	3.67 (0.17)
Postnuclear supernatant	8.05B (1.73)	1.78 (0.22)	13.05B (4.08)	2.76 (0.86)
9,000 x g supernatant	10.50A (2.56)	2.25 (0.46)	18.19A (4.28)	4.05 (0.69)
12,000 x g supernatant	7.30B (0.88)	1.62 (0.61)	14.85B (3.22)	3.31 (0.70)
104,000 x g microsome pellet in buffer	4.82C (0.34)	3.58 (0.70)	6.05C (1.61)	4.45 (0.64)
104,000 x g microsome pellet in 104,000 x g supernatant	7.91B (0.47)	1.81 (0.26)	15.89B (2.31)	3.64 (0.45)

1. Enzyme source was prepared as described in methods.
2. Mean +/- SEM for 3 rats: number in bracket represents SEM.
3. Means that are not followed by the same letter are
   significantly different from one another, P<.05. (Duncan's Mul-
   tiple range test)

TABLE 9. AMINOPYRINE DEMETHYLASE AND ANILINE HYDROXYLASE
ACTIVITIES IN VARIOUS SUBCELLULAR FRACTIONS OF CONTROL
RAT LIVER

Enzyme Source[1]	Aminopyrine demethylase[2]		Aniline hydroxylase[2]	
	nmoles/min /gm liver[3]	nmoles/20min /mg protein	nmoles/min /gm liver[3]	nmoles/20min /mg protein
Crude homogenate	54.46E (7.6)	8.82 (0.88)	6.16C (1.9)	.959 (0.26)
Postnuclear supernatant	141.05D (15.9)	29.93 (3.48)	13.12B (2.6)	2.78 (0.55)
9,000 x g supernatant	212.31C (26.2)	46.13 (5.64)	20.09A (5.9)	4.36 (1.27)
12,000 x g supernatant	224.79B (21.1)	49.99 (4.39)	17.88A (5.8)	3.97 (1.24)
104,000 x g microsome pellet in buffer	308.16A (40.7)	230.55 (11.27)	26.82A (5.8)	19.99 (2.8)
104,000 x g microsome pellet in 104,000 x g supernatant	256.85B (9.9)	58.94 (3.4)	23.05A (5.1)	5.26 (0.94)

1. Enzyme source was prepared as described in methods.
2. Mean +/- SEM for 3 rats: number in bracket represents SEM.
3. Means that are not followed by the same letter are
   significantly different from one another, P<.05. (Duncan's Mul-
   tiple range test)

Discussion

SATO and NAKAJIMA used headspace sampling following vial equi-
libration to measure metabolism of hydrocarbons by comparing GC
chromatograph peak heights (13). A headspace sample was injected
onto the GC column using an airtight syringe. In the present

study, a Valco 6-port valve was used to automate sampling and more accurately control the injection of the headspace. Metabolism was measured by comparing chromatographic peak area ratios rather than peak heights, this proved to be faster and more accurate.

It was previously reported that the pH optimum range for benzene metabolism was between 7.0 and 7.8 (5). In the present research the optimum range has been further defined to be between 7.3 and 7.4. The metabolism of benzene was linear for 20 minutes under conditions used. Protein concentrations which gave the best results were approximately 9 mg/assay when using 12,000 x g supernatant. Benzene inhibits microsomal metabolism at a concentration of 50 mM (5). Under the conditions used, optimal benzene concentration was 36.30 uM, well below that which inhibits benzene metabolism. PB treatment caused a reduction in benzene metabolism. The Km value was lower in controls than in PB treated rats, possibly due to higher enzyme affinities for benzene in controls than PB treated rats. The Km value of 13.89 uM reported in this study is much lower than the 0.98 mM value reported by Gut (8).

The rate of benzene metabolism was found to be lower than toluene metabolism. IKEDA et al (9) observed the same results. This may be explained by the fact that a larger amount of energy is needed to break the aromatic C-H bond of the benzene than the aliphatic C-H bond of toluene.

Pretreatment of rats with three known hepatic drug metaboliz-
ing enzyme inducers (PB, 3MC and PCB) did not result in an in-
crease in in vitro benzene metabolism. IKEDA and OHTSUJI (9)
found that PB treated rats did not result in an increase in in
vivo benzene metabolism. GONASUM et al (7) reported that although
PB induced mouse liver cytochrome P-450, benzene metabolism was
not elevated. There are at least two reports (5,8) that indicate
PB markedly increases in vitro benzene metabolism. These discre-
pencies could be due to various research groups using different
strains, age or sex of rats.

The rate of toluene metabolism was significantly higher in
treated groups (PB, 3MC or PCB) than their respective control
groups. The induction of toluene metabolism by PB or 3MC has been
previously reported (9). The observed fact that significant in-
crease of toluene metabolism and apparently no increase in ben-
zene metabolism following pretreatment of PB, 3MC or PCB indi-
cates the possibility of involvement of two different types of
enzymes or pathways in the metabolism of toluene and benzene.

Induction of aniline hydroxylase activity was observed with
the pretreatment of 3MC and PCB. These results agree with previous
reports (4,9,10). Aminopyrine demethylase activity was increased
in rats by the pretreatment with all three incucers.

It was initially observed in this research that the 12,000 x g
supernatant metabolized benzene and toluene at a faster rate than
the 104,000 x g microsomes. As a result of this finding the liver
was fractionated into a number of components; each studied to de-
termine their ability to metabolize benzene and toluene.

It was observed that the metabolism rate of benzene and toluene were highest in crude homogenate, and the lowest in microsomal suspension. The metabolic rate of the microsomal suspension was restored to that of the 12,000 x g supernatant when the microsomes were resuspended in the 104,000 x g supernatant. The data suggests that there is something in the 104,000 x g cytosol which influences benzene and toluene metabolism. It had been found that glutathione S-transferase is in cytosol and plays an important role in metabolizing xenobiotics (6,14). The increase in benzene and toluene metabolic rates when the microsomes were resuspended in the 104,000 x g cytosol could be due to the presence of glutathione and glutathione S-transferase in the cytosol. Further research will be required to determine if only glutathione and glutathione S-transferase or if other factors found in the cytosol are also involved in stimulating the rate of benzene and toluene metabolism.

References

1. Berlin, M., J.C. Cage & E. Johnson (1974). Increased aromatics in motor fuels: a review of the environmental and health effects, Work, Environ. Health 22, 1.

2. Bresnick, E., H. Mukhtar, T.A. Stoming, P.M. Dansette & D.M. Jerina (1977). Effect of phenobarbital & 3-methylcholanthrene administration on epoxide hydrase levels in liver microsomes, Biochem. Phar. 26, 891-92.

3. Browning, E. (1965). In toxicity and metabolism of organic solvents, 3, 40, 66 Elsevier, Amsterdam.

4. Bruckner, J.V., K.L. Khanna & H.H. Cornish (1973). Biological responses of the rat to polychlorinated biphenyls, Toxicol. & Appl. Pharmacol.. 24, 434-48.

5. Drew, R.T. & J.R. Fouts (1974). The lack of effects of pretreatment with phenobarbital and chlorpromazine on the acute toxicity of benzene in rats, Toxicol. & Appl. Pharmacol. 27, 183-93.

6. Glatt, H, & F. Oesch (1977). Inactivation of electrophilic metabolites by glutathione S-transferase and limitation of the system due to subcellular localization, Arch. Toxicol. 39, 87-96.

7. Gonasun, L.M., C. Witmer, J.J. Kocsis & R. Snyder (1973). Benzene metabolism in mouse liver microsomes, Toxicol. & Appl. Pharmacol. 26, 398-406.

8. Gut, I. (1976). Effect of phenobarbital pretreatment on in vitro enzyme kinetics and in vivo biotransformation of benzene in the rat, Arch. Toxicol. 35, 195-206.

9. Ikeda, M. & H. Ohtsuji (1971). Phenobarbital induced protection against toxicity of toluene and benzene in the rat, Toxicol. & Appl. Pharmacol. 20, 30-43.

10. Johnstone, G.J., D.J. Ecobichon & O. Hutzinger (1974). The influence of pure polychlorinated biphenyl compounds on hepatic function in the rat, Toxicol. & Appl. Pharmacol. 28, 66-81.

11. Puyear, R.L., K.J. Fleckenstein & J.D. Brammer (1983). Solubility of major JP-4 jet fuel alkylbenzenes in water of different salinity and temperature, Bull. Environ. Contam. Toxicol., in preparation.

12. Read, S.M. & D.H. Northcote (1981). Minimization of variation in the response to different proteins of the Coomassie blue G dye-binding assay for protein, Anal. Biochem. 116, 53-64.

13. Sato, A. & I. Nakajima (1979). A vial equilibration method to evaluate the drug metabolizing enzyme activity for volatile hydrocarbons, Toxicol. & Appl. Pharmacol. 47, 41-46.

14. Tunek, A., K.L. Platt, M. Przybylski & F. Oesch (1980). Multistep metabolic activation of benzene. Effect of superoxide dismutare on covalent binding to microsomal macromolecules and identification of glutathione conjugates using high pressure liquid chromatography and field desorption mass spectrometry, Chem. Biol. Interactions 33, 1-17.

15. Williams, D.A. (1974). Drug metabolism, Principles of Medicinal Chemistry, Chapter 5, W.G. Foye, editor, Lea & Febiger.

IV. Toluene metabolism and activities of aminopyrine demethylase and aniline hydroxylase in the liver of sunfish, Lepomis spp

Introduction

Selected hepatic microsomal enzymes were studied. The initial goal was to develop the techniques and manual skills with equipment needed in metabolic studies. Laboratory rats were chosen for this preliminary work because their hepatic metabolic activity towards xenobiotics has been well documented. (5, 6, 12, 13, 14, 21) Analogous studies of the liver microsmal enzymes of sunfish (Lepomis spp.) were then performed. Sunfish from Leaf Lake in Becker Co., MN, served as the test organisms. These fish, though displaying a predominantly bluegill phenotype (L. macrochirus) also evidenced some influence of the green sunfish (L. cyanellus) and the pumpkinseed (L. gibbosus). No attempt was made to measure the relative genetic input of these three species. Use of the larger Lepomis spp., rather than Pimephales promelas (fathead minnow), decreased both the need to pool livers, and the time between sacrificing fish and running the assays.

Procedures

1. Treatment of test organisms with possible enzyme inducing agents:

Male Wistar-Furth rats were treated with phenobarbital at the rate of 75 mg/kg body weight (BW). Intraperitoneal (i.p.) injections of PB in glass distilled water were made daily for four days prior to sacrificing. Rats in a second group were sham injected with glass distilled water. A third group of rats, which

received no treatment , served as controls. Body weights were recorded daily for all animals.

The fish were treated on the first and third days of a six day experiment with Aroclor 1254 (PCB) dissolved in 100% ethanol, with peanut oil acting as the carrier. Intramuscular (i.m.) injections were made above the lateral line at an estimated dosage of 0.75 mg/kg BW. Sham injections of the carrier were made on a second group of fish. A third group served as controls. Body weights were recorded when the fish were sacrificed.

2. Preparation of hepatic microsomes

Test organisms were food-deprived for twenty-four hours prior to being sacrificed. Rats were guillotined, whereas fish were held 3-4 minutes in ice water, concussed, and opened ventrally. In all cases livers were immediately removed to ice cold 0.154 M KCl buffer. Buffering agents were either 0.1 M sodium phosphate or 0.05 M Tris with pH adjusted to 7.4 at 25 C. After being rinsed in additional buffer and dried of excess fluids, livers were weighed and homogenized. A 10% liver homogenate was used in rats (1 gm liver:10 ml total volume). In fish the homogenate ratios were 2:5 for aminopyrine demethylase assays, 1:4 for aniline hydroxylase assays, and 1:5 for toluene metabolism assays. All homogenates were centrifuged at 12,000 x g for twenty minutes (0-4 C) to remove whole cells, nuclei, mitochondria, and other cell fragments. Supernatants were transferred to clean test tubes, vortexed, and saved on ice.

3. Enzyme assay reaction mixtures

Reaction mixtures contained 12,000 x g supernatant, nicotinam-
ide adenine dinucleotide phosphate (NADP), glucose-6-phosphate
(G-6-P), $MgCl_2$, KCl, the appropriate substrate, and the appropri-
ate buffer. Reaction blanks contained all of the above, omitting
NADP and G-6-P. See Table 1 for a detailed list of components in
the enzyme assays reaction mixture.

TABLE 1. COMPONENTS (MG) OF THE THREE ENZYME ASSAY REACTION
MIXTURES

	Enzyme Assays					
	APDM[1]		AH[2]		Toluene Metabolism	
	Rat	Sunfish	Rat	Sunfish	Rat	Sunfish
Total Volume[3]	3.0ml	1.0ml	3.0ml	2.05ml	3.1ml	2.1ml
Components[4]						
LWW	100	120	100	125	100	100
NADP	0.372	0.123	0.372	0.250	0.372	0.250
G-6-P	2.60	0.858	2.60	1.80	2.60	1.75
$MgCl_2$	2.40	1.20	2.40	2.40	2.40	2.40
Aminopyrine	3.50	0.88				
Aniline			7.15	1.43		
Toluene					.00867	.00867

1. Aminopyrine Demethylase
2. Aniline Hydroxylase
3. Buffers used to prepare reaction mixtures contained
   0.154 M KCl.
4. LWW=Liver Wet Weight, NADP=Nicotanimide Adenine Dinucleotide
   Phosphate, G-6-P=Glucose-6-Phosphate

3.1 Aminopyrine demethylase assay

Rat assays contained 100 mg liver wet weight (LWW), 0.167 mM
NADP, 3.33 mM G-6-P, 8.33 mM $MgCl_2$, and 5.04 mM aminopyrine in a
final volume of 3.0 ml 0.154 M KCl/0.1 M phosphate buffer, pH
7.4.

Lepomis assays contained 120 mg LWW, 0.165 mM NADP, 3.30 mM G-6-P, 12.5 mM $MgCl_2$, and 3.80 mM aminopyrine in a final buffer, pH 7.4.   3.2 Aniline hydroxylase assay

Rat assays contained the same reactants as in the aminopyrine demethylase assay except the substrate was 25.6 mM aniline. The final volume was 3.0 ml KCl/phosphate buffer or 0.154 M KCl/0.05 M Tris buffer, pH 7.4.

Lepomis assays contained 125 mg LWW, 0.164 mM NADP, 3.38 mM G-6-P, 8.13 mM $MgCl_2$, and 7.49 mM aniline in a final volume of 2.05 ml of the KCL/Tris buffers at pH 7.7.

3.3 Toluene Metabolism Assay

Rat assays contained 100 mg LWW, 0.161 mM NADP, 3.22 mM G-6-P, 8.13 mM $MgCl_2$, and 0.0304 mM toluene in a final volume of 3.1 ml of either of the two buffers

Lepomis assays contained 100 mg LWW, 0.161 mM NADP, 3.20 mM G-6-P, 12.0 mM $MgCl_2$, and 0.0448 mM toluene in a final volume of 2.1 ml of Tris buffer, pH 7.4 at 37 C.

4. Enzyme assay procedures

4.1 Aminopyrine demethylase assay

Rat liver assays were incubated at 37 C in a Dubnoff water bath, 120 oscillations/minute for 20 minutes. Sunfish liver assays however were incubated for 10 minutes under the same conditions. All reactions were stopped with 1.0 ml 10% (w/v) trichloroacetate (TCA). Samples were centrifuged at 14,000 x g for 10 minutes to settle the protein precipitate. To measure formaldehyde concentrations equal volumes of the clear supernatant and

Nash's Reagent B were vortexed and incubated for 8 minutes at 60 C. Absorbances were read at 412 nm against blanks made with reaction blank supernatants after cooling to room temperature. Standard curves of known formaldehyde concentrations were run. The protein pellet was dissolved in 5.0 ml 0.1 M KOH and saved for protein analysis.

4.2 Aniline hydroxylase assay

Media containing rat liver enzymes were incubated as above. Those containing fish liver were incubated at 25-27 C for 60 minutes. Hydroxylase activity was stopped by adding 1.0 ml 20% (w/v) TCA. Following centrifugation 1.0 ml of 1.0 M Na_2CO_3 and supernatant were combined. One ml 1% Phenol (v/v) was then added. Following each addition samples were vortexed. After 20-25 minutes of room temperature incubation absorbances were read at 630 nm to determine concentrations of p-aminophenol (PAP). The protein pellets were treated as above.

4.3 Toluene metabolism

The possible metabolism of toluene was investigated using headspace sampling procedures (16). Capped 17 ml vials fitted with Teflon-lined septa were incubated at 37 C. Those containing rat liver supernatant were incubated for 10 minutes. Vials with 12,000 x g fish liver supernatant were incubated for 60 minutes at 37 C in a Dubnoff waterbath (120 oscillations/minute). Vials were then held for 10 seconds in water at room temperature and sampled using a Valco six-port valve evacuated to negative 15 psi. Comparison of peak areas of samples from reaction vials

with those of reaction blanks determined the relative decrease of toluene in the gaseous phase. Standard curves of known toluene concentrations were periodically run to assure the GC was responding linearly. Following headspace sampling proteins were precipitated with 1.0 ml 20% TCA and centrifuged. The pellets were treated as in previous assays.

5. Determination of protein concentrations

The protein precipitates of all samples were dissolved in 5.0 ml of 0.1 M KOH. Aliquots of these solutions were diluted either 1:5 or 1:10 with more KOH as necessary. 0.100 ml portions of these dilutions were added to 5.0 ml of Serva Blue G solution. Absorbances were read at 595 nm with a dual-beam spectrophotometer. Standard curves were prepared with bovine serum albumin (BSA) in 0.1 M KOH. Linearity of response was noted between 10 and 60 ug BSA per 5.1 ml Serva Blue G/protein solution.

Results

1. Development of assay procedures

1.1 Aminopyrine Demethylase

The initial experiment designed to look for aminopyrine demethylase activity in sunfish liver microsomes compared enzyme activity at five pH levels and five aminopyrine concentrations. Reaction mixtures contained the equivalent of 60 mg liver wet weight (LWW), 0.124 mg NADP, 0.867 mg glucose-6-phosphate, and 2.4 mg magnesium chloride in .154M KCl/.1 M sodium phosphate buffer at one of the following pH's; 6.8, 7.1, 7.4, 7.7, & 8.0. Aminopyrine concentrations were 4.32, 5.18, 6.06, 6.96, and 7.78

mM. Livers from two fish were pooled to decrease overall variability. Assay mixtures were incubated for 15 minutes at 30 C before being killed with 0.33 ml of 10% trichloroacetate (TCA). There was little difference found among the various pH's. It was decided that the mean pH of 7.4 would be used for ensuing experiments.

Aminopyrine demethylase activity (APDM) was next studied by varying both substrate concentrations and quantities of liver in the reaction tubes. Livers from three fish were pooled and general reaction conditions were the same as above. Aminopyrine concentrations were as follows; 0.86, 1.73, 2.59, 3.46, and 4.32 mM. Quantities of liver used were 30, 60, or 90 mg. The results showed that test tubes having 30mg of liver yielded the highest reaction rates although the overall prouction of formaldehyde was somewhat lower. To keep product formation at levels where it could consistently be measured with our equipment it was decided that higher quantities of liver should be used.

The effects of temperature and substrate concentration on APDM was then studied. Since previous work was done at 30 C the following temperatures were selected; 33 c, 38 C, and 44 C. (Table 2) Five concentrations of aminopyrine were used; 2.59, 4.32, 6.05, 7.78, and 9.51 mM. Livers from five fish were pooled for these assays. Each sample used 120 mg LWW and samples were incubated for 20 minutes. Linearity of the reaction rates was noted at all three temperatures, but the overall reaction rates were highest at 38 C.

TABLE 2. COMPARISON OF INCUBATION TEMPERATURES AND
AP CONCENTRATION OF RATES OF AMINOPYRINE DEMETHYLASE*

Temperature	AP concentration					r^2
	2.59	4.32	6.05	7.78	9.51	
APDM Activity (umoles/g protein/hour)						
33	5.19	6.59	7.49	8.39	8.85	.969
38	7.75	8.39	9.67	10.60	11.20	.986
44	6.21	8.02	9.03	9.03	9.49	.829

*Liver was obtained from a pool of 5 fish.

APDM was studied at various time intervals up to 40 minutes.
(Table 3) Aminopyrine concentrations were the same as in the
temperature experiments, as were the general reaction conditions.
Livers from four fish were pooled for the assays incubated 10,
20, 30, and 40 minutes. Both reaction rates and total formaldeh-
yde production declined linearly over time at all concentrations.
(Table 3, 4) Formaldehyde production was linear relative to sub-
strate concentration. These results indicated that formaldehyde,
a volatile compound, was being lost from the open reaction tubes.
That loss was occurring more rapidly during longer incubations
than formaldehyde production. Reaction rates in a second experi-
ment at five minutes of incubation were inconsistent so a ten
minute incubation period was chosen for later trials.

Time (min)	AP concentration (mM)					
	2.59	4.32	6.05	7.78	9.51	R^2
	ADPM Activity (umoles/g protein/hour)					
5	33.9	28.8	34.7	33.2	38.0	.323
10	21.1	22.6	24.4	23.0	26.6	.754
20	9.93	10.7	11.4	12.3	12.1	.908
30	5.56	6.43	6.87	7.22	7.36	.915
40	4.21	4.36	4.64	4.87	6.07	.821
r^2	.747	.858	.832	.854	.815	
R	-.865	-.926	-.912	-.924	-.903	

*Livers of 4 fish pooled for 10,20,30 and 40 min.
 Livers of 3 fish pooled for 5 min.

TABLE 4. EFFECT OF INCUBATION TIME AND SUBSTRATE CONCENTRATION
UPON RECOVERY OF CH_2O DURING ADPM ENZYME ASSAYS

Time	AP concentration (mM)				
	2.59	4.32	6.05	7.78	9.51
	total moles CH_2O recovered				
5	31.4	26.6	32.1	30.7	35.1
10	34.4	36.8	39.9	37.5	43.5
20	32.4	34.8	37.2	40.2	39.6
30	27.3	31.5	33.6	33.4	36.0
40	27.5	28.5	30.3	31.8	39.6

A Lineweaver-Burk Plot of aminopyrine concentrations rela-
tive to resulting reaction rates using averages from four dif-
ferent fish or groups of fish yeilded an expected maximum ve-

locity of 21.7 umoles formaldehyde recovered/g protein/hour with a Km value of 2.25 mM aminopyrine. The r-value for the plot was 0.981. Reaction tubes contained 120 mg of LWW and were incubated at 38 C for 10 minutes. The following concentrations of aminopyrine were used; 2.59, 4.32, 6.05, 7.78, and 9.51 mM.

1.2 Aniline hydroxylase

Aniline hydroxylase activity was studied first in sunfish using sodium phosphate buffer at pH 7.4. Little or no activity was measured. Low aniline hydroxylase activity (AH) was found in sunfish liver using 0.154 M/0.1 M Tris buffer, pH 7.7 at 25 C. Reaction mixtures contained 167 mg LWW, .186 mg NADP, 1.3 mg glucose-6-phosphate, and 2.4 mg magnesium chloride in a final volume of 2.0 ml of the Tris buffer. Aniline concentrations were as follows; 15.4, 30.7, 46.1, 61.4, and 76.8 mM. Incubation at 37 C yielded higher reaction rates than incubation at 27 C but the latter rates were more consistent and showed much greater linearity relative to aniline concentrations. Livers from 5 fish were pooled to decrease the influence of individual variability. In later experiments it was found that .05 M Tris buffer produced equivalent results to 0.1 M Tris and so was often used.

In a subsequent experiment run under similar conditions, reaction rates measuring amounts of p-aminophenol/g protein/hour showed relatively high degrees of linearity with increasing concentrations of aniline. The reaction rates at 36 C declined

however with increasing substrate concentration while those at 26 C increased with concentration of aniline. (r-values = -.793 and .863 respectively) Later experiments were run at ambient temperatures in the laboratory ranging from 25-27 C.

AH was further studied by holding temperature constant at 25 C and varying pH and aniline concentrations. Tris buffer was used at one of four pH's; 7.1, 7.4, 7.7, and 8.0. Aniline concentrations were 1.54, 3.07, 4.61, 6.14, and 7.68 mM. (These were only one-tenth those used previously, but yielded comparable reaction rates.) Reaction rates generally increased with pH and with aniline concentration. The reaction rates at pH 7.7 were the most linear with respect to aniline concentration (r-square = .900). These results are the average of two experiments. In the first experiment livers from two fish were pooled for each series of tests at each pH. In the second experiment livers from two or three fish were pooled for the series at each of the pH's. Pooling of livers was done to mininmize the effects of individual variability in the population. (Enzyme activity was quite variable from individual to individual.)

A Lineweaver-Burk Plot was run on the data from the above experiment at both pH 7.7 and pH 8.0. In the former, maximum velocity was predicted to be .75 umoles/g protein/ hour with a Km of .59 mM aniline (r = .75). In the latter case maximum velocity was 1.0 umoles of PAP formed/g protein/ hour with a Km of .59 mM aniline (r=.75) Later experiments were run at a pH

of 7.7 because of the greater consistency achieved at that pH. A concentration of 7.68 mM aniline was used because the sensitivity of our spectrophotometer was simply not great enough to measure accurately concentrations of PAP we often found with lower substrate concentrations.

1.3 Toluene metabolism

The disappearance of toluene was only found to occur in samples containing fish liver homogenate supernatant under the following conditions. Reaction vials were closed to the atmosphere with caps fitted with teflon-lined septa. The vials contained 0.25 mg NADP, 1.75 mg glucose-6-phosphate, 2.4 mg magnesium chloride, 8.67 ug of toluene, and 100 mg LWW in a final volume of 2.05 ml .154 M KCl/.05 M Tris buffer, pH 7.4 at 37 C. Reactions were allowed to continue for 60 minutes at 37 C before being sampled for toluene in the headspace.

2. Results of the three assays

2.1 Results of the assays using rat liver enzymes

Aminopyrine demethylase activity resulted in 141.0 and 129.7 umoles formaldehyde recovered/g protein/hr of incubation in control or sham injected rats respectively. Formaldehyde was recovered at the rate of 370.6 umoles/g protein/hour in the PB treated rats. (p much less than 0.05). (Table 5)

TABLE 5. REACTION RATES OBSERVED IN RAT AND SUNFISH LIVER
12,000 X G SUPERNATANTS FOR APDM, AH, AND TOLUENE METABOLISM

Assay	Rat metabolism[1] umoles/g protein /hr incubation	N	Fish metabolism[1] umoles/g protein /hr incubation	N
APDM[2]				
Control	141.0(23.4)	4	18.2(2.87)	10
Sham injected	129.7(12.8)	4	23.6(2.32)	5
PB treated	370.6(27.8)	4		
PCB treated			25.7(1.77)	10
AH[3]				
Control	5.43(0.95)	4	0.206(.063)	10
Sham injected	6.42(1.41)	4	0.520(.018)	5
PB treated	13.37(4.45)	4		
PCB treated			0.525(.038)	10
Toluene				
Control	7.44(0.44)	4	0.118(.036)	9
Sham injected	6.47(0.72)	4	0.168(.044)	9
PB treated	9.44(0.55)	4		
PCB treated			0.226(.045)	9

1.Mean +/- SEM: number in bracket represents SEM.
2.Aminopyrine Demethylase
3.Aniline Hydroxylase

Aniline hydroxylase activity was more variable. PAP was formed at the rate of 5.42 and 6.41 umoles/g protein/hr in control and sham injected rats respectively. Reaction rates in the PB treated rats averaged 13.32 umoles/g protein/hr of incubation. (p less than 0.05)

The disappearance of toluene occurred at the rate of 7.43 and 6.48 umoles/g protein/hr of incubation in control and sham injected rats respectively. The rate of substrate metabolism in

PB treated rats was 9.43 umoles/g protein/hr. This reaction rate is significantly different from those rates in the first two groups (p less than .05).

Body weights of the three groups of rats were very similar, with less than 2 g separating the means of the heavy and light groups. Liver wet weights, expressed as a per cent of the total body weight varied significantly (p=0.005) with the percentage being higher in PB treated rats than in shams and controls. (4.38 vs. 3.63 and 3.58% respectively) Using ANOVA and Duncan's Multiple Range Test the latter 2 groups did not vary significantly. Protein concentrations of livers in the 3 groups of rats did not vary significantly.

The relative effects of the two buffers used (sodium phosphate or Tris) were also analyzed. It was found that reaction rates were essentially the same using either buffer. 2.2 Results of the assays using sunfish liver enzymes

The results of assays performed using livers from _Lepomis_ _spp._ are more ambiguous. The rates are more variable and as such, not always significantly different. In the aminopyrine demethylase assay the rate of formaldehyde recovery was 18.2 and 23.6 umoles/g protein/hr of incubation in controls and sham injected respectively. PCB treated fish liver produced formaldehyde at the rate of 25.7 umoles/g protein/hour. Using the Statistical Analysis Systems (SAS) program for the Kruskal-Wallis rankings test there appears to be a significant difference between the reaction rates of fish in the control and those

treated with PCB group (p=0.05). However, there is an overlap
in the reaction rates of the sham injected group with either of
the other two experimental groups. (Table 5)

It was determined that the in vitro rate of aniline hydroxy-
lation using fish liver supernatants was higher at a pH of 7.7
than at the pH of 7.4. PAP was formed at a rate of 0.206
umoles/g protein/ hr of incubation in the control group of sun-
fish. Rates increased significantly in PCB-treated and sham
injected fish. These rates were 0.520 and 0.525 umoles/g pro-
tein/hr respectively.

The rate of toluene metabolism in the vials containing _Le-
pomis_ _spp._ liver homogenate was very slight under the condi-
tions used. In comparing the reaction vials of the controls
with their respective blanks (those vials not containing the
NADPH regenerating system) it was found that there was an aver-
age loss of 118.2 nmoles of toluene/g protein/hr of incubation.
The loss in the sham injected group averaged 167.8 nmoles/g
protein/hr. The average loss detected in the PCB treated group
of fish was 225.5. These losses do not differ significantly,
due to the high degree of individual variability. (These re-
sults were from livers of individual sunfish.)

Discussion

The metabolism or possible metabolism of three substrates
(aminopyrine, aniline, and toluene) by enzymes associated with
the 12,000 G supernatant fraction of liver homogenates (male
Wistar-Furth rats and sunfish of the genus _Lepomis_) was inves-
tigated.

The possible metabolism of toluene was measured by determining the decrease of this volatile substrate in the gaseous phase of an air-tight incubation vial containing appropriate reactants and liver supernatant. Mathematically it can be shown that the ratio of peak areas between control and reaction vials accurately reflects changes in toluene concentrations within those vials. (16) The consistent loss of toluene from the gaseous phase in reaction vials compared to control vials has been interpreted as a measure of the metabolism of this compound.

In the rats baseline data was collected on the mixed-function oxidase activity (MFO) of control rats then compared to the MFO activity of rats treated with phenobarbital (PB) at the rate of 75 mg/kg body weight (BW)/day for four days and in rats treated only with the carrier (sham injected). In all three instances the MFO activities of the control rats and the sham injected rats were significantly different from the activty in the PB-treated rats (p less than 0.05) but were not different from each other.

Treatment of the rats with PB caused a significant increase in liver size compared to body size. (p less than 0.05)

In both the toluene metabolism assays and the aniline hydroxylase assays the effects of two buffers were tested. Those two buffers were 0.1 M Na-phosphate and 0.05 M Tris. In neither case did the use of either buffer result in significantly different results.

The results support what has been already extensively reported in the literature. (Reviews; 5, 12, 13, 14, 21)

Brodie, et.al. (5) and Brodie and Maickel (6) reported that fish lacked the ability the metabolize foreign compounds. These early reports have been decisively rejected by many investigators (1, 2, 3, 9, 19, 20 to name a few of the more recent articles) Metabolism of toluene in Lepomis spp. was considered of interest because this group of fish plays an integral role in freshwater ecosystems due to its nearly ubiquitous distribution in the United States. The structure of toluene (ie. a single benzene ring with a methy constituent) suggests that during metabolism it may be demethylated or hydroxylated. Therefore the aminopyrine demthylase and aniline hydroxylase assays seemed very appropriate as conjunctive studies. These MFO enzyme systems have also been reported in other fish as well as their induction by various agents. (4, 7, 8, 10, 11, 15, 17, 19)

It was determined that in sunfish aminopyrine demethylase activity was not particularly dependent on pH. APDM was, however, temperature dependent with the highest reaction rates over several substrate concentrations occurring at a temperature of 38 C. Lower activity over those same concentrations was noted at both 33 and 44 C.

The reaction rate was also substrate dependent, with increasingly higher rates being recorded at increasingly higher concentrations. Time was a critical factor in measuring APDM

activity. The open test tubes used for the assays allowed for-
maldehyde to presumably escape if incubation times were extend-
ed beyond 10 to 15 minutes. As a result, not only did reac-
tion rates decline linearly as incubation times increased, but
so did the total amount of formaldehyde measured in each sam-
ple.

Aniline hydroxylase activity was measured in assays using
Tris buffer, pH ranging from 7.1-8.0. The higher pH's resulted
in greater reaction rates. The most linear rates were recorded
at a pH of 7.7. It was decided to run succeeding experiments
at this level. Early attempts to measure aniline hydroxylase
activity using phosphate buffer were unsuccessful in the sun-
fish. Tests using rat liver, however, showed no significant
difference between the two buffers for this particular assay.
Whether the fish liver enzyme system is fundamentally different
is not known and perhaps a return to the phosphate buffer and
an incorporation of the modifications of later experiments
would yield results equivalent to those achieved with Tris.

AH was also shown to be temperature dependent in the sunfish
liver assay media. As incubation temperatures increased, reac-
tion rates decreased. This phenomenon was so pronounced that
at 36 C the reaction rates were actually decreasing as sub-
strate concentration increased. This might display some corre-
lation of temperature to substrate-concentration inhibition.

The metabolism of toluene by sunfish liver 12,000 G superna-
tant was finally achieved near the end of the fall season.

Thus the supply of fish was limited and necessitated the use of the only procedure successfully showing a decrease in toluene in the reaction vials. It is quite possible that some modification of the procedure will yield higher reaction rates than those shown so far. The temperature used was 37 C. If toluene is metabolized by an enzyme system related to the one metabolizing aniline as it may well be, a reduction in the temperature may result in higher reaction rates. Changes in pH and substrate concentration may also successfully increase the particular enzyme activity. Finally, 60 minutes may well be an inappropriate incubation time.

Aroclor 1254, a Monsanto product, contains various polychloro- biphenyls (PCB). This substance has been shown to be an MFO inducer. (2, 10, 18) Methods of treatment in these studies were by aquatic exposure to the water-soluble fraction of Aroclor 1254 or by ingestion along with food pellets. It was decided that intramuscular injection of the PCB's might prove satisfactory, providing a more rapid increase in MFO activity than other possible methods and providing more control of the dosage each fish received. were also used to better control dosage. Injections were made at the approximate dosage of 750ug/kg BW, using peanut oil and ethanol as a carrier on day 1 of the experiment and were repeated on day 3. Fish were sacrificed on day 6. The results were somewhat ambiguous. Formaldehyde recovery rates were elevatsignificantly elevated in PCB-treated fish. The same type of elevation also occurred in

the AH assays as well a the toluene metabolism assays. In the latter two cases, though, that elevation was not significant. Also, in all three assay procedures, the enzymatic activity of the sham-injected sunfish was somewhat higher than in the controls. The peanut oil/ethanol carrier may have caused some induction of MFO activity. Finally, the great deal of variability exhibited by the population implies, that, with a greater sample size PCB induced enzymatic activity could be shown to be statistically significant. The broad variability in the activity of the fish liver enzymes is presumalby the phenotypic display of the great deal of genetic heterogeneity one expects to find in a wild population of hybrids.

BIBLIOGRAPHY

1.   Addison, R.F., et.al. (1977). Mixed-Function Oxidase enzymes in trout, Salvelinus fontinalis, liver; absence of induction following feeding of p,p'-DDT or p,p'-DDE. Comp. Biochem. Physiol. 57C,39-43

2.   Addison, R.F., et.al. (1978). Induction of hepatic mixed-function oxidase (MFO) enzymes in trout (Salvelinus fontinalis) by feeding Aroclor 1254 or 3-methylcholanthrene. Comp. Biochem. Physiol. 61C, 323-325

3.   Balk, L., et.al. (1980). Initial characterization of drug-metabolizing systems in the liver of the northern pike, Esox lucius. Drug Metab. Disp. 8, 98-103

4.   Bend, J.R., et.al. (1976). Hepatic microsomal mixed-function oxidase systems from the little skate, Raja erinacea, a marine elasmobranch. Microsomes and Drug Oxidations, 1976

5.   Brodie, B.B., et.al. (1958). Enzymatic metabolism of drugs and other foreign compounds. Ann. Rev. Biochem. 27,427-454

6.   Brodie, B.B. and R.P. Maickel (1962). Comparative biochemistry of drug metabolism. Proc. First Int. Pharmac. Meet. 6, 299-324

7.   Buhler, D.R. and M.E. Rasmusson (1968). The oxidation of drugs by fishes. Comp. Biochem. Physiol. 25, 223-239

8.   Gerhart, E.H. and R.M. Carlson (1978). Hepatic mixed-function oxidase activity in rainbow trout exposed to several polycyclic aromatic compounds. Environ. Res. 17, 284-295

9.   Hansson, T., et.al. (1980). Effects of some common inducers on the hepatic microsomal metabolism of androstenedione in rainbow trout with special reference to cytochrome P-450-dependent enzymes. Biochem. Pharmacol. 29, 583-587

10.   Hill, D.W., et.al. (1976). Induction of hepatic microsomal enzymes by Aroclor 1254 in Ictalurus punctatus (Channel Catfish). Bull. Environ. Contam. Toxicol. 16,495-502

11.   James, M.O., et.al. (1979). Hepatic microsomal mixed-function oxidase activities in several marine species common to coastal Florida. Comp. Biochem. Physiol. 62C, 155-164

12. Kappas, A. and A.P. Alvares (1975). How the li
    metabolizes foreign substances. Sci. Am. 232:6, 22-31

13. Kuntzman, R. (1969). Drugs and enzyme induction. Ann. Rev.
    Pharmacol. 9, 21-36

14. La Du, B.N., et.al. (editors) (1971). Fundamentals of Drug
    Metabolism and Drug Disposition The Williams and Wilkins Co.
    Baltimore, Md.

15. Pohl, R.J., et.al. (1974). Hepatic microsomal mixed-
    function oxidase activity of several marine species from
    coastal Maine. Drug Metab. and Disposit. 2:6, 545-555

16. Sato, A. and T Nakajima (1979). A vial-equilibration method
    to evaluate the drug-metabolizing enzyme activity for
    volatile hydrocarbons. Toxicol. and Appl. Pharmacol. 47,
    41-46

17. Stegeman, J.J., et.al. (1979). Hepatic and extrahepatic
    microsomal electron transport components and mixed-function
    oxygenases in the marine fish Stenotomus versicolor.
    Biochem. Pharmacol. 28, 3431-3439

18. Stegeman, J.J. and R.L.Binder (1980). Induction of aryl
    hydrocarbon hydroxylase activity in embryos of an estuarine
    fish. Biochem. Pharmacol. 29, 949-951

19. Stegeman, J.J. and M. Chevion (1980). Sex differences in
    cytochrome P-450 and mixed-function oxygenase activity in
    gonadally mature trout. Biochem. Pharmacol. 29, 553-558

20. Varanasi, U. and D.J. Gmur (1980). Metabolic activation and
    covalent binding of benzo(alpha)pyrine to deoxyribonucleic
    acid catalyzed by liver enzymes of marine fish. Biochem.
    Pharmacol. 29, 753-761

21. Williams, D.A. (1974). Drug Metabolism (Ch. 5 of Principles
    of Medicinal Chemistry, W.O. Foye, ed. Lea and Febiger,
    1974

V. Bioaccumulation and time distribution of ^{14}C benzene and ^{14}C toluene by fathead minnows using a closed static bioassay system.

Introduction

Aromatic hydrocarbons are components of water soluble fractions derived petroleum products such as JP-4 jet fuel and gasoline (7, 5). These water soluble aromatic hydrocarbons gain access to an aquatic organsim by consumption of hydrocarbons laddened food (6), skin (9) and quite likely the gills. The uptake of hydrocarbons by coho salmon has been reported to be dependents upon the number of benzene rings present in the aromatic hydrocarbon, i.e. anthracene > naphthalene > benzene. Tissues which concentrate greatest amounts of hydrocarbons are in the following order: bile > liver > brain > muscle (6).

Fish during various stages of embryonic development are permeable to hydrocarbons. Pacific herring eggs accumulate more hydrocarbon than larval forms at a later stage of development (3). The spawning Pacific herring when exposed to hydrocarbons accumulate them in the ovary and unfertilized egg. This ultimately resulted in reduced fertility (8). Toluene has been reported to produce developmental abnormalities in the fathead minnow (2).

This investigation was performed to compare the uptake and tissue distribution of toluene and benzene in the fathead minnow (Pimephales promelas).

Materials

Scintisol, Unisol and Complement were purchased from Isolab, Inc. Omnisolv methanol and 30% hydrogen peroxide were obtained from Matheson Coleman and Bell. Uniformly labeled ^{14}C benzene and toluene (ring-1-^{14}C) were purchased from New England Nuclear, with specific activities (SA) of 10-20 mCi/mmole and 1-5 mCi/mmole respectively. Both digested tissue and water samples were counted in a Beckman LS 6800 liquid scintillation counter (LSC).

Methods

Water was prepared for in vivo fathead minnow (Pimephales promelas) metabolism studies as follows. The pH of one liter of charcoal filtered tap water (pH 8.9) was adjusted to 7.0 and filtered with a Whatman GF/A 1.6 um filter. The pH was lowered to reduce the effects of chemiluminescence during liquid scintillation counting. Filtering was done to reduce the cloudy appearance of the water when experiments were run over extended periods of time. One liter of water was placed in a two liter screw cap type Erlenmeyer flask and slowly bubbled with oxygen for five minutes before adding the minnows. Two minnows were added to the flask. Ten ul of 1:10 isotope (diluted with either toluene or benzene depending on the isotope) was added just before the flask was closed with a modified screw cap. Approximately 8.9×10^5 DPM was added to the water of each flask. The specific activity of toluene and benzene used was 8.43×10^{-3} uCi/uM and 8.08×10^{-3} uCi/uM respectively. The cap was modified by drilling a hole and inserting a Teflon septum so that the system could permit

withdrawl of aqueous samples without exposing the flask to the atmosphere. Water samples were removed by puncturing the septum with a 12" long, 22 gauge needle attached to a 3 ml glass syringe. In all cases one ml samples of the aqueous phase were removed and placed in a scintillation vial one hour after starting and immediately before termination of the experiment. Water samples were prepared for counting by adding 10 ml of Scintisol to each vial. Samples were analyzed in the LSC and counted to a 2sigma=1%.

The experiment continued for 4,8,12,18 or 24 hours. Duplicate flasks were used at each time interval. Following withdrawl of the final aqueous sample for LSC counting, the flask was opened and the water poured off. Minnows were placed in a beaker containing a lethal solution of MS222 in water. When the minnows were no longer active they were weighed (wet weight), dissected, and the following tissues were transferred to counting vials: bile (gall bladder), brain, intestine, lipid, liver, muscle, developed ovary, skin, and spleen. 1 cm skin samples came from an area posterior to the anal opening, muscle samples were also taken from this region. One ml of Unisol/100 mg tissue was used to solubilize various tissues.

Tissues were digested for 12 hours or longer with Unisol at room temperature and then prepared for liquid scintillation counting. A one ml aliquot of solubilized tissue was placed in a scintillation vial, to this was added 0.5 ml 100% methanol and 10 ml Complement. Four drops of 30% hydrogen peroxide were added to

each vial to reduce color quenching. After each addition the vials were capped and shaken. Samples were stored overnight before counting in the LSC. All samples were allowed to sit in the dark at least 30 minutes in the LSC before counting to reduce chemiluminescent effects.

Due to the fact that some experimental sample's H numbers fell below the built-in quench curve of the LS 6800 system separate quench curves were prepared for both aqueous and solubilized tissue samples. The new curves entered in the LSC encompassed experimental H numbers, improving accuracy and efficiency. Samples were counted in the appropriate file. The aqueous quench curve contained: 0.5 ml glass distilled water, 10 ml Scintisol, 0-64 ul methyl nitrate (quenching agent) and 50 ul of ^{14}C toluene standard (20,500 DPM). A solubilized tissue quench curve contained 1 ml Unisol, 0.5 ml 100% methanol, 10 ml Complement, 4 drops of 30% hydrogen peroxide, 0-64 ul methyl nitrate and 50 ul of ^{14}C toluene standard (20,500 DPM). Quench curve samples were prepared according to methods described above.

Count data obtained from the LS 6800 was calculated efficiency, H number, and CPM. Plots of calculated efficiency versus H number were made for each quench curve. Using a given sample's H number, the efficiency could be determined from the quench curve plot. DPM values were calculated by dividing CPM by efficiency. DPM/mg tissue values were found by dividing DPM by mg of tissue (wet weight) taken at the time of dissection.

Results

Under conditions of our static bioassay system two fathead minnows can survive 24 hours and longer in a closed 2 liter Erlenmeyer flask with 1 liter of water. Activity of ^{14}C in the water remained constant for the duration of the experiment for benzene and in the case of toluene actually increased slightly. A good deal of time was devoted to determine why the toluene content of the flask increased, but to no avail. The closed system worked well for the static bioassay using the fathead minnow, and presumably would work equally well with other small fish for relatively short periods of time.

The ability of the fathead minnows to bioaccumulate benzene and toluene is represented in Figures 1 & 2. Bile had the greatest amount of activity in both exposure groups, while muscle had the least. Peak accumulation of ^{14}C activity in bile occured at 12 hours in benzene exposed fish, while it continued to increase for 24 hours in ^{14}C toluene exposed minnows. Comparing the two exposure groups the bile in fish exposed to toluene accumulated 2 to 3 times more activity. Spleen accumulated a maximal amount of benzene by 12 hours, with a rapid decline by 18 hours. The spleen accumulated toluene gradually up to 18 hours, where activity was greater than benzene activity. Benzene accumulation in lipid showed a similar pattern as did the spleen. Toluene accumulated in lipid to a maximal amount by 12 hours. Liver accumulated the greatest amount of benzene by 8 hours with nearly 50% decline by 24 hours. Liver in the toluene exposed fish accumulated toluene

to a near maximal level by 8 hours. Only a slight increase oc-
cured over the next 10 hours, which was followed by a decline at
24 hours. The ovary accumulated more toluene than benzene. Fat-
head minnows appear to bioconcentrate toluene to a greater extent
than benzene.
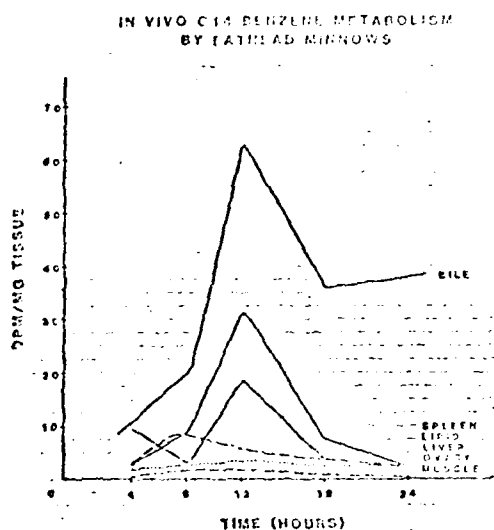
Figure 1
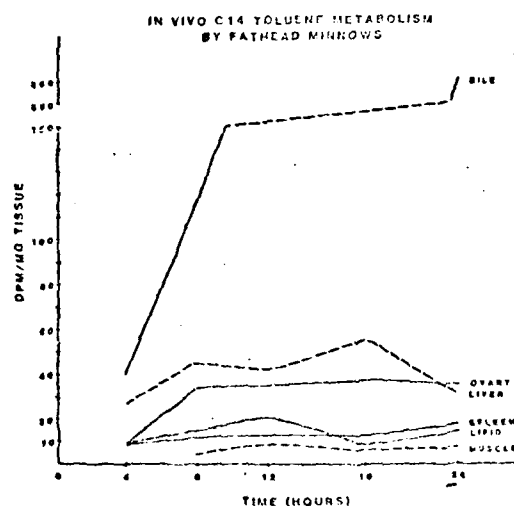
Figure 2

The bioconcentration of ^{14}C benzene and ^{14}C toluene from water
into several tissues as a function of time. Ten ul of benzene or
toluene containing 8.9 X 10^5 DPM each was added to a 2 liter Er-
lenmeyer flask and closed to the atmosphere with a Teflon or alu-
minum foil lined cap. Fish were removed from the flask at
4,8,12,18 or 24 hours, tissues were removed, digested, and ^{14}C
incorporation determined. Values represent the means of 4-6 min-
nows.

Discussion

The ability of the fathead minnow to bioconcentrate toluene was greater than benzene. A possible explaination for this could be due to the slight differences in the molecular configuartion of these two molecules. Toluene has a methyl group attached to the benzene ring which could provide for greater membrane permeability and this would provide for an increased rate of entry into the minnow. VARANASI et al (9) reported that naphthalene was removed from water by rainbow trout. ELDRIDGE et al (3) found that larvae of Pacific herring bioaccumulated benzene from water, and reached equilibrium within 6-12 hours. The data presented in Figure 1 indicates that equilibrium was reached in muscle and ovary upon exposure of minnows to benzene. Other tissues were not in equilibria. The bile may have reached a steady state between 18 and 24 hours, but more work would be required to more acurately determine this. Toluene bioaccumulation in the various tissues, with the exception of bile, reached equilibria after about 8 hours (Figure 2). Toluene continued to accumulate in the bile for the entire 24 hour period. It was found that the liver concentrated more toluene than it did benzene.

ROUBAL et al (6) found that injecting or feeding benzene, naphthalene or anthracene resulted in the greatest amount of bioconcentration in the liver and brain followed by muscle. They also found bioconcentration was associated with molecular weight, i.e. anthracene>naphthalene>benzene. The difference in molecular weights range from three to one benzene ring in each molecule re-

spectively. They observed the same order of bioconcentration in the bile. We observed the same relationship of bioconcentration between toluene and benzene. The difference in molecular weights between these two molecules is a single methyl group. It would be interesting to see if increased substitution on the benzene ring would increase bioconcentreation activities.

A single experiment was preformed to determine if the liver mixed function oxidase (MFO) system was involved in bile formation and bioconcentrating toluene. Minnows were permitted to swim in a weak solution of piperonyl butoxide (1 mg/liter of filtered tap water) for 24 hours. Piperonyl butoxide inhibits MFO activity in fish and other organisms when used either in vivo or in vitro (MELANCON et al,). The fish were then treated in the manner described above to ^{14}C toluene. After 24 hours the bile was analyzed for ^{14}C content. The radioactivity in the bile was near background. This strongly implicates MFO activity in toluene metabolism. Further studies would be required to determine the toluene metabolites in the bile.

References

1. Collier, T.K., M.M. Krahn, & D.C. Malins (1980). The disposition of naphthalene and its metabolites in the brain of rainbow trout (Salmo gairdneri), Environ. Research 23, 35-41.

2. Devlin, E.W. (1982). Developmental studies on the fathead minnow, (pimephales promelas, raf). Ph.D. thesis, 1-138.

3. Eldridge, M.B. & T. Echeverris (1978). Fate of ^{14}C benzene in eggs and larvae of Pacific herring (Clupea harengus pallasi), J. Fish. Res. Board Can. 35, 861-65.

4. Melancon, M.J.Jr., J. Saybott & J.J. Lech (1977). Effect of piperonyl butoxide on disposition of Di-2-ethylhexyl phthalate by rainbow trout, Xenobiotica 7, 633-40.

5. Montz, W.E. Jr., R.L. Puyear & J.D. Brammer (1982). Identification and quantification of water-soluble hydrocarbons generated by 2-cycle outboard motors, Arch. Environm. Contam. Toxicol. 11, 561-65.

6. Roubal, W.T., T.K. Collier & D.C. Malins (1977). Accumulation and metabolism on Carbon-14 labeled benzene, naphthalene, and anthracene by young coho salmon (Oncorhynchus kisutch), Arch. Environm. Contam. Toxicol. 5, 513-29.

7. Puyear, R.L., K.J. Fleckenstein & J.D. Brammer (1983). Solubility of major JP-4 jet fuel alkylbenzenes in water of different salinity and temperature, Bull. Environ. Contam. Toxicol., in preparation.

8. Struhsaker, J.W. (1977). Effects of benzene (a toxic component of petroleum) on spawning Pacific herring, clupea harengus pallasi, Fishery Bulletin 75, 43-49.

9. Varanas_ _., M. Uhler & S.I. Stranahan (1978). Uptake and release __ naphthalene and its metabolites in the skin and epidermal mucus of salmonids, Toxicol. & Appl. Pharmacol. 44, 277-89.

VI. Prehatching Development of the

fathead minnow (Pimephales promelas Raf.)

INTRODUCTION

A number of excellent studies on teleostean embryonic development have been published: the killifish (Fundulus heteroclitus) by Armstrong and Child (1965), the zebra fish (Brachyderio rerio) by Hisaoka and Firlit (1960), the whitefish (Coregonus clupeaformis) by Price (1934), the salmonids (Oncorhynchus keta) by Mahon and Hoar (1955), (Salmo gairdneri and Salvelinus fontinalis) by Ballard (1973), the white sucker (Catostomus commersoni) by Long and Ballard (1976), the diamond killifish (Adinia xenica) by Koenig and Livingston (1976), as well as many others.

The fathead minnow (Pimephales promelas Raf.) is a small, hardy cyprinid found in southern Canada, the United States and northern Mexico (Andrews and Flickinger, 1974). The extensive use of the fathead minnow as a forage fish, coupled with its ubiquitous distribution and ease of maintenance in the laboratory, have made it a highly useful indicator species for toxicity testing (Manner and Dewese, 1974). Yet in spite of its widespread use in laboratory studies, descriptions of its early development are incomplete. Results of this study indicate the pre-hatching development of the fathead minnow is typical for cyprinids. The timing of appearance of various embryonic structures differ somewhat among cyprinids, but the overall pattern is the same. Our study describes the posthatching development of the fathead minnow under controlled conditions. The development is divided into 32 stages.

METHODS

Fathead minnow were obtained from stock cultures at the U.S. Environmental Re h Laboratory Duluth, Minnesota. Breeding facilities in our ratory consisted of 28 ten-liter tanks, each containing a U-sha ile, one mature male and two mature females. All tanks were fitted th standpipes and individually supplied with air and water. Fargo city water (pH 8.3, hardness 80 mg/l $CaCO_3$) passed through activated carbon was used in all tanks. Water temperature was maintained at 24 C +0.5 C. The whole culture system was enclosed in a light-tight, insulated room with a photoperiod of 16 hours light (100 lux at the water surface) and 8 hours dark. Mature fish were fed frozen brine shrimp and Glenco No. 2 enriched trout food twice daily. Larval fish were fed live brine shrimp twice daily.

In order to observe events at fertilization mature ova were obtained by removal of fully developed ovaries from gravid females and added to sperm suspensions obtained from mature minced testis. Embryos attached to the underside of the U-shaped tiles were removed from the breeding tanks, placed in areated two liter tanks maintained at 25 C +0.2 C. (See Figure 1), and maintained under the same photoperiod (25 lux at the water surface) as the adults. At predetermined intervals 5-10 embryos were gently removed from the tiles for observation.

Embryos for light microscopy were dissected out of their chorion, photographed with a compound microscope, fixed in FAA (formalin-acetic acid-alochol) (Humason, 1979), embedded in paraffin, serially sectioned at six and ten microns, and stained with Harris hematolylin and eosin.
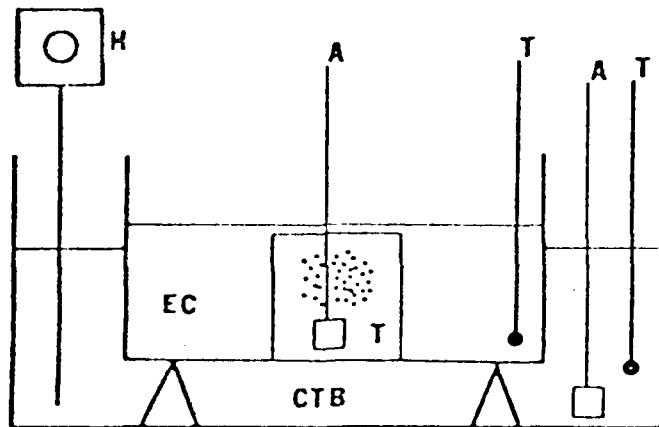
Figure 1. System used to hold embryos; air supply (A), constant temperature bath (CTB), embryo chamber (EC), heater (H), thermometer (T), and tile (Ti) with attached embryos.

Stained slides were photographed with a compound microscope. Measurements of average length were determined with an ocular micrometer calibrated in hundreths of a millimeter from a sample of fifteen embryos.

Embryos for scanning electron microscopy were fixed in 4% phosphate-buffered glutaraldehyde (pH 7.4) overnight, rinsed three times in buffer, then post-fixed in 2% OsO_4 for 3-5 hours. Fixations were carried out at 4 C. Following osmium fixation, embryos were again rinsed in buffer, dehydrated in ethanol at room temperature, and immediately critically point dried with liquid CO_2 in a Samdri PVT-3. Embryos were mounted on stubs and coated with gold in a Hummer II sputter coater. A JOEL JSM-35 scanning electron microscope was used to examine specimens.

RESULTS

Plate 1. Stage 1 Unfertilized ovum

Figure A. Unfertilized Ovum (80X).

The chorion (C) surrounds the yolk mass (YM). The micropyle (M) forms a channel through the C and a depression in the YM. The perivitilline space has not yet formed.

Figure B. Line Drawing (80X).

The opaque YM is represented by small dots.

The mature unfertilized ovum is spherical and surrounded by a closely appressed chorion. The distinctive micropyle is funnel-shaped with seven ridges and protrudes into the yolk mass which consists of yolk platlets mixed with cytoplasm. Cortical alveoli in the cortical cytoplasmic layer lie on the surface of the whitish, transluscent yolk mass.
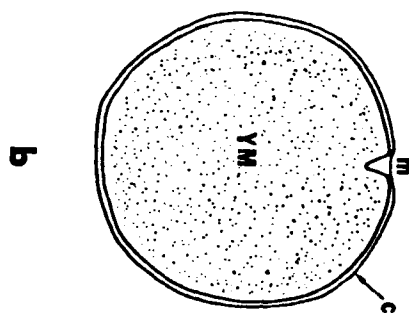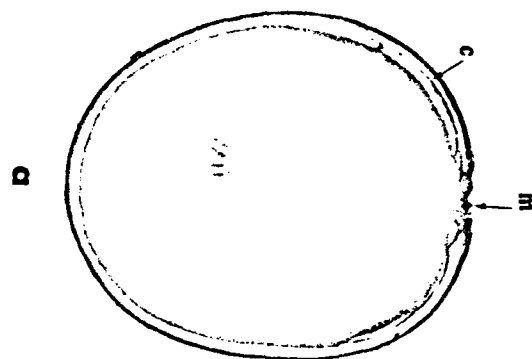
Plate 2.   Stage 2   Recently fertilized ovum

Figure A. Scanning Electron Micrograph (66X).

The cytoplasmic cap (CC) is visible above the yolk mass (YM).

Figure B. Live Embryo (80X).

The CC is visible as an elevated clear region of the peripheral cytoplasm. The YM has started to clear although aggregates of large yolk platlets are still present. Note this embryo has been dechorionated.

Figure C. Line Drawing (80X).

In addition to the CC and YM this figure shows the surrounding chorion (C) with its micropyle (M) and the perivitilline space (PvS) that has formed.

Following fertilization the cortical alveoli break down starting in the region just under the micropyle. This results in the separation of the chorion from the cytoplasmic layer with the subsequent formation of the perivitelline space. Large yolk platelets flow together and the yolk mass becomes clear and remains clear throughout subsequent development. In living embryos cytoplasm is visible streaming through and around the yolk mass to the animal pole where a low, broad cytoplasmic cap is forming, establishing the polarity of the embryo. The chorion is still soft and fragile, making it difficult to collect embryos without damaging them. The thin plasma membrane which completely surrounds the embryo is covered with microvilli. In later stages these microvilli will only be found on the blastomeres, but not on the thin plasma membrane surrounding the yolk mass.
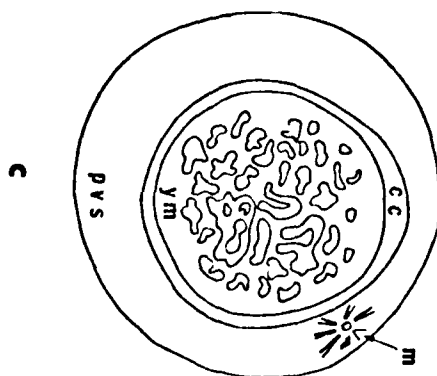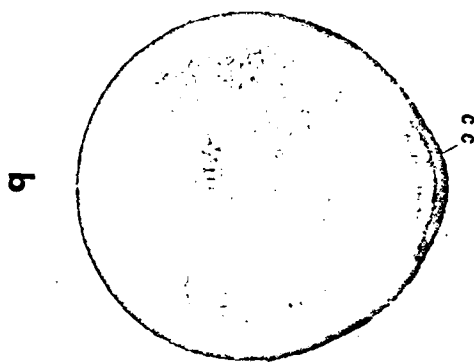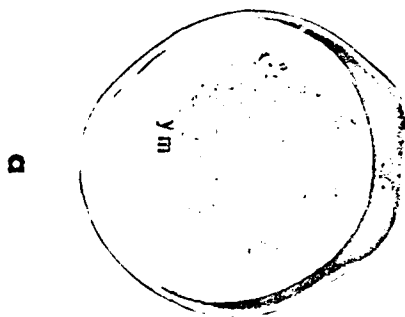
Plate 3. Stage 3   One celled blastodisc

Figure A. Scanning Electron Micrograph (66X).

The cytoplasmic cap (CC) is visible as an elevated cap on the mass (YM). The smooth transition of the CC into the YM is not seen in living embryos and is thought to be a fixation artifact.

Figure B. Live Embryo (80X).

The CC appears as a clear elevated mass of cytoplasm on the YM.

Figure C. Serial Section (90X).

Small yolk platlets (YP) are visible in the cytoplasm (Cy) of the CC.

Figure D. Line Drawing (80X).

This figure shows the chorion (C), CC, YM, and cytoplasmic streaming (CS). Note the arrows indicating the direction of the cytoplasmic flow. The solid line shown in this and subsequent drawings forming the ventral border of the early blastomeres represents a transition zone rather than an abrupt line.

The one celled blastodisc consists of a large cytoplasmic cap which bulges above the yolk mass. Small yolk particles are carried along into the granular cytoplasm of the blastodisc by cytoplasmic streaming. The blastodisc is in close contact with the yolk and is continuous with a thin cytoplasmic layer covering the yolk.
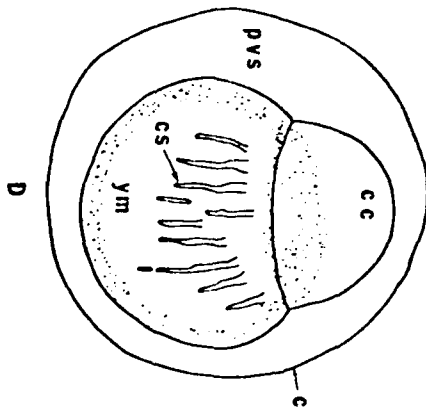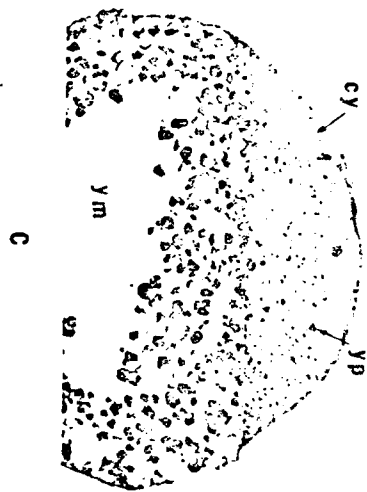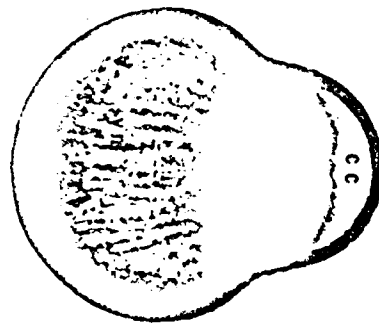
Plate 4.   Stage 4   Two celled blastodisc

Figure A.   Scanning Electron Micrograph (65X).

   The cleavage furrow (ClF) and two blastomeres (B) are visible on
   the yolk mass (YM).

Figure B.   Live Embryo. (80X)

   This figure shows the continued streaming of the cytoplasm (CS)
   toward the blastomeres, and the ClF.

Figure C.   Line Drawing. (80X)

   The chorion (C), ClF, B, YM, are all illustrated.

Figure D.   Serial Section. (200X)

   This light micrograph shows a metaphase mitotic figure (MF) found
   in a blastomere prior to the the four cell stage.

Figure E.   Scanning Electron Micrograph (480X).

   This figure shows the cleavage furrow (ClF) separating the two
   blastomeres (B).

The first cleavage plane appears initially as a slight depression in

the blastodisc and then deepens into a vertical furrow. Cleavage takes

about seven minutes from start to finish. The division is meroblastic

and meridional resulting in two equal sized blastomeres which are

elevated above the yolk mass. A mitotic figure is visible in serial

sections in each blastomere prior to stage 5. Cytoplasmic streaming

toward the blastomeres continues.

- 72 -

a

ym

clf

b

clf

cs

b

c

ym

clf

b

c

d

b

e

clf
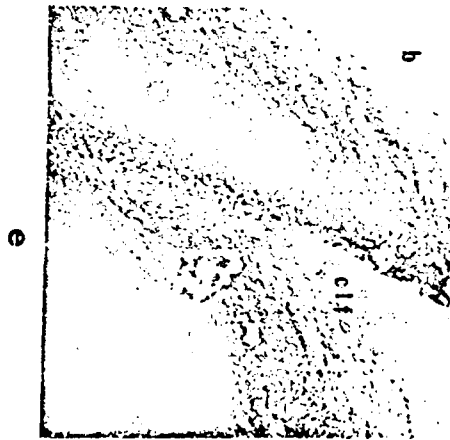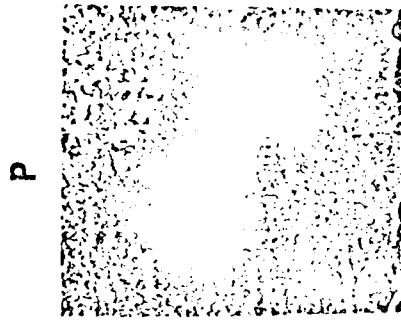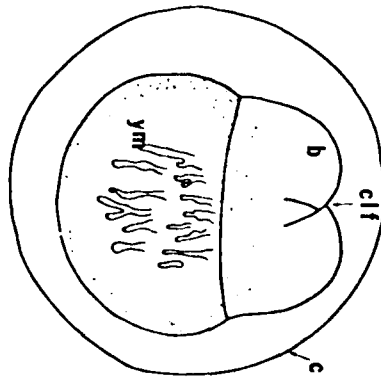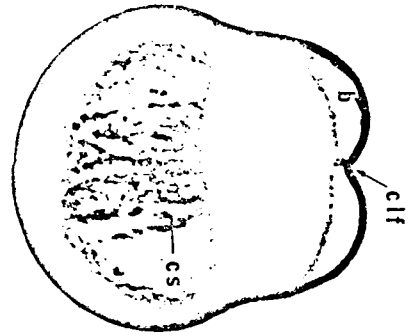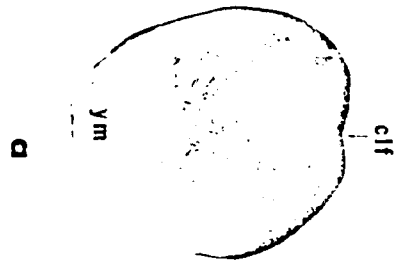
Plate 5. Stage 5   Four celled blastodisc

Figure A. Scanning Electron Micrograph (66X).

This figure shows the four globular blastomeres (B) and the cleavage furrow (ClF) separating them.

Figure B. Live Embryo (80X).

The four blastomeres (B) are visible on the yolk mass (YM).

Figure C. Serial Section (90X).

This section shows the cleavage planes (CP) that separate the four blastomeres.

Figure D. Line Drawing (80X).

The plane of section (C) for figure C is represented by the dashed line.

A second meridional cleavage cuts across the plane of the first at right angles and creates four equal-sized, globular blastomeres. This cleavage also takes about seven minutes. Some cytoplasmic streaming is still visible. The embryo rotates freely within the chorion.
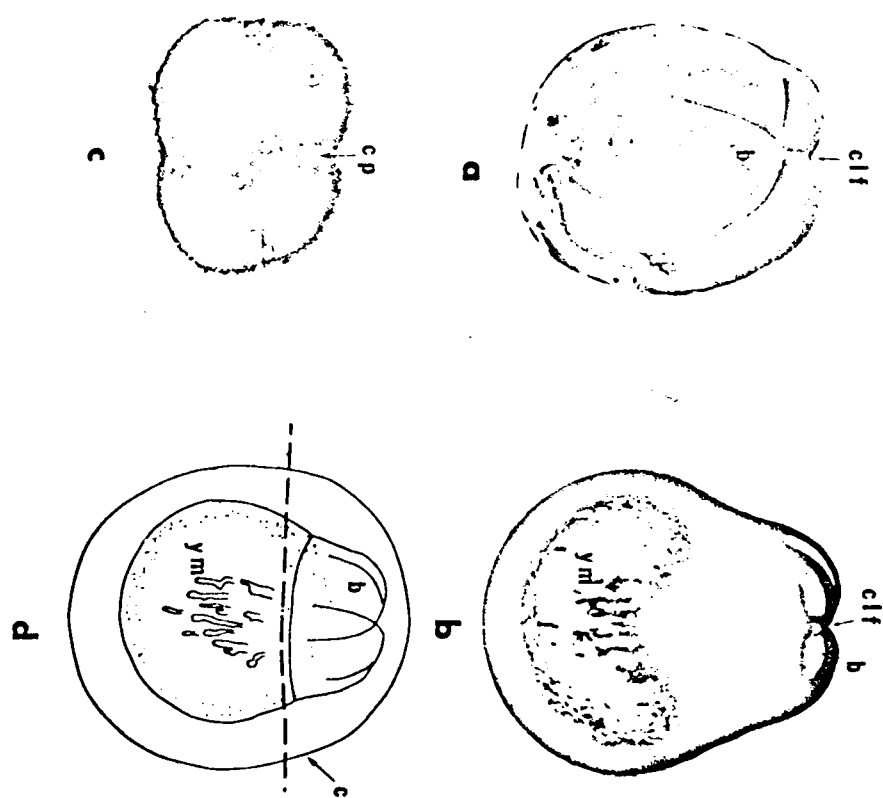
Plate 6. Stage 6   Eight celled blastodisc

Figure A.   Scanning Electron Micrograph (65X).

   This dorsal view shows the two parallel rows of four blastomeres
   (B) and the ClF separating them.

Figure B. Live Embryo (80X).

   In this view four of the eight B are visible on the yolk mass
   (YM).

Figure C. Serial Section (80X).

   This section shows four B on the YM. Two of the B contain mitotic
   figures (MF).

Figure D. Line Drawing (80X).

   The large perivitilline space (PvS) is still present, as is a
   limited amount of cytoplasmic streaming (CS).

Four synchronous meridional cleavages occur parallel to the first
cleavage plane, resulting in eight equal-sized blastomeres arranged in
two rows of four cells each. Minor irregularities in this arrangement
are not uncommon.

Small yolk granules are visible in the blastodisc cytoplasm adjoining
the yolk mass and extending upward along the cleavage planes. Yolk
platelets appear smaller immediately underlying the blastodisc.
Cleavage planes cut completely through the blastodisc to the surface of
the yolk. Spindle fibers and mitotic figures are clearly visible.
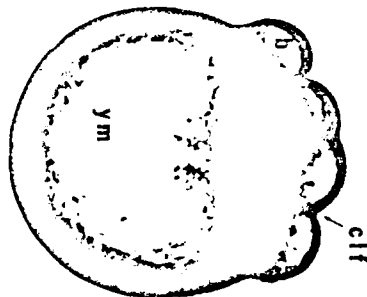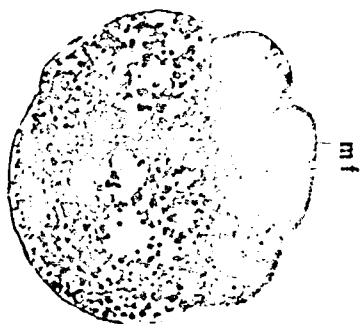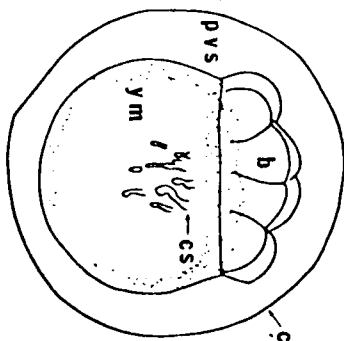
Plate 7. Stage 7   Sixteen celled blastodisc

Figure A. Scanning Electron Micrograph (66X).

This figure shows the sixteen blastomeres (B) on the yolk mass (YM). Note the B are in four rows, each consisting of four blastomeres.

Figure B. Live Embryo (80X).

figure C. Line Drawing. (80X).

Cleavage planes are parallel to the second and at right angles to the first and third. Cleavage is synchronous and generally results in four parallel rows of four blastomeres of approximately equal size. Cleavage furrows at this stage do not cut completely through the cytoplasm, but leave a continuous layer of cytoplasm adjoining the yolk. This layer is the presumptive periblast. A limited amount of cytoplasmic streaming still occurs.

A
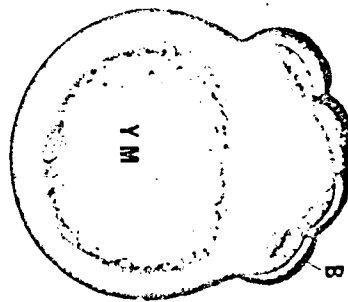
B
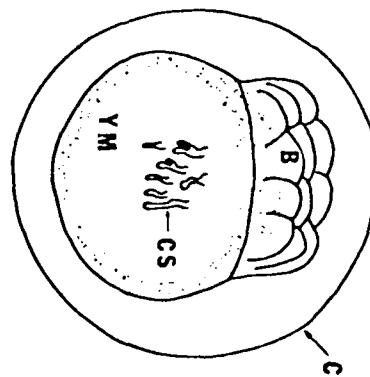
C

Plate 8.   Stage 8   Thirty two celled blastodisc

Figure A.   Scanning Electron Micrograph (66X).

Approximately 32 blastomeres (B) form a mound on the yolk mass (YM).

Figure B.   Live Embryo (80X).

Figure C.   Line Drawing. (80X).

The last remnant of cytoplasmic streaming (CS) is visible on the yolk mass (YM).

Cleavages are irregular and difficult to follow. The cleavage planes are no longer strictly perpendicular to yolk mass. Blastomeres are two cells deep in the center of the blastodisc. No intercellular spaces are present between blastomeres. The periblast layer has migrated from under the blastodisc to form a limited periblast corona. The chorion has hardened and averages 1.4 mm in diameter.

a

ym

b

ym

b

c

ym

cs

b

c
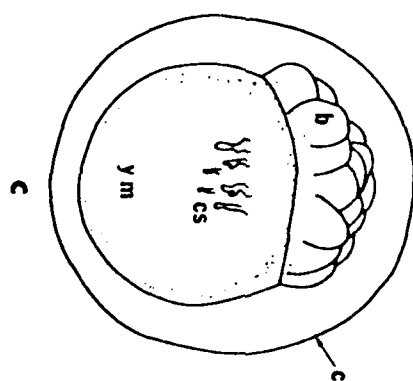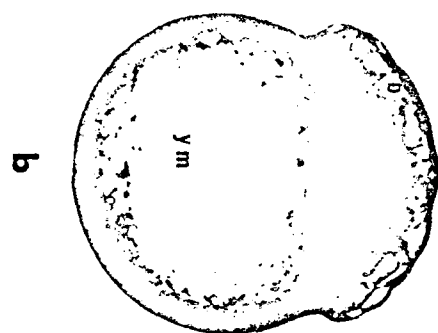
Plate 9. Stage 9   Late cleavage

Figure A. Scanning Electron Micrograph (66X).

This figure shows the early epidermal stratum (ES), the surface layer of blastomeres.

Figure B. Live Embryo (80X).

The outermost layer of blastomeres which form the ES is visible. Note the lack of cytoplasmic streaming.

Figure C. Serial Section (80X).

This figure shows the individual blastomeres and small yolk particles (YP) within their cytoplasm.

Figure D. Line Drawing (80X).

This illustration shows the limited periblast corona (PC) extending from the B. Plane of section for figure C is indicated by dashed line.

The individual blastomeres form an elevated cap upon the yolk mass. Asynchronous cleavages result in an increase in blastomere number along with a decreased blastomere size.

Spaces between the blastomeres are present. These spaces later become continuous and form the ventral segmentation cavity or blastocoele. The closely packed outermost layer of blastomeres form the early epidermal stratum which surrounds the loosely spaced inner cells. The periblast corona has enlarged. Yolk particles are visible in the cytoplasm of the deep lying blastomeres.
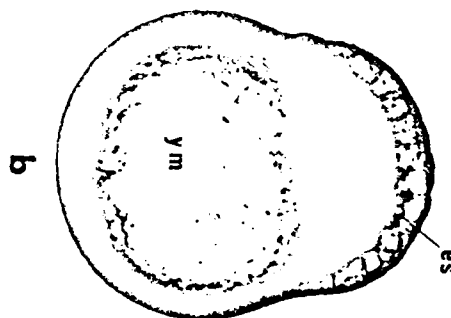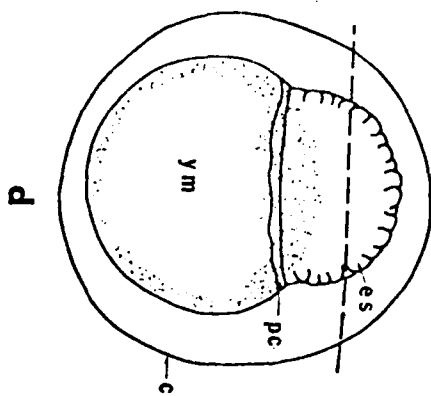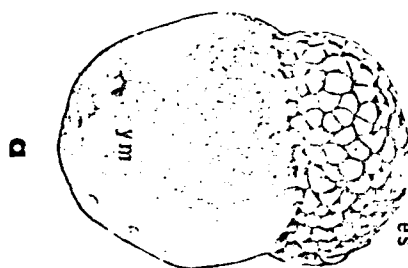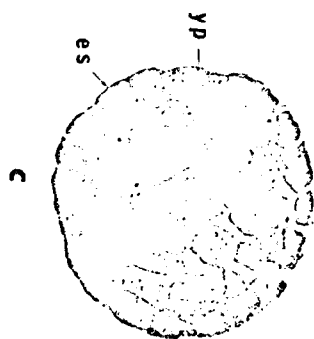
Plate 10. Stage 10   High blastula

Figure A. Serial Section (80X).

This section shows the epidermal stratum (ES), consisting of blastomeres which are flatter and more squamous in appearance than the deeper lying blastomeres (B). The segmentation cavity (Sg) and the region of thickened periblast (TP) are also easily seen.

Figure B. Live Embryo (80X).

The outermost ES is visible.

Figure C. Line Drawing (80X).

The periblast corona (PC) has enlarged while the blastomeres have decreased in size. The perivitilline space (PvS) separates the embryo from the chorion (C)

Figure D. Scanning Electron Micrograph (120X).

This figure shows the ES covering the mass of blastmeres which rest on the underlying yolk mass (YM).

Figure D. Scanning Electron Micrograph (7400X).

The blastomeres (B) which form the ES are covered with numerous microvilli (Mv). A cleavage furrow (ClF) between two B is present.

Further cleavages in the high blastula result in an elevated cap of blastomeres. The epidermal stratum is distinct and surrounds loosely packed globular interior cells. Blastomere nuclei are large and distinct. The blastoderm rests on the periblast. The periblast corona has expanded and covers approximately one fifth of the yolk mass. Periblast nuclei appear to arise at the edge of the blastoderm from divisions of the marginal cells, although mitosis in isolated periblast nuclei is also visible. Yolk platelets are excluded from the blastoderm by the periblast layer. Spaces between blastomeres have increased to form the low, broad segmentation cavity which is bordered dorsally by globular cells of blastoderm and ventrally by the periblast layer. One portion of the periblast corona has become thickened and lies immediately adjacent a thickened region of the blastoderm. This is where the embryonic shield will form. Microvilli are present on the plasma membrane of the blastomeres.
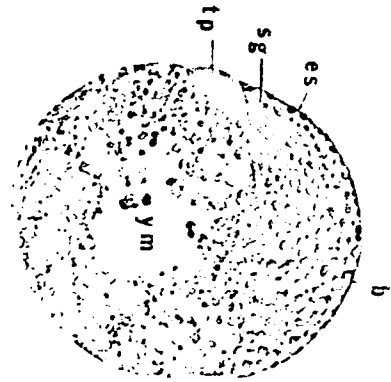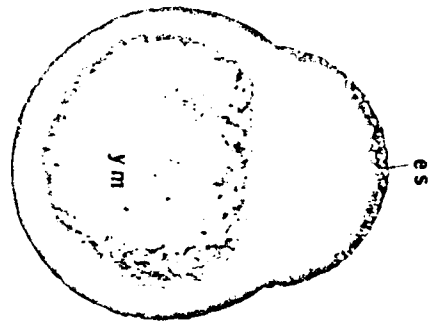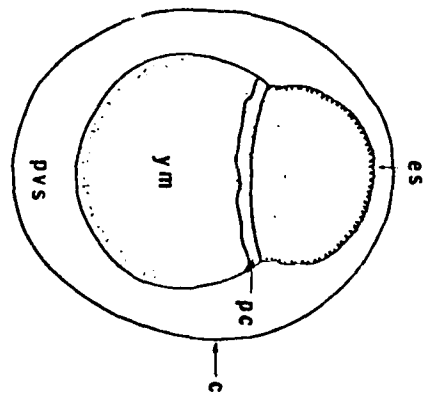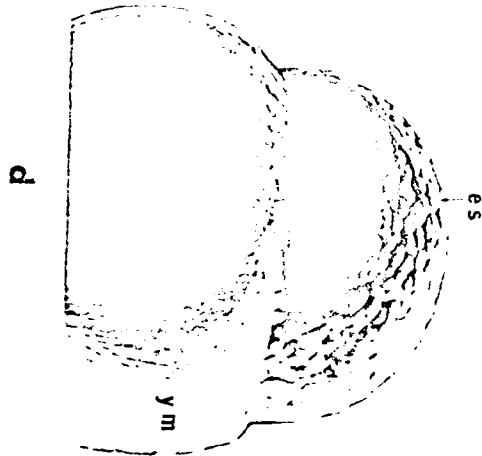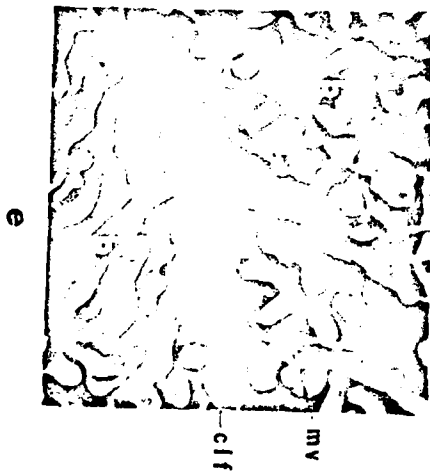
Plate 11. Stage 11 Flat blastula

Figure A. Live Embryo (80X).

Figure B. Line Drawing (80X).

   This drawing illustrates the further increase in size of the periblast corona (PC) and decrease in size of the blastomeres of the epidermal stratum (ES).

Figure C. Serial Section (200X).

   In this section mitotic figures are visible in the region of thickened periblast (TP). Also note the ES and the distinct nucleus (Nu) of a blastomere.

Figure D. Serial section (80X).

   This section shows the location of the blastocoele (Bc) and the thin layer of under-lying periblast (P).

The blastoderm forms a flattened, lens-shaped structure called the flat blastula that caps the yolk mass. There is a further reduction in size and an increase in number of individual blastomeres. Extensive mitotic activity is visible within the blastomeres and in the periblast layer. Cells of the epidermal stratum continue to flatten. It is often difficult to distinguish the flat blastula from the early gastrula stages in living embryos. The broad segmentation cavity or blastocoele is still present.
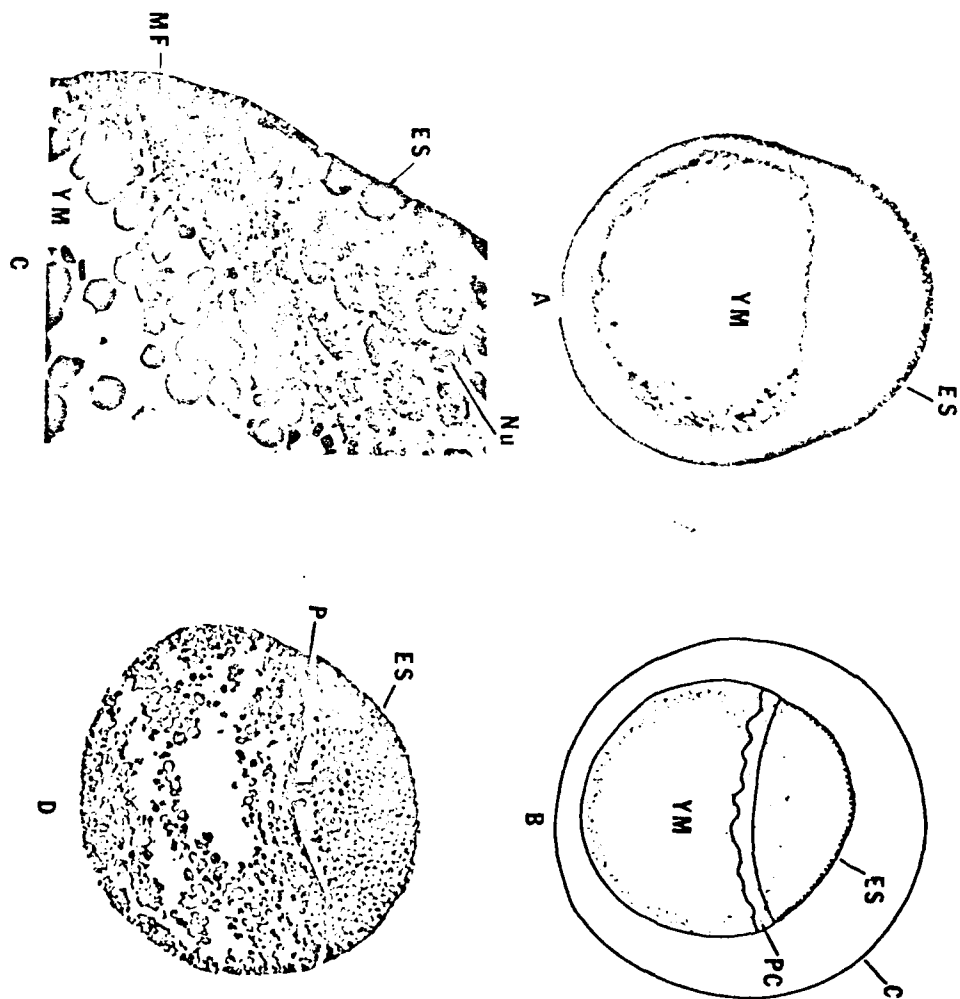
Plate 12.   Stage 12   Early gastrula

Figure A.   Serial Section (80X).

The germ ring (GR) forms the advancing edge of the blastoderm, and is bounded by the epidermal stratum (ES). Much yolk has been lost during sectioning.

Figure B.   Live Embryo (80X).

The flattened mass of cells of the blastoderm (Bl) have started migrating over the yolk mass (YM).

Figure C.   Line Drawing (80X).

The periblast corona (PC) continues to enlarge and migrate down over the yolk mass (YM).

At the onset of gastrulation the edge of the blastoderm becomes elevated to form the early germ ring, which causes a slight depression in the yolk mass. The embryonic shield anlage is visible as an enlargement of one portion of the germ ring that is preceeded by the region of thickened periblast. Much mitotic activity is visible in this thickened periblast layer. The number of cells within the central blastoderm has decreased while the segmentation cavity has enlarged.

A

B

C
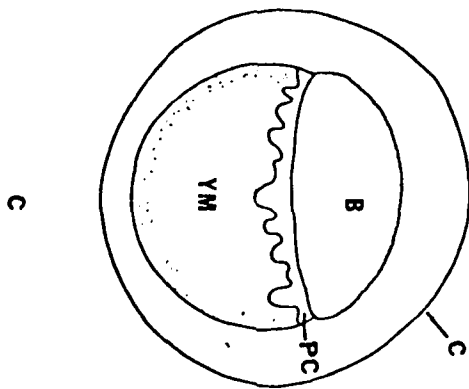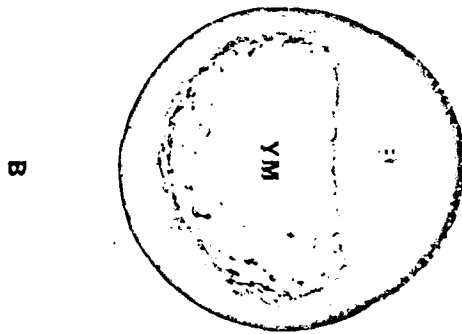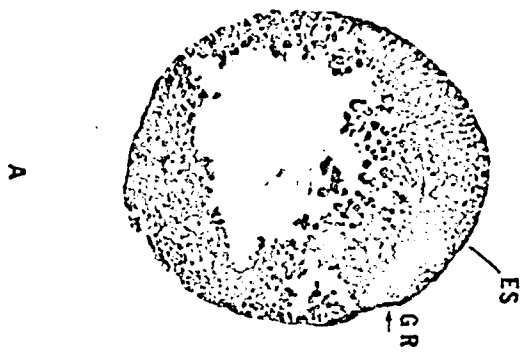
Plate 13. Stage 13 One quarter epiboly

Figure A. Serial Section (80X).

    The large segmentation cavity (Sg) is bordered ventrally by the periblast layer (P) and dorsally by the blastomeres (B). Considerable amounts of yolk have been lost during the preparation of this section.

Figure B. Live Embryo (80X).

    The germ ring (GR) is present as the edge of the migrating blastoderm.

Figure C. Line Drawing (80X).

    This drawing shows the thickened GR, the chorion (C), periblast corona (PC), and yolk mass (YM).

The germ ring has migrated one quarter of the way over the yolk mass and has thickened to become elevated above the blastodisc. Much?mitotic activity is evident in the blastomeres. An extensive segmentation cavity is still present. The periblast corona is visible in living embryos.
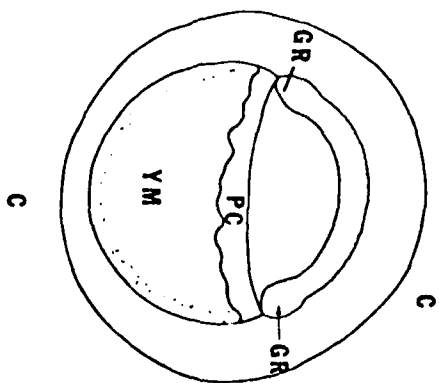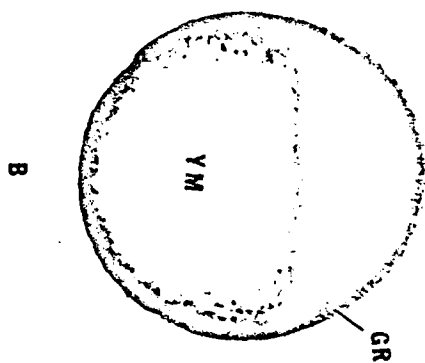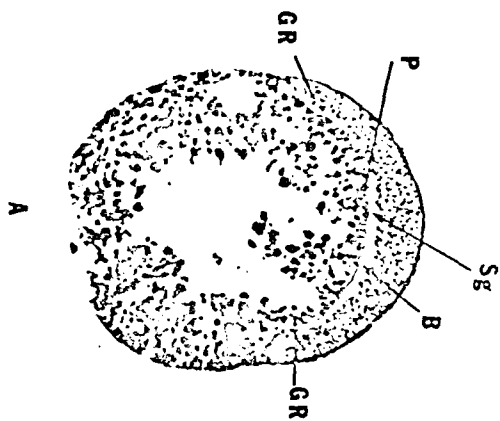
Plate 14. Stage 14   One half epiboly

Figure A. Scanning Electron Micrograph (66X).

This figure shows the thickened germ ring (GR), and the blastomeres (B) that make up the epidermal stratum (ES).

Figure B. Live Embryo (80X).

The germ ring (GR) continues to migrate over the yolk mass (YM). Note the elevated region of the GR that forms the embryonic shield (EmS).

Figure C. Line Drawing (80X).

This drawing illustrates the elevated edge of the advancing blastoderm. The embryonic shield (EmS) is a slightly thickened region of the GR.

Figure D. Serial Section (80X)

This section shows the thickened GR.

Figure E. Scanning Electron Micrograph (3000X).

The surface of the individual blastomeres have an irregular contour. The number of microvilli, compared to earlier stages, is reduced. Cleavage furrows separate the four blastomeres seen in this view.

Figure F. Serial Section (200X).

This section shows the thickened periblast (TP) containing the large primordial germ cells (PGC) in front of the EmS. Also note the ES layer.

Epiboly continues with the germ ring covering one half of the yolk mass. The central area of the blastoderm is thinning and will later form the extra embryonic membrane of the yolk sac epithelium. Mitotic figures are no longer visible in the periblast layer but are evident in the blastomeres. Large oval cells lacking a distinct nucleus are visible in the thickened periblast layer preceeding the embryonic shield. This is the first appearence of the primordial germ cells (Johnson, 1951). The embryonic shield appears as a thickened region of the germ ring slightly closer to the animal pole than is the surrounding germ ring.
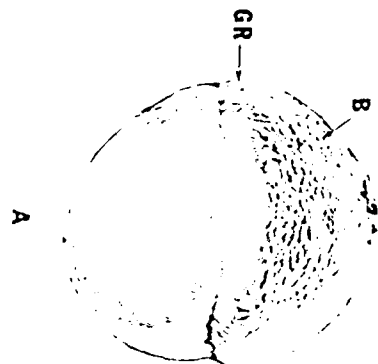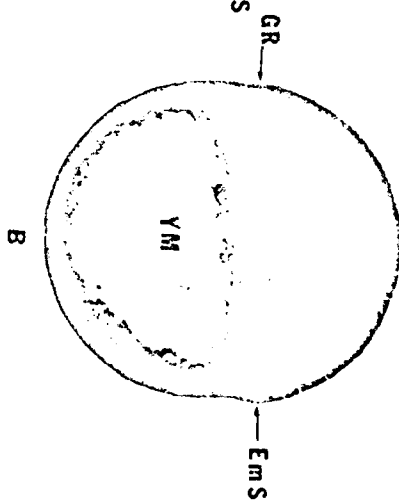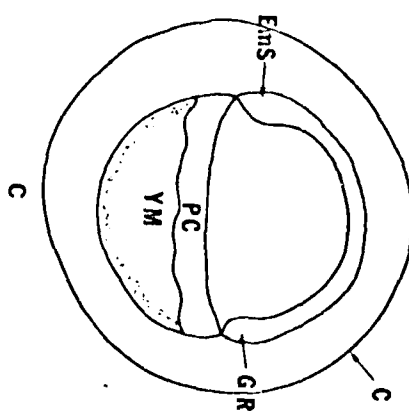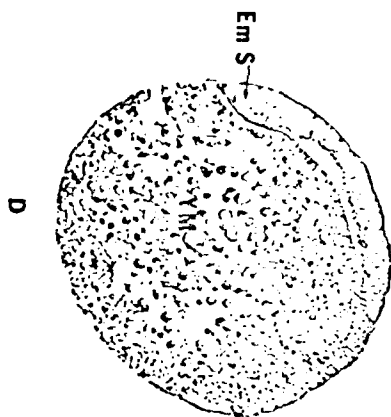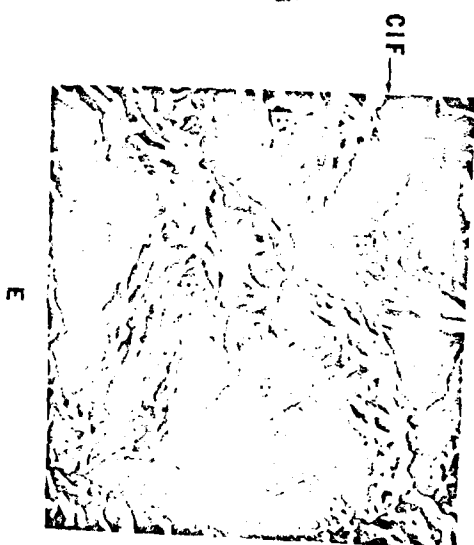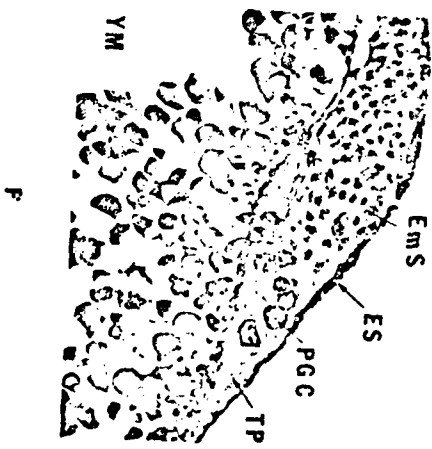
Plate 15. Stage 15   Three quarters epiboly

Figure A. Serial Section (80X).

   This sagittal section shows where the anterior (A) and caudal (Ca) regions of the embryo will form.

Figure B. Live Embryo (80X).

   This figure shows the thickened ridge of cells that make up the embryonic shield (EmS). The yolk plug (YlP) has not been covered by the advancing germ ring (GR).

Figure C. Line Drawing (80X).

   This illustration shows the future caudal end of the embryo. The plane of section of figure E is indicated by a dashed line. The periblast corona (PC) almost completely covers the YlP.

Figure D. Serial Section (400X).

   This section shows an unlined vesicle (V) and the underlying primordial germ cells (PGC) in the thickened periblast (TP).

Figure E. Serial Section (100X).

   This section shows the area of the presumptive caudal knob (CK), as well as the lateral somite anlagen (SA). The unlined vesicle (V) and surrounding TP and PGC are also visible.

Epiboly continues with the germ ring covering three quarters of the yolk mass. An unlined vesicle in the periblast under the advancing edge of the embryonic shield is visible in serial sections and creates a depression in the yolk mass. A streak of cells is being laid down as the embryonic shield moves down over the yolk mass. Elsewhere there is continued thinning of the cells of the blastoderm. Prior to stage 16, this streak of cells thickens and forms the neural keel anlage. The neural keel in teleosts forms as a solid mass of neurectoderm, with the neurocoele forming later. The yolk plug protrudes slightly from the edge of the germ ring. Mesodermal cells of the somite anlagen have aligned themselves lateral to the neural keel. Mesodermal cells forming the notochord anlage are located ventral to the neural keel. The primordial germ cells have poliferated in the periblast layer under the presumptive caudal knob.

- 94 -

END
DATE
FILMED
7 83
DTIC
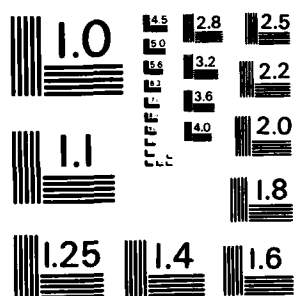
MICROCOPY RESOLUTION TEST CHART
NATIONAL BUREAU OF STANDARDS-1963-A
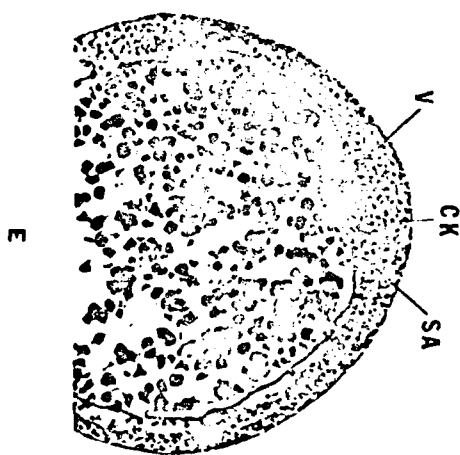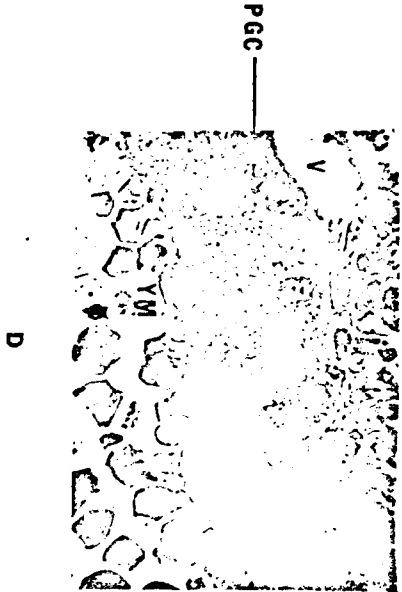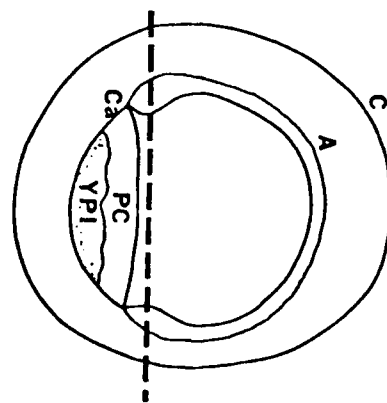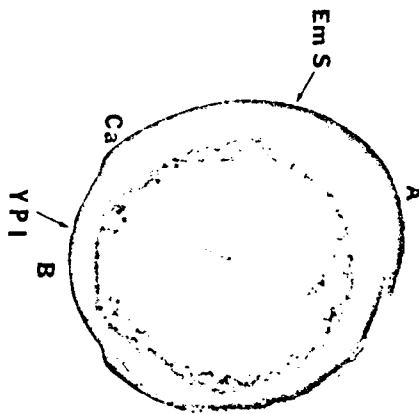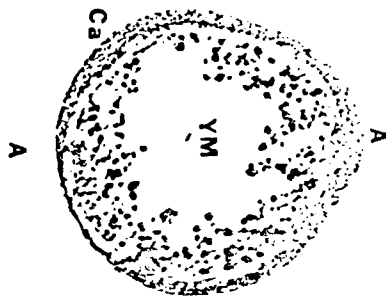
Plate 16. Stage 16   Closure of germ ring

Figure A. Living Embryo (80X).

This figure shows the elevated caudal knob (CK) and the head region (HR) at the anterior end of the embryo. Note the large fluid filled presumptive pericardial coelom (PC).

Figure B. Line Drawing (80X).

The plane of section for figure D is indicated by a dashed line. Note the site of closure of the germ ring (GR).

Figure C. Serial Section (80X).

This section shows the elevated undifferentiated mass of neuroectoderm in the head region (HR).

Figure D. Serial Section (100X).

This transverse section shows the undifferentiated mesodermal cells of the lateral somite anlagen (SA) that flank the notochord (N).

This stage marks the end of epiboly with the closure of the germ ring over the yolk plug. An elevated caudal cluster of cells is present at the posterior end of the embryonic axis where the germ ring closed. A depression in the yolk mass is visible immediatedy below this caudal knob. The primoridal germ cells continue to proliferate in the caudal periblast under the caudal knob. A second cluster of cells is visible at the anterior end of the embryo, forming the head region. The optic anlagen are visible as two lateral enlargements of the anterior cell cluster. Anterior and caudal cell clusters are connected by a low, broad ridge of cells, the presumptive neural keel. A group of undifferentiated mesodermal cells that form the presumptive notochord are present ventral to the neural keel. There is a migration of lateral mesoderm cells toward the embryonic axis. These cells constitute the somite anlagen. The ectoderm layer lifts free of the yolk mass anterior to the head region to form the precursor to the pericardial coelom.

- 96 -
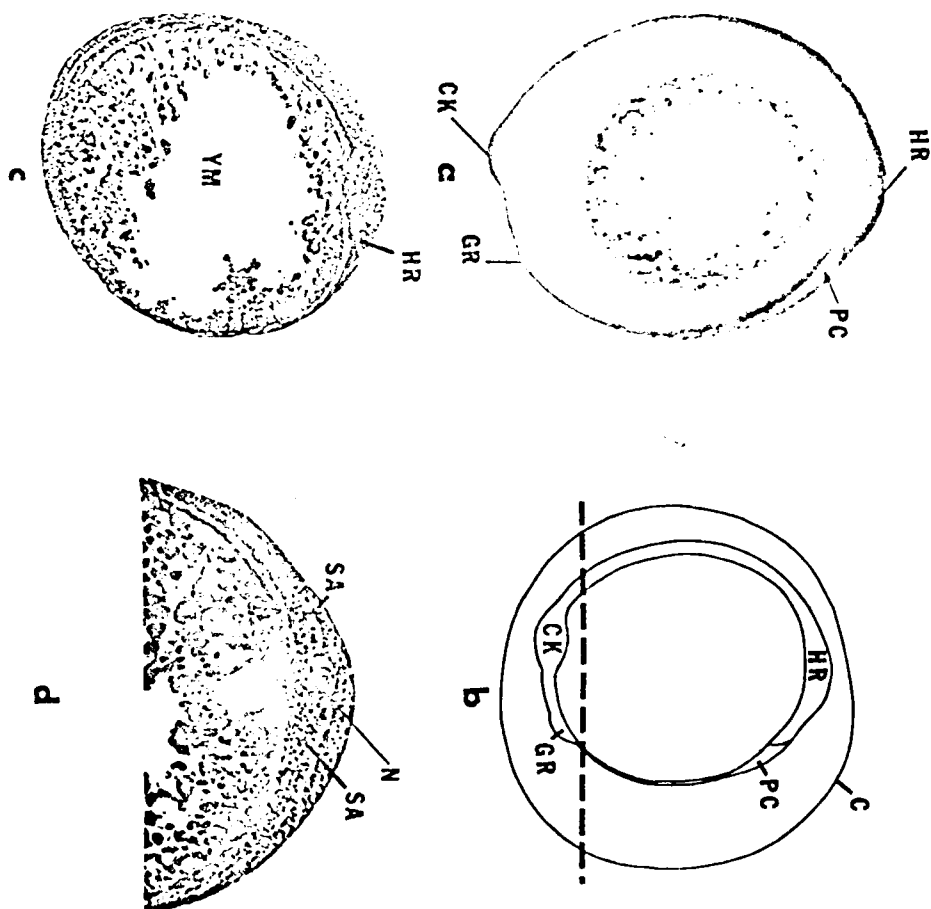
Plate 17. Stage 17 Neurula

Figure A. Serial Section (80X).

This sagittal section shows an optic anlage (OA) and the somites (S).

Figure B. Live Embryo (80X).

This figure shows the three regions of the brain: the prosencephalon (Pr), mesencephalon (Me) and rhomencephalon (R). Also note the anterior-most presumptive pericardial coelon (PC).

Figure C. Line Drawing (80X).

This diagram shows the three brain regions, Pr, Me, R, the caudal knob (CK), Kupffers vesicle (KV) and four somites (S). Plane of section for figure D is indicated by a dashed line.

Figure D. Serial Section (80X).

This transverse section shows the optic anlage (OA) as lateral evaginations of Pr. The presumptive infundubulum (I) is present as a ventral evagination of the Pr. Also note the paired block-like caudal somite anlage (SA).

Figure E. Serial Section (400X).

Kupffers vesicle (KV) bounded by columnar epithelial cells is visible above the thick region of caudal periblast (CP). Note the large primordial germ cells (PGC) in the CP.

The prosencephalon, mesencephalon, and rhombencephalon regions of the brain can be distinguished. The neural keel consists of a solid wide band of cells that extend caudally from the rhombencephalon. The notochord is visible as a solid rod of mesodermal cells ventral to the neural keel and extends from the rhombencephalon to the undifferentiated caudal knob. The notochord is flanked laterally by mesodermal cells which have differentiated into 4-5 pairs of somites. Kupffers vesicle is present as an oval shaped vesicle ventral to the caudal knob and is lined with columnar epithial cells. Optic anlagen are visible as lateral swellings of the prosencephalon. The presumptive infundibulum is visible as a ventral evagination of the presumptive diencephalon. Thin sheets of slightly darker staining neural crest cells are visible both dorsally and ventrally on the lateral aspects of the optic anlagen.
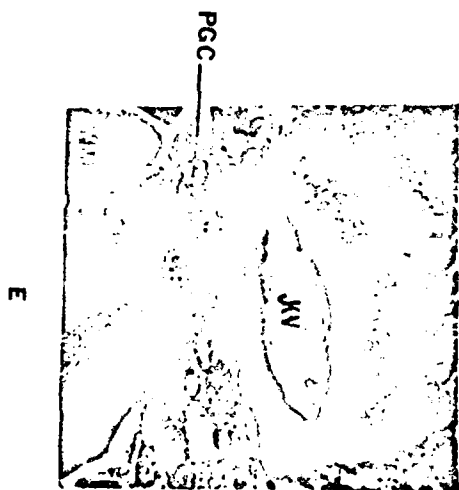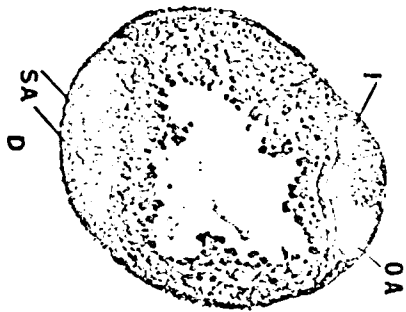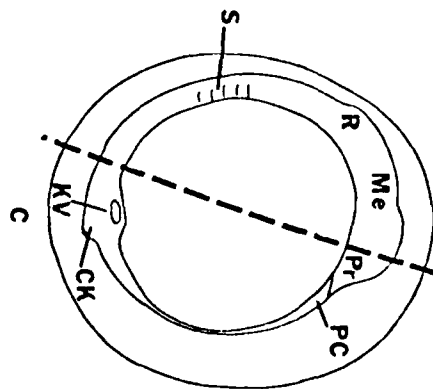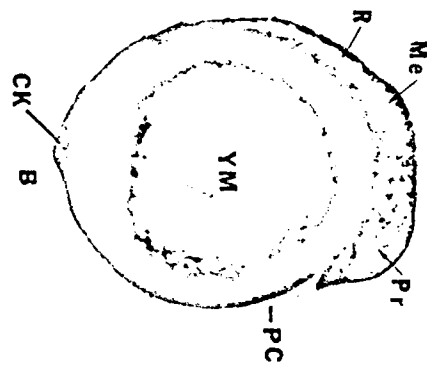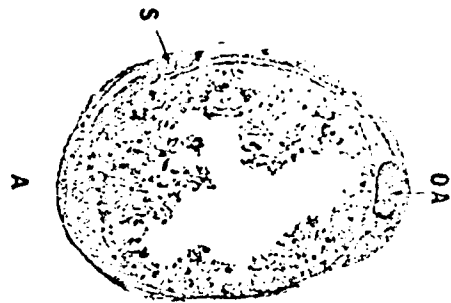
Plate 18. Stage 18 Optic vesicles

Figure A. Serial Section (200X).

This transverse section shows the optic vesicles (OV) situated lateral to the diencephalon (D). Note the lack of neurocoele in the D. Neural crest cells (NCC) are visible dorsal and lateral to the D. Plane of section is the dashed line "a" in figure C.

Figure B. Live Embryo (80X).

This figure illustrates the OV, pericardial coelom (PC), caudal knob (CK), notochord (N), and ten somites (S).

Figure C. Line Drawing (80X).

This drawing illustrates the OV, CK, N and ten somites (S).

Figure D. Serial Section (200X).

The triangular neural keel (NK) is visible above the N. A small coelomic cavity (CeC) is visible in the segmental mesoderm (SM). Plane of section is indicated by dashed line (d) in figure C.

Figure E. Serial Section (400X).

This figure shows Kupffers vesicle (KV) and an unlined vesicle in the caudal periblast (CP) layer.

The site of invagination of the optic vesicles in live embryos appears as a horizontal slit on their lateral aspects. The prosencephalon and optic vesicles are arrowhead-shaped when viewed from above. A depression is forming on the dorsal aspect of the brain between the mesencephalon and the rhombencephalon. Rudiments of the first and second ventricles of the forebrain are visible as small lateral slits in the anterior end of the prosencephalon. The third ventricular rudiment is a narrow dorsal-ventral slit which is continuous with narrow cavities in the optic vesicles. Cells of the solid neural keel have become aligned parallel to the yolk mass and have segregated
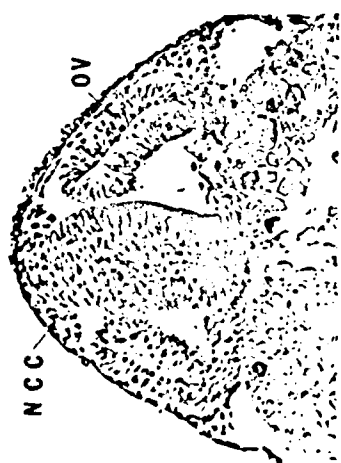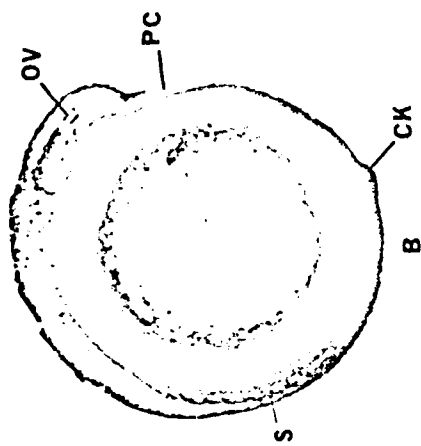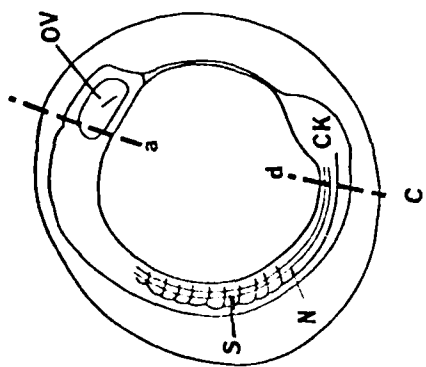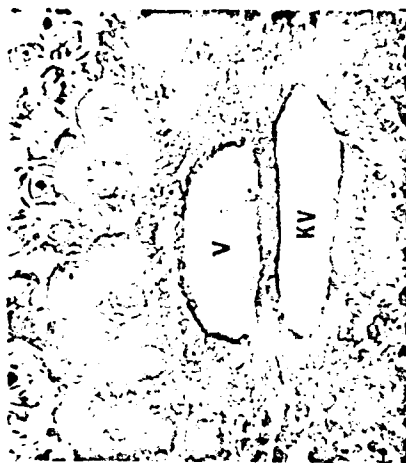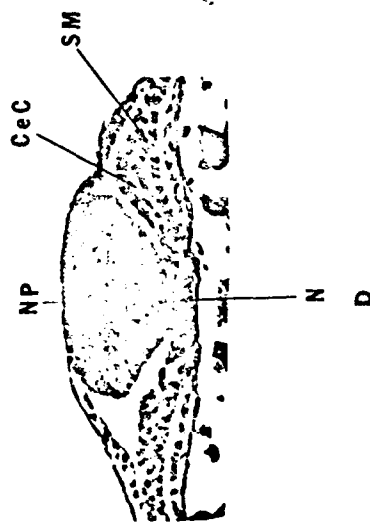
into two lateral masses, although no neurocoele is present. The neural keel is oval in cross section anteriorly and becomes triangular-shaped caudally. A large infundibulum extends ventrally from the diencephalon. Cells of the notochord are elongating and becoming vacuolated. Caudally, the notochordal cells become increasingly disorganized until they grade into undifferentiated mesoderm of the caudal knob. Several unlined vesicles are present in the thick periblast layer ventral to Kupffers vesicle. The number of primordial germ cells in the caudal periblast continues to increase. The pericardium is present as a fluid-filled sac anterior to and ventral to the first one-third of the optic vesicles. Nine to ten pairs of somites are present. Somites are six to seven cells thick adjacent to the notochord but taper off into lateral plate mesoderm laterally and flattened segmental mesoderm caudally. A small coelomic cavity is present in the segmental mesoderm. The epidermal ectoderm layer covers the embryo. There is no indication of circulatory or digestive system rudiments. Neural crest cells are visible as diffuse masses of cells dorsal-lateral and ventral-lateral to the diencephalon and mesencephalon. They are also visible as diffuse masses of cells lateral to the nerve cord in mid- and caudal-regions.

Plate 19. Stage 19   Neuromeres

Figure A. Serial Section (80X).

The otic placodes (OtP) are visible in this sagittal section as thickenings in the ectodermal ectoderm (EE). Note Kupffers vesicle (KV) and the optic cup (OC) are still prominent structures.

Figure B. Live Embryo (80X).

A large optic cup (OC) is visible in the prosencephalon. The OtP is visible as a slightly clear region in the rhombencephalon.

Figure C. Line Drawing (80X).

Neuromeres (Nm) are visible as a series of small evaginations in the dorsal rhombencephalon. Fourteen somites (S) are visible as the distinctive OC and PE. Planes of section for figures D and E are indicated by dashed lines d and e respectively.

Figure D. Serial Section (80X).

This transverse section shows the solid nerve cord (NC) posterior to the rhombencephalon. The notochord (N) and KV are also visible in the caudal region.

Figure E. Serial Section (200X).

The posterior edge of the optic cup (OC) is visible, as is its connection with the diecephalon (D). Neural crest cells (NCC) are visible as dorsal and ventral masses of cells lateral to the D.

Neuromeres are visible as a series of small evaginations in the dorsal mylencephalon. A neurocoel is present only in the form of the reduced brain ventricles. The cavity within the optic cups is increasing in size. The ventrally located pericardium is enlarged and is moving both anteriorly and posteriorly. The otic placodes are visible as a pair of lateral thickenings in the epidermal ectoderm in the rhombencephalic region. The 14 pairs of somites are bounded by a layer of columnar cells and have condensed to form more block-shaped segments. Notochordal cells are becoming increasingly vacuolated and
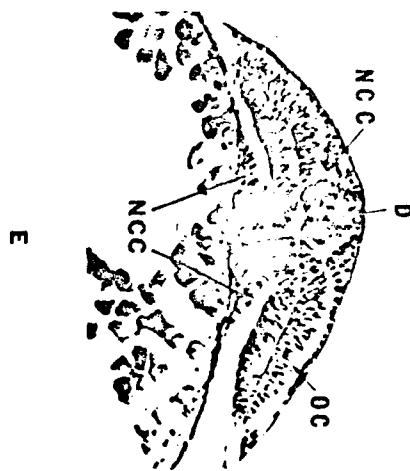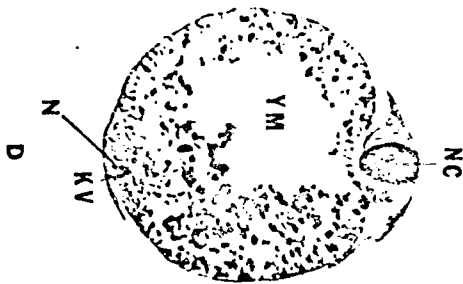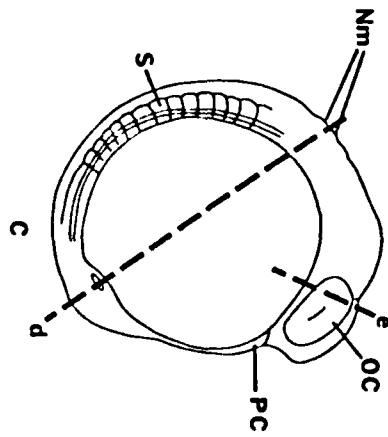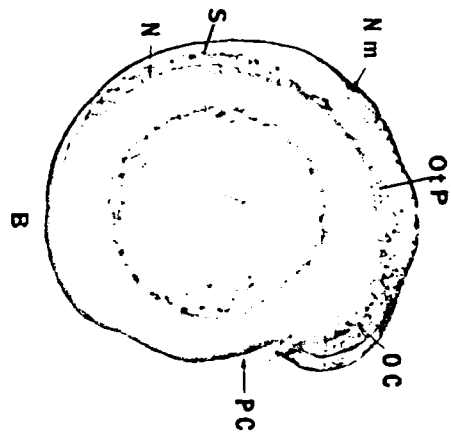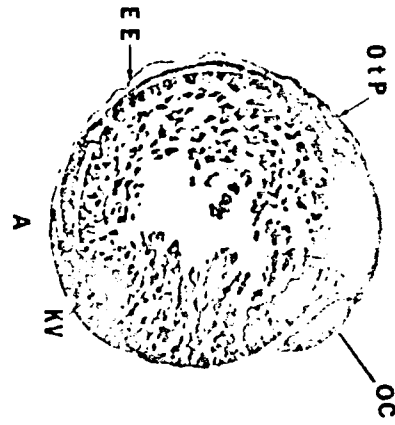
the notochord has increased in length anteriorly. A thick periblast with germ cells and Kupffers vesicle are present below the somewhat flattened caudal knob. The embryo is bounded by a squamous epithelial layer of ectoderm. Neural crest cells continue to migrate around the brain and nerve cord.

Plate 20. Stage 20 Otic vesicles

Figure A. Live Embryo (80X).

The otic vesicle (OtV) is visible as a clear region in the lateral rhombencephalon. The mesencephalon (Me) is elevated above the rest of the brain. Sixteen somites (S), the notochord (N), the diencephalon (D) and telencephalon (Te) are also visible. 1.in

Figure B. Line Drawing (80X).

This figure shows the location of Kupffers vesicle (KV) and the structures identified in figure A.

Figure C. Serial Section (200X).

The small lumen and columnar cells that make up the OtV are visible in this sagittal section.

Figure D. Serial Section (400X).

KV and an unlined ventral vesicle (V) are visible in this sagittal section of the caudal region. The embryo is bounded by the epidermal ectoderm (EE) layer.

Otic vesicles have formed and each possesses a small lumen surrounded by columnar cells with peripherally located nuclei. The three brain regions and neuromeres are easily distinguished in living embryos. The mesencephalon is markedly elevated above the rest of the brain. The 16 pair of somites are becoming more chevron-shaped. Primordial germ cells are moving anteriorly out of the caudal periblast layer. The pericardium continues to migrate posteriorly.
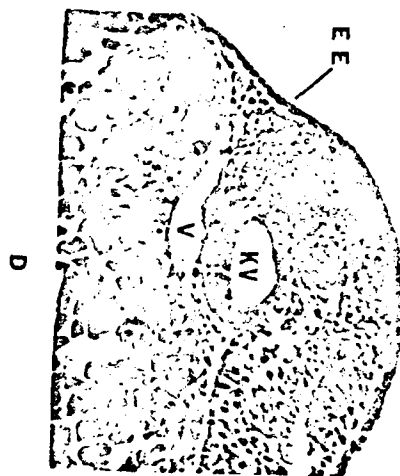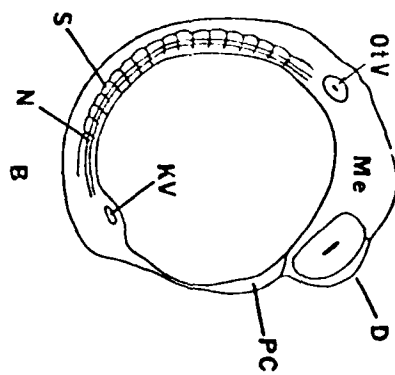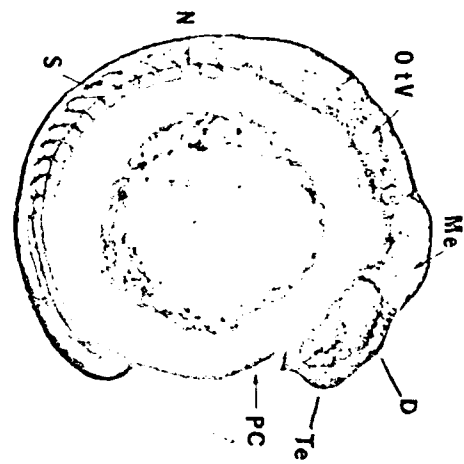
Plate 21. Stage 21 Tailbud

Figure A. Live Embryo (80X).

This figure shows the tailbud (TB), enlarged otic vesicle (OtV),
optic cup (OC), and the mesenmetencephalon fissure (MMF). Somites
(S) have increased in number since the previous stage.

Figure B. Line Drawing (80X).

The lens placode (LP) not visible in figure A is illustrated in
this line drawing. The plane of section of figure d is indicated
by the dashed line.

Figure C. Serial Section (80X).

This sagittal section shows how far posterior the pericardial
coelom (PC) has migrated. Also note the elongated cells of the
notochord (N).

Figure D. Serial Section (100X).

This transverse section shows the LP still attached to the
epidermal ectoderm (EE). Scattered neural crest cells (NCC) are
visible lateral to the diencephalon (D). The third ventricle (3V)
has enlarged within the D.

The tail bud has formed and is starting to lift free of the yolk
mass. The 18-20 pair of somites are becoming increasingly chevron-
shaped. A fissure separating the mesencephalon and the metencephalon
has formed perpendicular to the embryonic axis. The aqueduct of Sylvius
connects the slightly enlarged third ventricle with the fourth
ventricle. The spinal cord is oval in transverse section and contains a
narrow neurocoele. The olfactory placodes are visible as a pair of
thickenings in the ectoderm between the optic cups. The lens placodes
are rounded masses of undifferentiated ectodermal cells extending into
the optic cup but still attached to the epidermal ectoderm. The
periblast under the tail bud has become reduced in size. Primordial
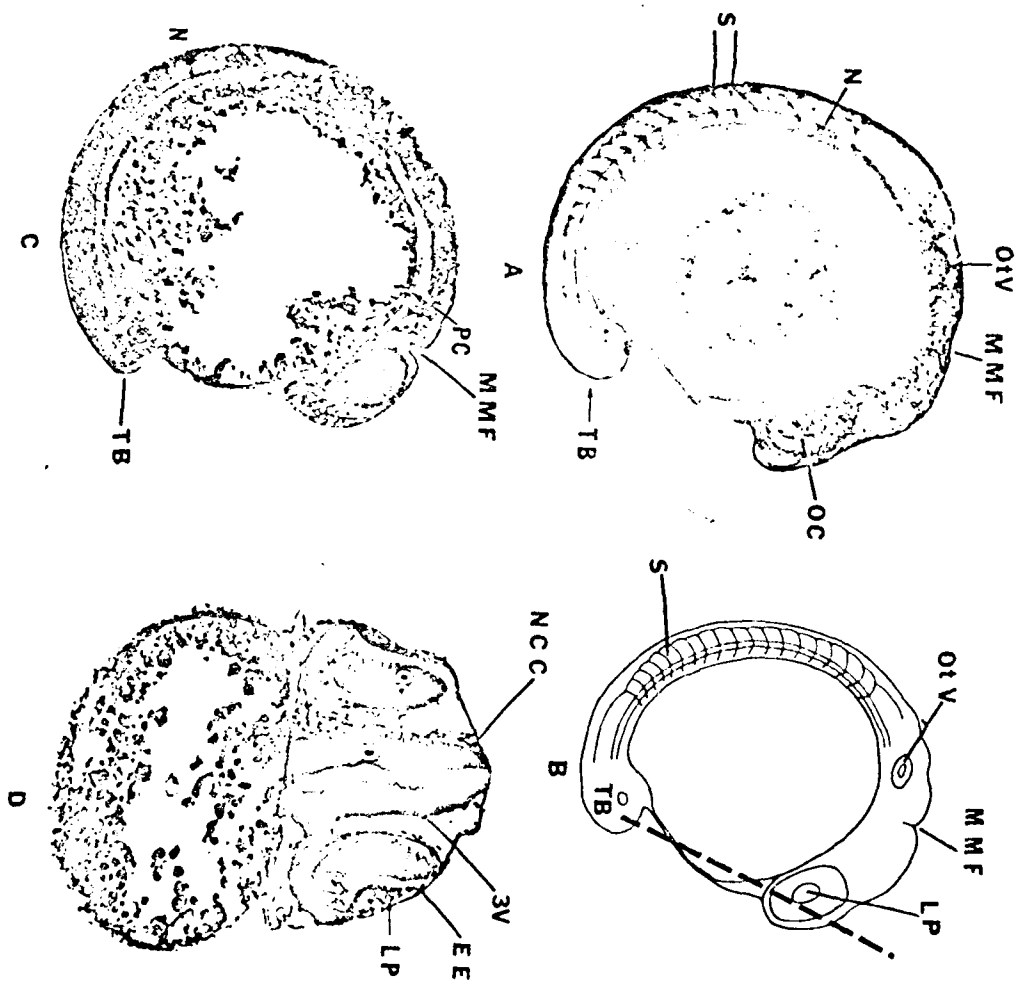
germ cells continue to migrate anteriorly in the yolk sac syncytium. There is no indication of the gut anlage at this stage. A broad ventral mass of mesoderm extending caudally from the optic cups will form the heart anlage in later stages. The pericadial coelom continues to migrate posteriorly.

Plate 22.   Stage 22   First movements

Figure A. Live Embryo (80X).

   This drawing illustrates the enlarged tailbud (TB), pericardal coelom (PC) and lens (L).

Figure B. Line Drawing (80X).

   The olfactory placode (OlP) is indicated by a line in the anterior telencephalon. The lens (L) and OtV have enlarged and are easily distinguished in living embryos. The plane of section for Figure C is indicated by a dashed line.

Figure C. Serial Section (80X).

   The enlarged L is visible in the optic cups. Note the large neurocoele (Nc) in the nerve cord (NC). Plane section is indicated by dashed line in figure B.

Figure D. Serial Section (200X).

   This sagittal section shows the enlarged lumen of the OtV. The heart anlage (HA) is visible as two sheets of mesoderm. The OlP is visible as a thickening in the epidermal ectoderm (EE) in the anterior telencephalon. The anterior border of the PC is bounded by a layer of EE.

Weak twitching movements are first observed in living embryos. The tail bud has elongated and is free of the yolk mass. Brain ventricles and the neurocoele of the spinal cord have enlarged. The olfactory pits have formed and are visible in living embryos. The otic vesicles have enlarged. The lens has formed and is clearly visible in the optic cups which remain connected to the diencephalon by a hollow cord of cells. Muscle fiber cell precursors in the 20 somite pairs are elongating and becoming multinucleated.

The pericardial cavity has enlarged considerably. The heart anlage is visible as an anterior-ventral evagination from a broad sheet of mesoderm located under the mesen-metencephalic fissure. The embryonic coelom is visible as a small cavity in the mesoderm lateral to the somites. Neuromast anlagen are visible as columnar thickenings of cells in the epidermal ectoderm lateral to the nerve cord in the mid-regions of the embryo.
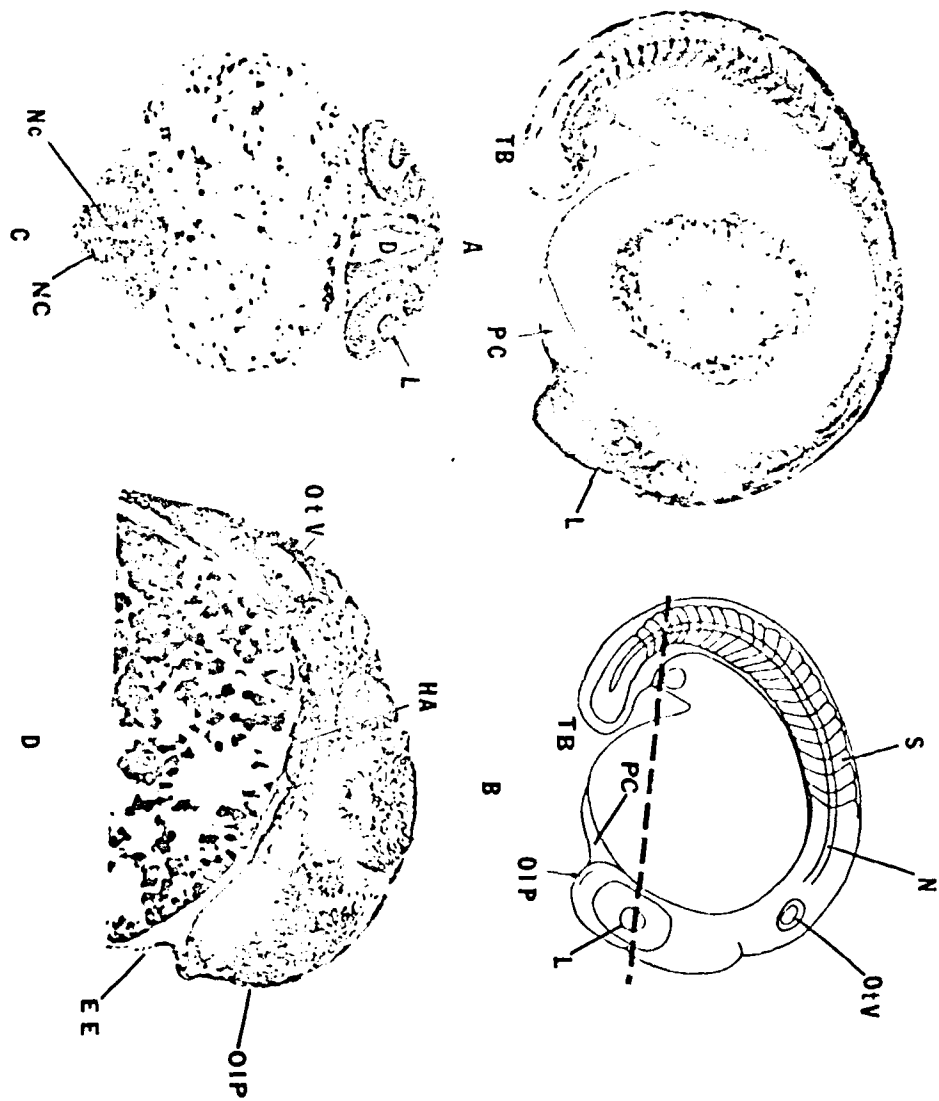
- 111 -

Plate 23. Stage 23 Heartbeat

Figure A. Live Embryo (80X).

　The figure shows the large pericardial coelom (PC) and otic
vesicle (OtV). The yolk mass (YM) is considerably reduced in size
compared to the rest of the embryo.

Figure B. Line Drawing (80X).

　The ventral choroid fissure (CF), enlarged somites (S) and the PC
are all visible. The mesen-metencephalic fissure (MMF) and OtV
are easily distinguished in living embryos. The plane of section
of Figure C is indicated by the dashed line.

Figure C. Serial Section (80X).

　The large lens (L) is visible in the optic cup (OC). The
infundibulum (I) has expanded laterally. The dorsal spinal cord
(SC) and ventral notocord (N) are visible in the caudal region.

Figure D. Serial Section (80X).

　This sagittal section shows the somites (S). Their distinctive
appearence is due to the elongated muscle fibers. The optic cup
(OC), lens (L) and OtV are clearly visible. Note the large
Kupffers vesicle (KV) and the vacuolated cells of the notochord
(N).

　The S-shaped tubular heart lies in a depression in the yolk ventral
to the left eye. A colorless fluid is visible moving in the heart as it
beats sporadically, although no peripheral circulation is present.
Blood islands are forming as clumps on the yolk mass. The pericardium
continues to form posteriorly. The embryo exhibits extensive tail
thrashing movements. The brain ventricles have enlarged and the roof of
the rhombencephalon has started to become thinner. The meso-
metencephalon fissure is more pronounced than previously. The spinal
cord, notochord and otic vesicle continue to differentiate. The large
infundibulum has expanded laterally. The lens and the ventral choroid
fissure are distinct. Germ cells continue to migrate laterally and

- 113 -
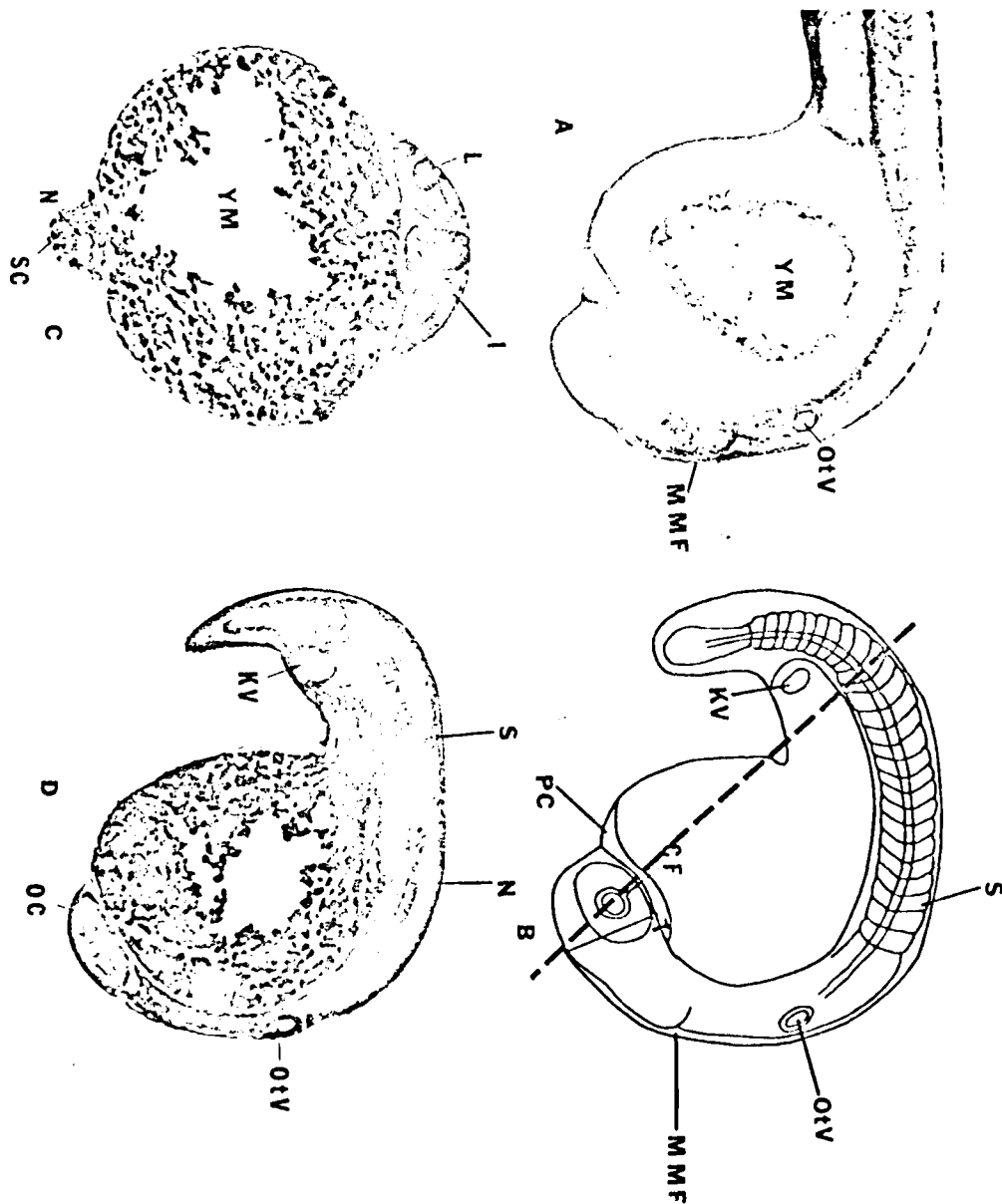
anteriorly from the periblast region under Kupffers vesicle. In the caudal region the dorsal and ventral medial fin folds are visible as thickened evaginations in the epidermal ectoderm. Muscle fibers remain immature but continue to elongate. The olfactory pits are lined with columnar epithelal cells and are located medial to the optic cups. The paired pronephric ducts are present in the caudal region as a pair of thin-walled, laterally located tubes, each having a small lumen. They merge anteriorly to form a single thin-walled structure, the urinary bladder anlage.

Plate 24.   Stage 24   Circulation

Figure A.   Live Embryo (80X).

   The distinctive third (3V) and fourth (4V) brain ventricles are
   easily seen in living embryos.

Figure B.   Line Drawing (80X).

   Otoliths (O) are visible as a pair of small concretions in the
   otic vesicle.   The liver diverticulum appears as a depression in
   the yolk sack (YS). The olfactory grove (OG) is visible in the
   anterior telencephalon.   Planes of section for figure C and D are
   represented by dashed lines, c and d respectively.

Figure C.   Serial Section (80X).

   The heart (H) is visible as a thin tube of mesoderm under the
   optic cup.   The lens (L) is surrounded by columnar epithelium.
   The infundubulum (I) is also visible.

Figure D.   Serial Section (200X).

   This transverse section shows the spinal cord (SC), notochord (N)
   encased in a hyaline sheath (HS), and the caudal artery (CA) and
   vein (CV).   The lensshaped neuromasts (Nm) are visible lateral to
   the CA.

Figure E.   Serial Section (200X).

   The optic cup (OC), third and fourth ventricles (3V, 4V) and heart
   (H) are visible in this section.

   Blood islands resting on the yolk mass consist of light yellow

aggregations of cells.   These cells are being washed into the large,

common cardinal veins by the blood flow.   Colorless nucleated blood

cells leave the heart and enter the ventral aorta which divides

anteriorly into the internal carotid and hyaloid arteries, and

posteriorly to form the dorsal aorta.   The large caudal artery lies

immediately under the notochord and extends to the sixth pre-cloacal

somite.   The caudal vein is immediately ventral to the caudal artery.
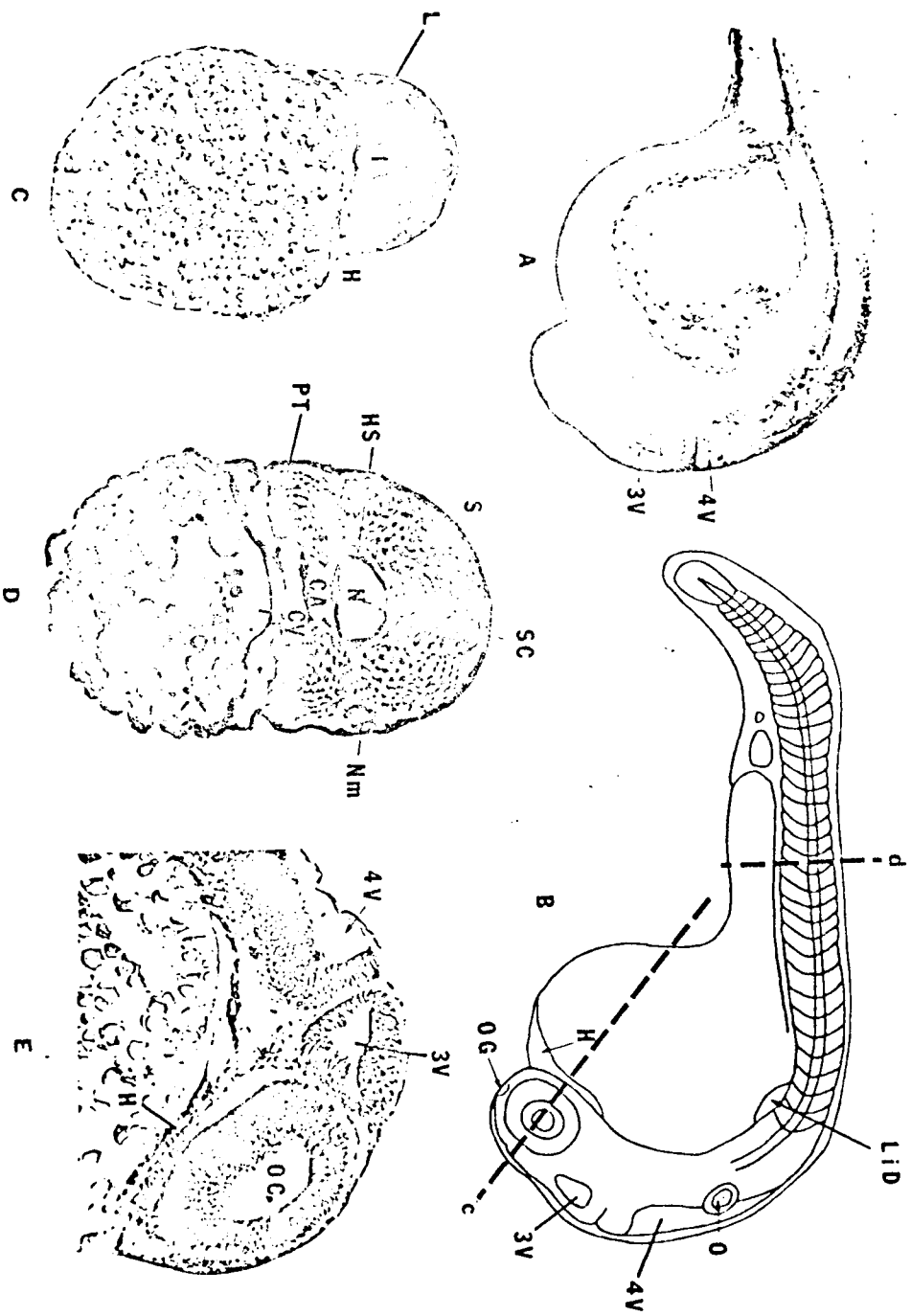
Elongated multinucleated skeletal muscle fibers contain a prominent nucleus. Otoliths are visible as two small concretions in each otic capsule. The lens has enlarged and is surrounded by a single layer of columnar epithelium. The dorsal and ventral median fin folds continue to form anteriorly. The gut can be seen as a thin-walled ventral tube of endoderm extending from the mesencephalon to the proctodeum. The proctodeum is visible as an invagination in the epidermal ectoderm ventral to the terminus of the hindgut. The liver diverticulum is visible as a mass of tissue budding off from the ventral foregut below the posterior mylencephalon. The paired pronephric ducts are ventral and lateral to the caudal vein, and are bounded by a single layer of columnar cells. Neuromasts of the lateral line system are visible as condensations of tissue under the epidermal ectoderm lateral to the somites. The tail has elongated and the embryo now possesses 35 to 37 pairs of somites. A lighter staining region (white matter) consisting of axons is visible on the lateral aspects of the diencephalon medial to the optic cups. The third and fourth ventricles have enlarged. Cells of the notochord are highly vacuolated. The notochord is encased in a thin hyaline sheath.

Plate 25. Stage 25   Retinal pigmentation

Figure A. Line Drawing (80X).

The median fin fold (MMF) is easily visible in living embryos. The somites (S), heart (H), liver (Li) and otiliths (O) continue to differentiate. The plane of section for figure C is indicated by the dashed line.

Figure B. Live Embryo (80X).

The olfactory groove (OG) is visible in the anterior telencephalon. The O appear as dark concretions in the otic capsule.

Figure C. Serial Section (200X)

This transverse section shows the lateral tectal lobes (TL) of the presumptive tectum and the thin layer of white matter (WM).

Figure D. Serial Section (100X).

This sagittal section shows the chorid plexus (ChP) on the roof of the rhombencephalon. The optic nerve (ON) is just visible as a light staining region ventral to the optic cup (OC). The OG is a dark staining area anterior to the OC. Liver tissue (Li) forms a depression in the yolk mass (YM).

The outermost layer of flattened cells surrounding the eyecup, the tapetum nigrum, has become pigmented, giving the optic cups a darkened color. The head is beginning to lift free of the yolk mass. The marked cephalic flexure occurs at the mesen-metencephalic transition. The optic nerve leaves the optic cup through the ventral chorid fissure. The white matter continues to increase in volume on the ventral surface of the brain and spinal cord. The tectal lobes which later form the tectum are visible as evaginations on the dorsal and lateral surfaces of the mesencephalon.

On the ventral surface of the anterior yolk mass, a large sac of blood is filled by the cardinal veins and drained by the sinus venosus. Blood islands are still present on the yolk sac. The heart has a
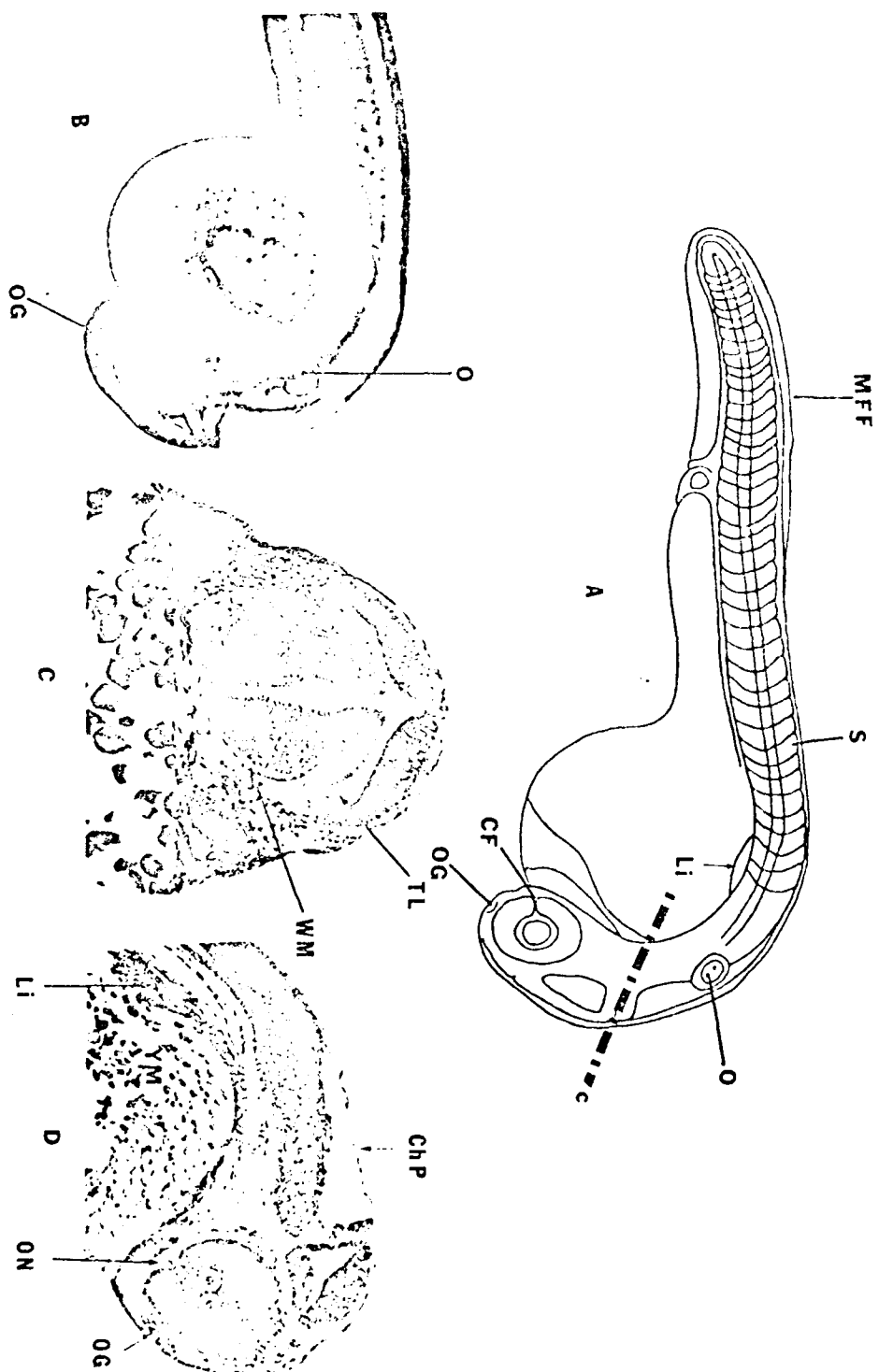
definite S-shape and lies primarily on the yolk sac under the right optic cup. Blood flow extends to the third post-caudal somite.

Small thickenings or deposits in the epidermal ectoderm are located throughout the head region and surrounding the cloacal opening. The median fin fold continues to form anteriorly. The lens-shaped neuromasts of the lateral line system are visible at intervals below the epidermal ectoderm lateral to the somites in the caudal region. Masses of mesenchyme and neural crest cells are condensing lateral and ventral to the rhombencephalon near the otic capsule. The anterior pituitary anlage is visible as an undifferentiated mass of ectodermal cells budding off the dorsal pharynx. Pharyngeal pouches 5 and 6 are visible as lateral pockets in the pharyngeal region anterior to the otic capsule. Axons extend from a placode posterior to the eyecups toward the mesencephalon and will later become part of cranial ganglion V. The fourth ventricle has enlarged. The thin roof of the rhombencephalon is now distinct and later forms the choroid plexus. Liver tissue continues to proliferate. Embryos are quite active, exhibiting frequent thrashing movements.

Plate 26. Stage 26 Intersegmental arteries

Figure A. Scanning Electron Micrograph (540X).

This micrograph shows a pectoral fin (PF) with its surface covered by epidermal ectoderm cells.

Figure B. Line Drawing (80X).

This drawing illustrates those structures easily seen in living embryos and in serial sections. The plane of section of figure D and E are shown as dashed lines "d" and "e" respectivly.

Figure C. Live Embryo

The median fin fold (MMF), optic capsule (OC), common cardinals (CC), and PF are visible.

Figure D. Serial Section (200X).

This frontal section shows the lens (L) in the optic cup (OC) as well as the large olfactory grooves (OG) in the epidermal ectoderm (EE).

Figure E. Serial Section (200X).

This figure shows white matter (WM) on the ventral and lateral surfaces of the spinal cord (SC). The pectoral fins (PF), notochord (N), liver tissue (Li), and gut (G) with a small lumen are visible.

The two pectoral fin buds which first became visible at about 45 hours have enlarged. Blood flow is seen for the first time in the intersegmental arteries. Blood cells are becoming more pigmented and blood flow now extends to the fourth post-caudal somite. The cardinal veins are well-defined and lie in depressions in the shrinking yolk sac.

The hindgut consists of a small lumen surrounded by a single layer of columnar epithelium and is located immediately ventral to the caudal vein. The lumen of the hindgut enlarges just anterior to the cloaca.

The sinus venosus, atrium, ventricle, and conus arteriosus of the heart can be distinguished in living embryos. Powerful ventricular contractions cause the head of the embryo to bob up and down. Circulation has increased in the head plexus. Guanine deposits give the eyes a silvery color. The embryo continues to elongate as the head lifts free of the yolk sac.
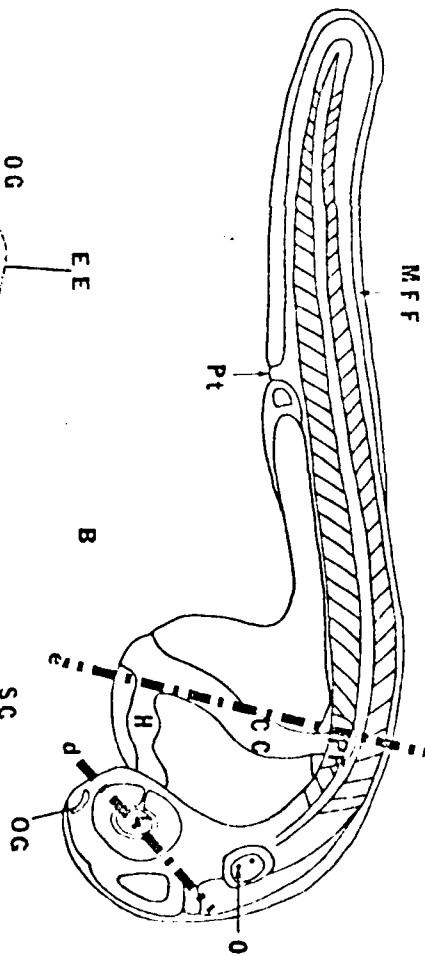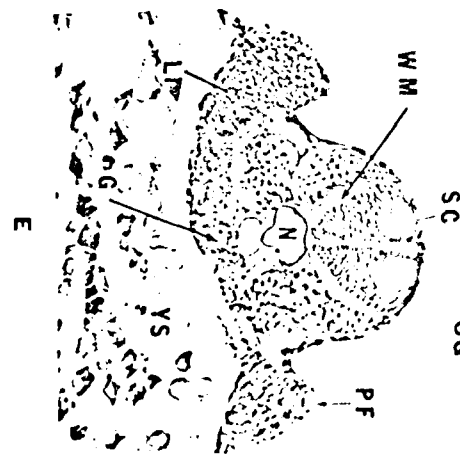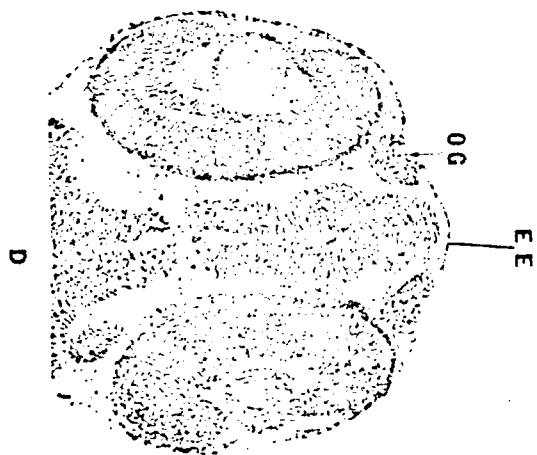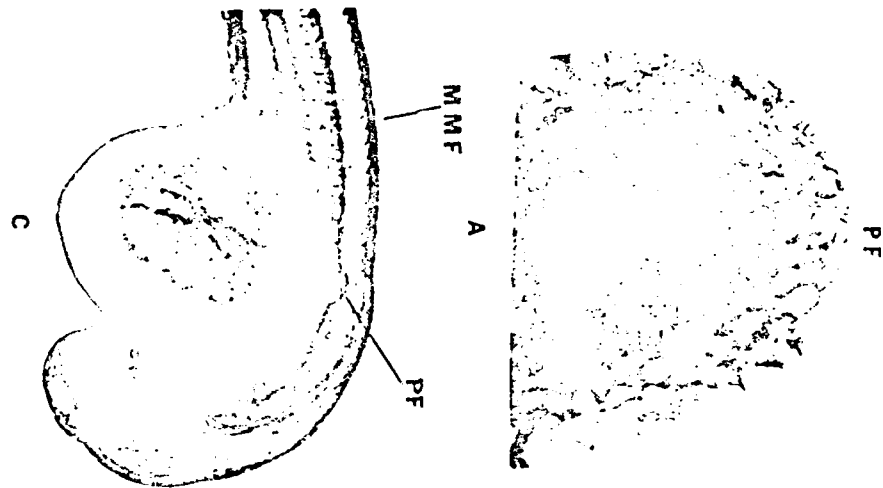
The enlarged olfactory grooves are lined by a layer of columnar cells. The epiphysis anlage appears as a small evagination from the roof of the diencephalon. White matter continues to increase in volume on the ventral and lateral surfaces of the brain and spinal cord. Kupffers vesicle persists anterior to the cloaca.

The highly vacuolated cells of the notochord are transparent and stacked in layers. The notochord tapers and terminates ventral to the anterior end of the otic capsule. The otic capsule is no longer oval, instead it is narrower at its base where the enlarged otoliths are located.

There is no indication of a stomodeum at this stage but the pharynx has enlarged laterally. The liver continues to enlarge. Muscle fibers continue to elongate and are developing the banding pattern typical of striated muscle. Neuromasts have continued to proliferate and migrate anteriorly. The eyes are connected to the diencephalon by the optic nerve. A small fold of cells connect the spinal cord with the dorsal medial fin fold. The pituitary anlage is visible as a compact mass of cells ventral to and closely appressed to the large infundibulum. The squamous epidermal ectodermal cells are pentagon-shaped. The pronephric ducts are more clearly defined.

Plate 27. Stage 27   Horizontal duct

Figure A. Line Drawing (80X).

   This drawing illustrates the perpendicular orientation of the otoliths (O) in the otic capsule. The notochord (N), pectoral fins (PF) and, heart (H) continue to differentiate. Plane of section of figure D is indicated by the dashed line.

Figure B. Live Embryo (80X).

   The large heart (H) is visible on the yolk sac. The N and PF are easily-seen in living embryos.

Figure C. Serial Section (100X).

   This sagittal section shows white matter (WM) on the the ventral hind brain. The thick optic nerve (ON) and extensive Li are also visible. The epiphysis (Ep) is visible as an evagination in the roof of the diencephalon.

Figure D. Serial Section (200X).

   This transverse section shows the small medial fin fold (MFF) as a fold in the epidermal ectoderm (EE). The large somites (S) are lateral to the spinal cord (SC) and notochord. The caudal artery (CA) and caudal vein (CV) are located dorsal to the gut (G).

The walls of the auditory capsule have thickened ventrally and thinned dorsally where the horizontal duct is forming. The paired otoliths are oval-shaped and have become perpendicular in orientation to each other. The olfactory grooves have elongated and are closely associated with the anlage of the olfactory lobes, although no connection is visible yet.

A strong blood flow is present in the intersegmental arteries. A short vessel extends caudally beyond the turn-around point of the caudal artery. Radial striations centered around the tip of the notochord have started to form in the caudal fin. The medial fin fold continues to enlarge and extend anteriorly. The surface thickenings in the epidermal ectoderm noted in previous stages are darkening. The notochord extends
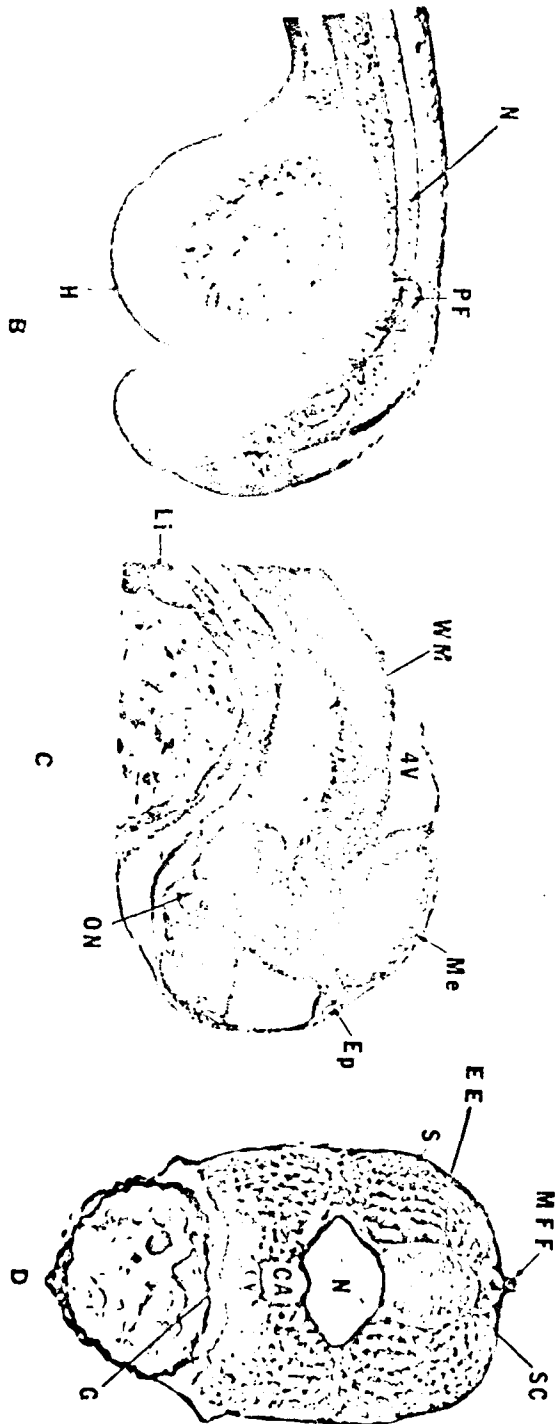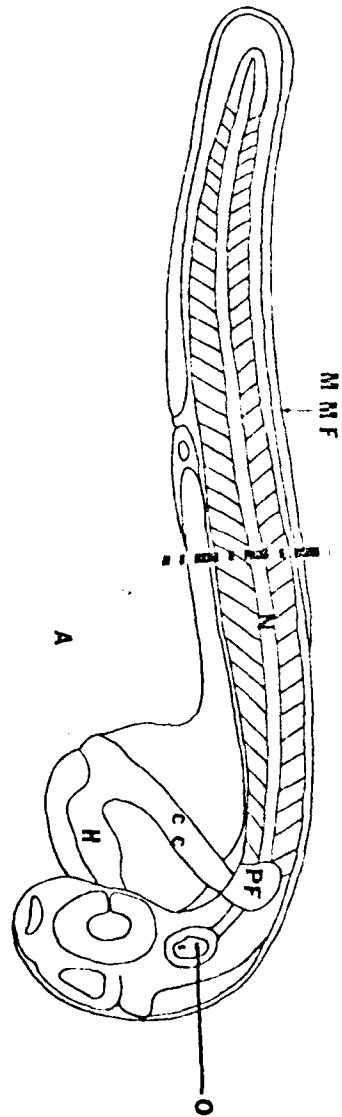
anteriorly to the mesen-metencephalic fissure and lies just dorsal to the pharynx. A small unlined vesicle and scattered large primordial germ cells are present at the posterior end of the yolk sac just anterior to the cloaca.

The presumptive cone cells have elongated inside the pigmented layer of the eye. The precursors of cranial ganglia IX and X are visible in serial sections as dorsal, lateral placodes sending bundles of axons toward the rhombencephalon. White matter continues to increase in volume. The two lateral cavities of the tectal lobes have enlarged in the mesencephalon. Neuromasts of the lateral line system are visible in lateral pairs throughout the head region. The mandibular, hyoid and pharangeal arches three and four are visible. Masses of tissue are condensing dorsal to the pharynx which later form the parachordal and trabecular cartilages. The early elements of the lower jaw are visible in sections as lateral and ventral condensations of tissue of the pharynx.

Plate 28. Stage 28   Blood in the pectoral fins

Figure A. Line Drawing (80X).

The cloaca (Cl) is visible as the common exit for the digestive
and urinary system. The otic vesicle (OtV) and heart (H) continue
to differentiate. The planes section for figures C and D are
indicated by dashed lines "c" and "d" respectively.

Figure B. Live Embryo (80X).

The liver (Li) is visible extending into the yolk sac of living
embryos. The optic cups (OC) appear as dark masses due to
extensive pigmentation.

Figure C. Serial Section (200X)

This oblique section shows the lens (L) and layers of the eye, the
sclerotic coat (ScC), the tapetum nigrum (TN), the outer nuclear
layer layer (ONC), the inner nuclear layer (INL), the axons (A),
and the ganglion cell layer (GCL).

Figure D. Serial Section (200X).

This transverse section shows the radial cartilage (RC) in the PF.
The thick-walled foregut (Fg) is medial to the liver tissue (Li).
Paired pronephric ducts (PD) are ventral and lateral to the N.

Blood flows through a single loop in the pectoral fins. Dark,
stellate melanocytes are present on the ventral surface of the yolk sac
anterior to the cloaca. An enlarged vessel dorsal to the myotomes
receives blood from the segmental arteries. The ventral aorta gives
rise to the six aortic arches. Ventral and lateral evaginations into
the lumen of the auditory capsule have appeared. The liver has
enlarged. The thick-walled heart lies completely on the yolk sac. The
angle of the cephalic flexure has decreased. The hyaline sheath
surrounding the notochord has thickened. The banding pattern of the
skeletal muscle is more apparent.

Cranial ganglia V, IX, and X have connected with the diencephalon and
mylencephalon. A bridge of tissue representing the semicircular canal
anlage is visible in the otic capsules. Neuromasts continue to
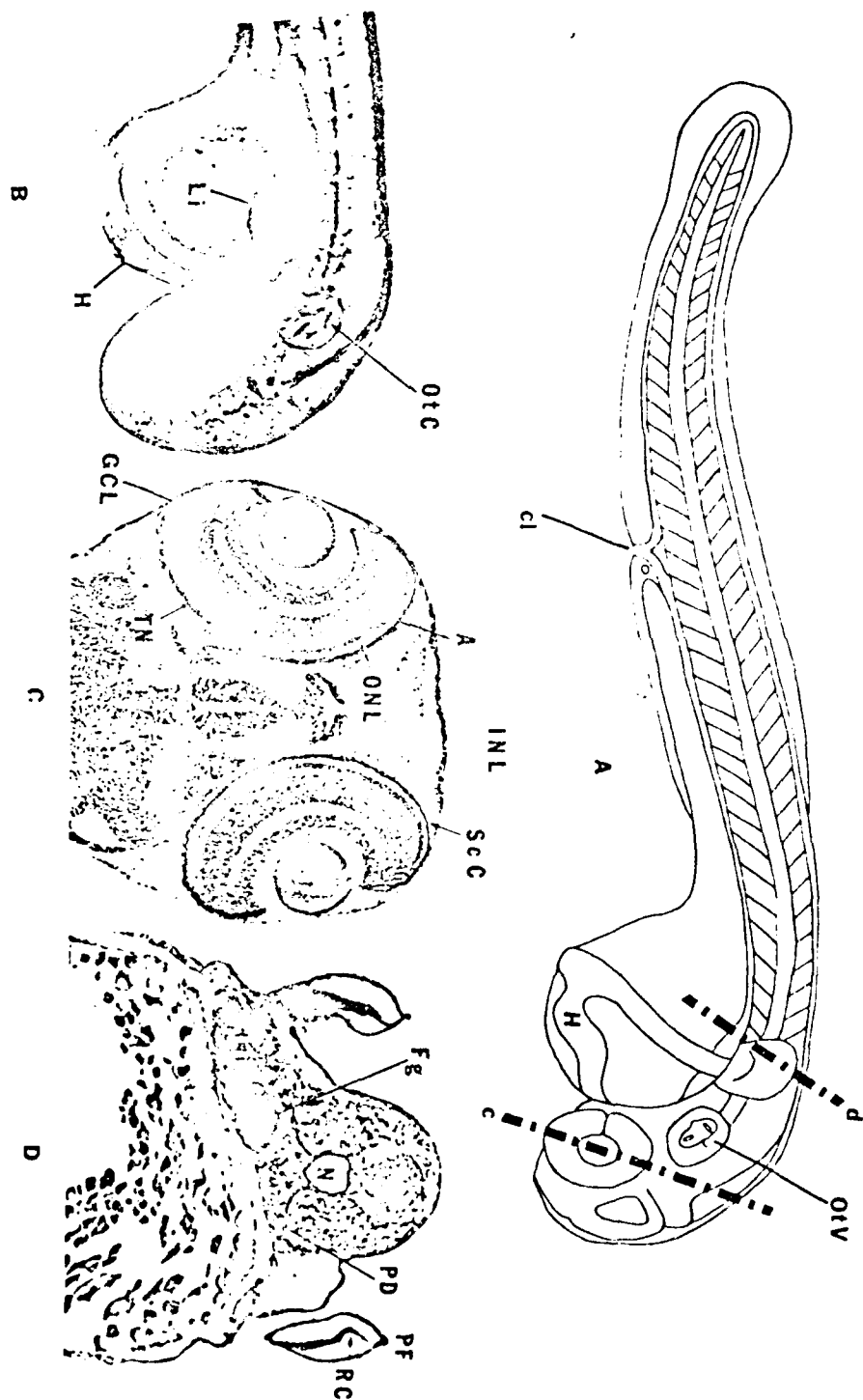
proliferate throughout the head region. The olfactory grooves have sent out axons which link up with the olfactory lobes of the telencephalon. The operculum extends caudally from the hyoid arch and covers branchial arches 3, 4, and 5. White matter extends along the dorsal and lateral sides of the spinal cord for most of its length.

The eyecup has darkened considerably, obscuring much of the lens. The eyes are enclosed in a two to three cell thick layer of undifferentiated mesoderm, the early sclerotic coat followed by the darkly pigmented tapetum nigrum. The retina itself has differentiated into a layer of columnar cone precursor cells, a bipolar layer, and the thick ganglion cell layer. The distinctive choroid fissure pierces all layers of the eye and is the route of exit for the optic nerve and entry for the hyaloid artery. The thin layer of epidermal ectoderm covering the eye has not yet differentiated into cornea.

The hindgut makes an abrupt ventral turn above the cloacal opening, then increases in size just prior to merging with the opening of the urinary bladder anlage. Paired posterior pronephric ducts join into a single enlarged duct lined with columnar epithelium, the urinary bladder anlage, which also makes an abrupt ventral turn prior to merging with the small cloaca. Paired pronephric ducts extend anteriorly to the pectoral fins. Cartilaginous tissue is differentiating in the upper and lower jaws. The pharynx is large and triangular shaped anteriorly, becoming compressed dorsally and ventrally prior to merging with the foregut. A bend in the foregut is visible under the pectoral fins. Radial cartilage is forming in the pectoral fins.

Plate 29. Stage 29   Bile formation

Figure A. Line Drawing (30X).

   This diagram illustrates the lower jaws (LJ) and the continued
   differentiation of the otic capsule (OtC). The plane of section of
   figure D is indicated by the dashed line.

Figure B. Live Embryo (80X).

   In this figure the OtC and the highly pigmented optic cup (OC) are
   seen.

Figure C. Serial Section (80X).

   This sagittal section shows the thick walled foregut (FG) and
   liver tissue (Li). Four aortic arches (AA) are visible in the
   branchial arches.

Figure D. Serial Section (100X).

   This oblique section shows the optic nerve (ON) in the optic cup.
   The large olfactory groove (OG) and pharynx (Pn) are also visible.

Further differentiation has occurred in the cartilage of the jaw

apparatus. Limited movement of the lower jaw and eyes in living embryos

is first seen at this stage. Yellowish bile in the gall bladder has

formed and is visible in living embryos. A dip is present in the median

fin fold around the cloacal opening. The number of stellate melanocytes

has increased on the ventral yolk sac. The caudal artery has replaced

the posterior dead-end vessel of the previous stage. Striated muscle

and basal cartilage is present in the base of the pectoral fins. The

ampullae anlagen at the base of the semicircular canal are visible as

thickenings in the walls of the otic capsule. The foregut has

differentiated into a thick walled stomach with an enlarged lumen.

Blood flow can now be observed in the liver sinusoids. The olfactory

groves are bordered internally by a squamous cell layer and externally
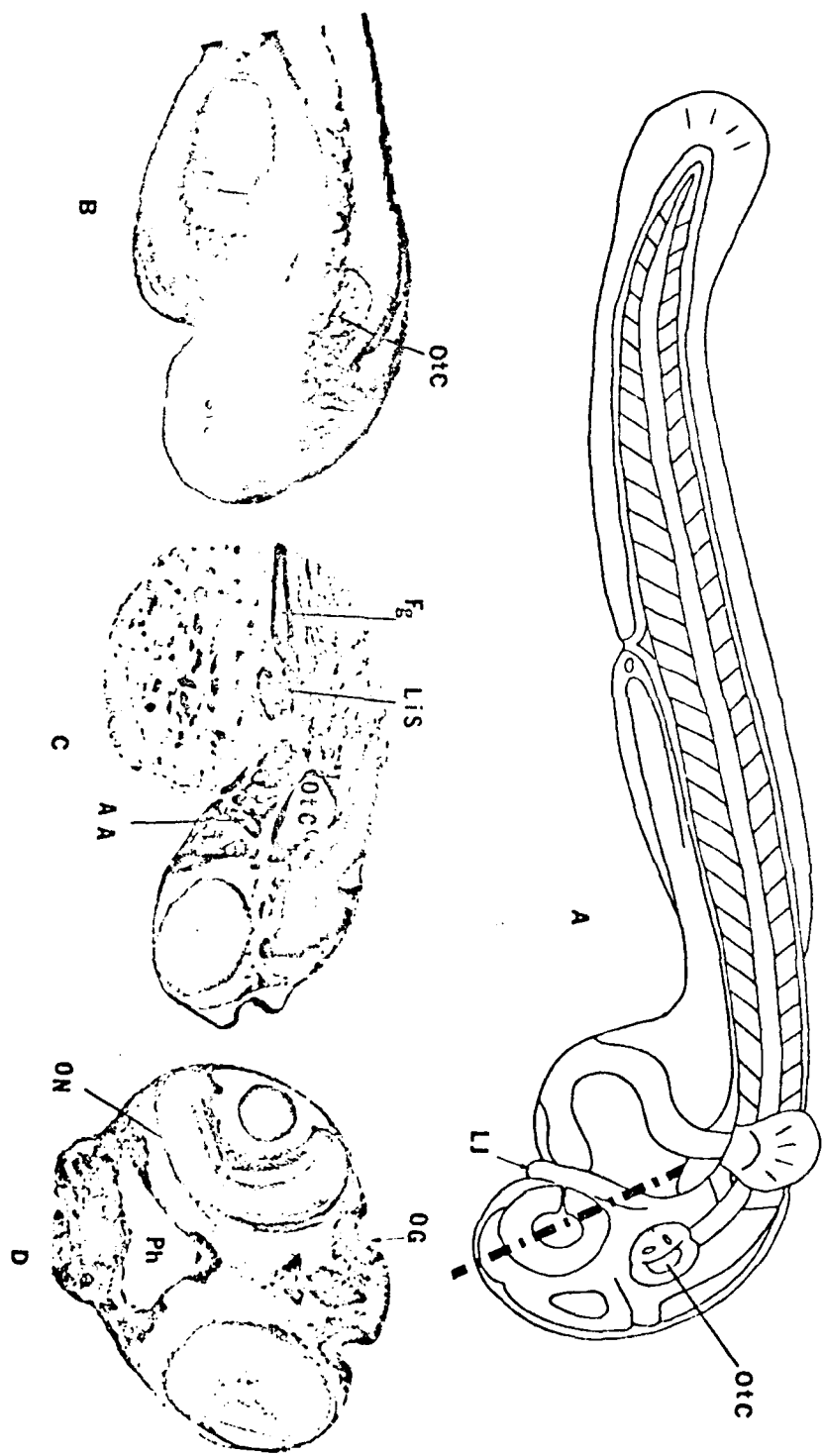
by a lighter staining sensory layer.

Plate 30.   Stage 30   Swim bladder

Figure A. Line Drawing (80X).

The dorsally pigmented swim bladder (SB) is illustrated caudal to the liver (Li). The heart ventricle (V) is large and thick walled. The planes of section for figure C and D are indicated by dashed lines c and d respectively.

Figure B. Live Embryo(80X).

The large paired otoliths (O) are clear and visible in the otic capsule. Stellate melanocytes (Mc) are visible on the yolk sac. The optic cups (OC) appear as heavily-pigmented masses in the head region.

Figure C. Serial Section (200X).

The dorsal tube (DT) that connects the thick walled stomach (St) to the swimbladder is visible ventral to the notochord (N). The gall bladder (GB) and bile duct (BD) are visible medial to the liver tissue. The large somites (S) are bounded by the layer of epidermal ectoderm (EE).

Figure D. Serial Section (100X).

The operculum (OP) can be seen lateral to the aortic arches (AA) in the gill arches (GA). The olfactory grooves (OG) are visible medial to the optic cups.

At this stage embryos hatch out of the chorion if disturbed by handling or bright lights. The swim bladder which appeared at 90 hours (25 C) has enlarged and is pigmented dorsally. It maintains its connection with the foregut through a thin hollow cord of cells. The stomach is thick walled and is developing internal folds. The lumen of the gall bladder is lined with a single layer of columnar cells and is connected to the intestine by a short bile duct. The yellow bile from the bile duct is visible extending caudally into the intestine.

The eyes, jaws, pectoral fins and operculum exhibit frequent movements. The mandibular adductor and levator muscles have formed in
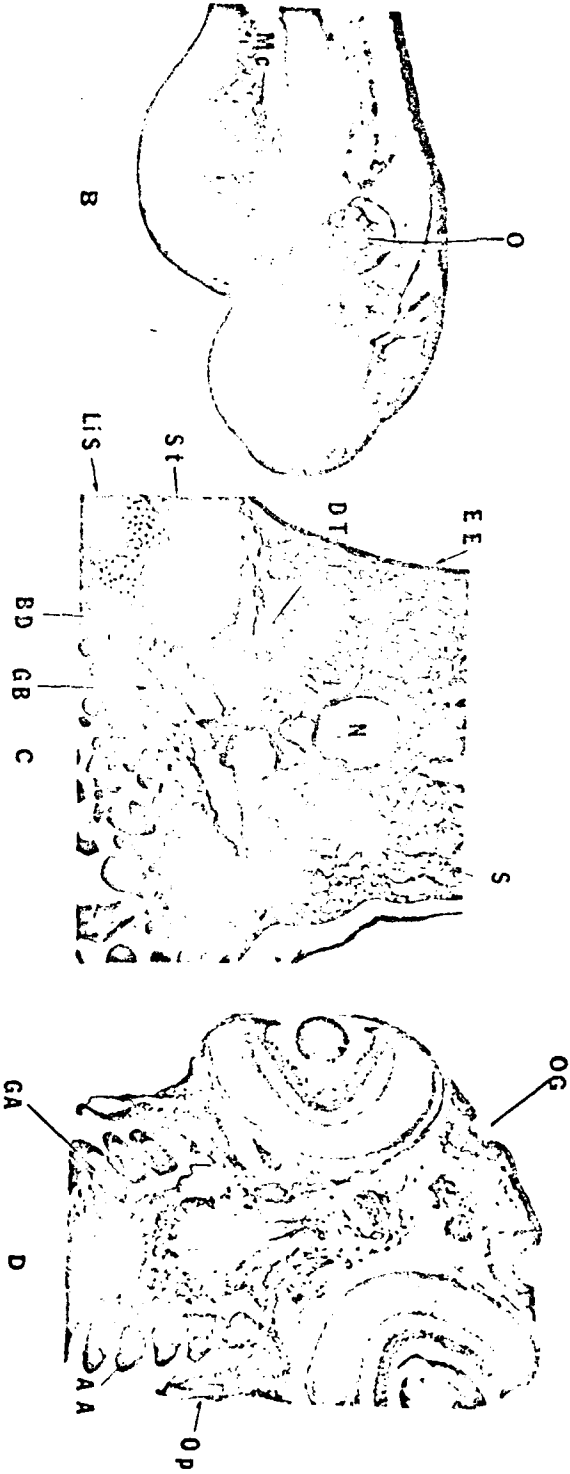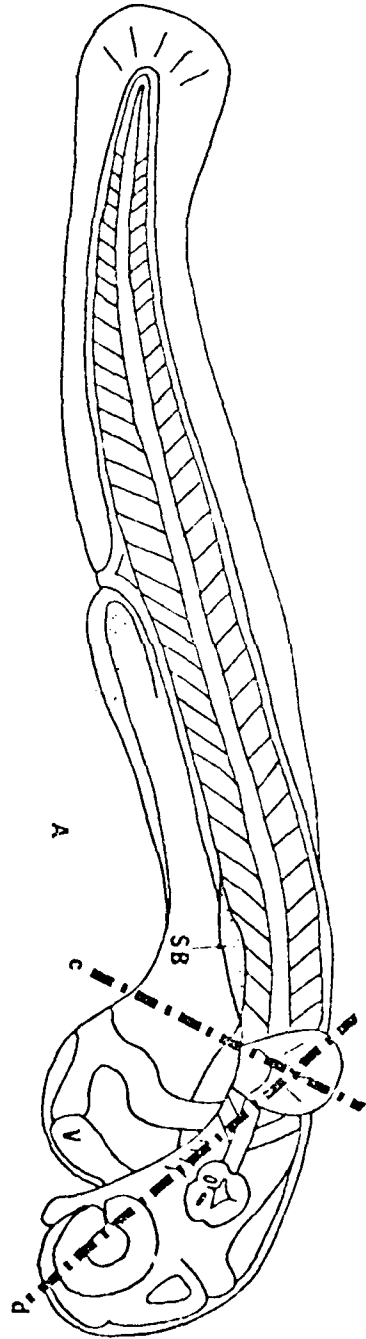
the head region in association with the protruding lower jaw. The mouth is now open. The epidermal ectoderm covering the shrinking yolk sac has a wrinkled appearance. The somites extend to the posterior edge of the otic capsule. Increased pigmentation is visible on the ventral yolk sac. Melanocytes are present at intervals along the lateral line system associated with the neuromasts. The number of striations in the caudal fin is increasing. A series of evaginations representing the gill anlagen are visible on the posterior surface of gill arches. The operculum has enlarged and covers all four gill arches.

Plate 31. Stage 31 Large operculum

Figure A. Line Drawing (80X).

The swimbladder (SB) and liver (Li) continue to enlarge. Planes of section of figure C and D are indicated by dashed lines "c" and "d" respectively.

Figure B. Live Embryo (80X).

The embryo becomes more streamlined in appearance.

Figure C. Serial Section (200X).

White matter (WM) is seen on the lateral aspects of the tectal lobes (TL) anterior to the otic capsule (OtC).

Figure D. Serial Section (200X).

This section shows the epiphysis (Ep) dorsal to the diencephalon (D). The lateral aspects of the (D) are covered with WM. Lens-shaped neuromasts (NM) are visible associated with the epidermal ectoderm (EE). The triangular shaped pharynx (Pn) is visible.

Under control conditions (25 C) a few fish hatch out of the chorion at this stage. Blood flow in the aortic arches has increased. The gill anlagen have enlarged. The operculum covers the otic capsule. The lower jaw is well formed. Striations are prominent in the caudal and pectoral fins. Pigment cells continue to migrate anteriorly on the ventral yolk sac. The swimbladder has increased in size and pigmentation and maintains its attachment to the gut by a small dorsal tube. The intestine has become pigmented. Bile production has increased as indicated by large areas of yellow pigment in the gall bladder and intestine.
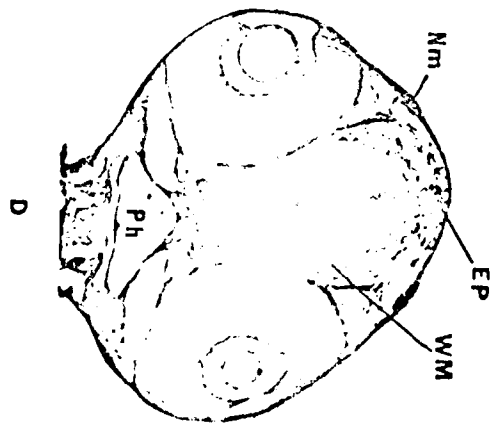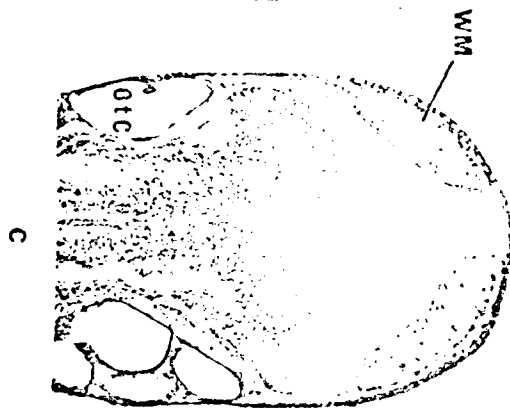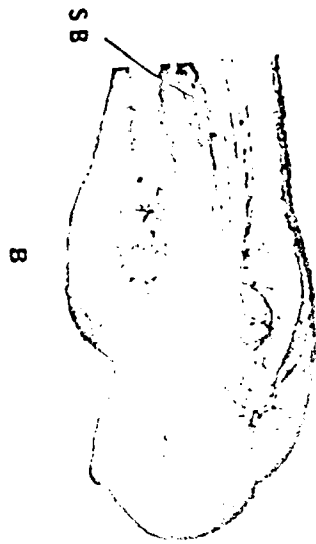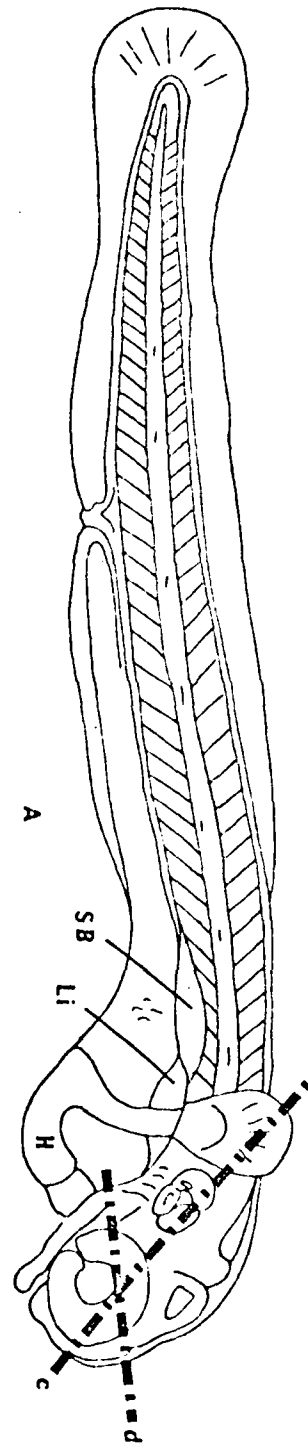
Plate 32.   Stage 32   Gill anlagen-hatching

Figure A.   Line Drawing (80X).

This drawing illustrates the large operculum (O) and the reduced yolk sac (YS). Plane of section of figure C is indicated by the dashed line.

Figure B.   Live Embryo (80X).

The notochord (N) is visible extending up to the posterior edge of the distinctive optic cup (OC). Stellate melanocytes (Mc) continue to migrate over the YS.

Figure C.   Serial Section(200X).

This transverse section shows the gall bladder (GB), the dorsal tube (DT) that connects the foregut (FG) with the swim bladder, the somites (S), the notochord (N), and the spinal cord (SC). The liver sinusoids (LiS) appear as clear spaces in in the liver tissue.

Figure D.   Serial Section (200X).

This sagittal section illustrates the large OtC as well as the ventral chorid fissure (CF) found in the optic cup.

The majority of the embryos have hatched out of the chorion at this stage. The operculum and lower jaw are well formed and move often. The superior, lateral, and medial rectus muscles are visible in serial sections and result in frequent eye movement. The yolk sac is much reduced and has become more streamlined in shape. A strong blood flow is present through the gill anlagen. The lumen of the stomach has enlarged and thickenings in its walls are visible histologically in both anterior and posterior regions.   Blood flow in the liver sinusoids has increased. A large neuromast is visible laterally on each operculum. The pronephric ducts are adjacent to the cardinal veins on their lateral ventral surface, although no glomeruli are present.
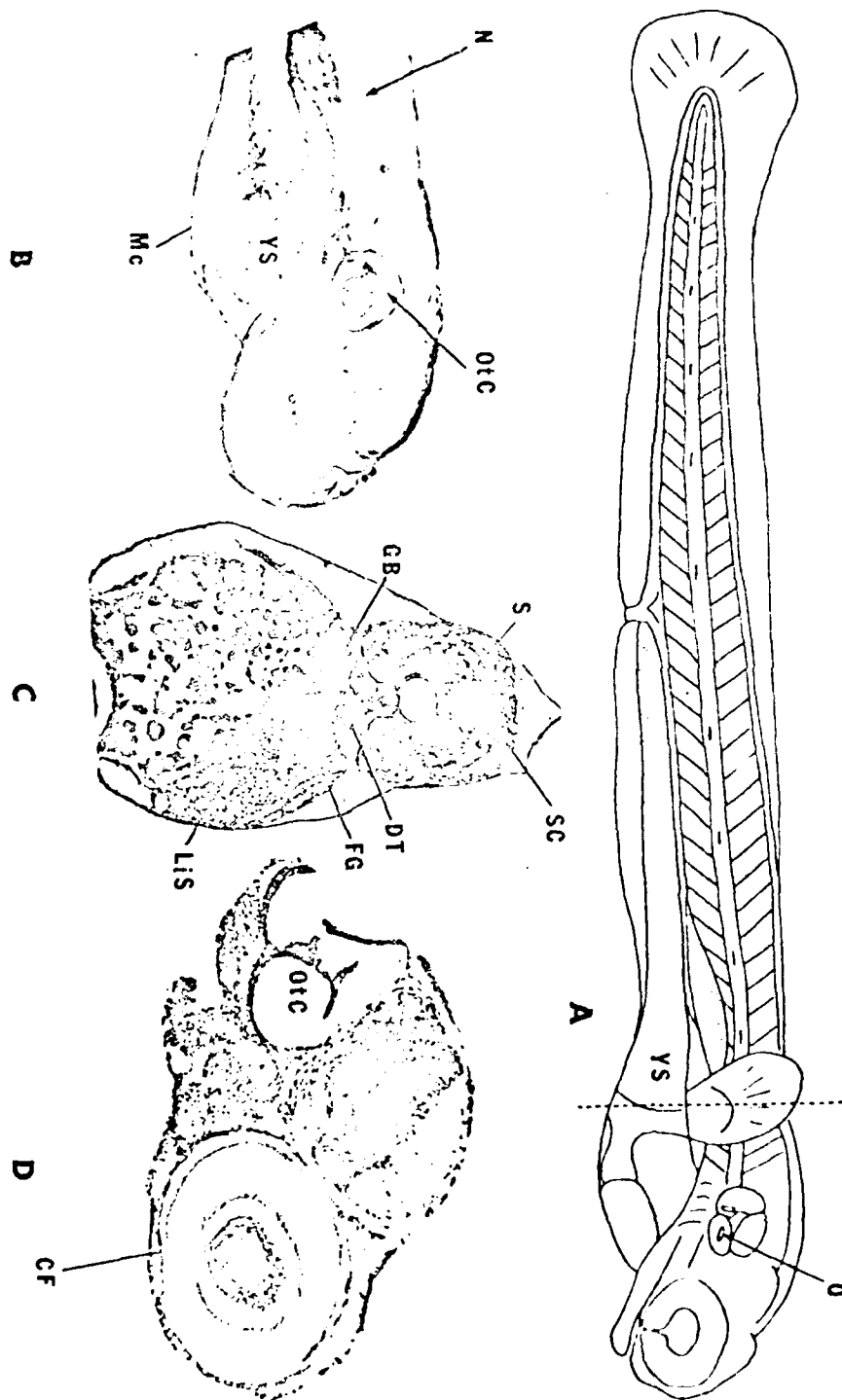
ACKNOWLEDGMENTS

LITERATURE CITED

Armstrong, P. B. and J. S Child. 1965. Stages in the normal development of Fundulus heteroclitis. Biol. Bull. 128:143-168.

Andrews, A. K. and S. A. Flickinger. 1974. Spawning requirements and characteristics of the fathead minnow. Proc. 27th Ann. Conf. S. E. Assoc. Game and Fish Comm. 759-765.

Ballard, W. W. 1973. Normal embryonic stages for salmonid fishes based on Salmo gairdneri (Richardson) and Salvelinus fontinalis (Mitchill). J. Exp. Zool. 184(1):7-26.

Hisaoka, K. K. and C. F. Firlit. 1960. Further studies on the embryonic development of the zebrafish, Brachydanio rerio (Hamilton-Buchanan). J. Morphol. 107:205-225.

Humason, G. L. 1979. Animal tissue techniques. W. H. Freeman and Co. San Francisco, p 21.

Johnson, P. M. 1951. The embryonic history of the germ cells of the largemouth bass, Micropterus salmoides, in Maine. J. Morphol. 88:471-542.

Koenig, C. C. and R. J. Livingston. 1976. The embryonic development of the diamond killifish, Adinia xenica. Copeia 3:435-444.

Long, L. W. and W. W. Ballard. 1976. Normal embryonic stages of the white sucker, Catostomus commersoni. Copeia 2:342-351.

Mahon, E. E. and W. S. Hoar. 1955. The early development of the chum salmon, Oncorhynchus keta (Walbaum). J. Morphol. 98:1-48.

Manner, W. H. and C. M. Dewese. 1974. Early embryology of the fathead minnow. Anat. Rec. 180(1):99-110.

Price, J.W. 1934. The embryology of the whitefish Coregonus clupeaformis. Ohio J. Sci. 34:287-305.

The stages are summerized in Table 1

TABLE 1

CHARACTERIZATION OF STAGES AT 25 C

Stage	Hours	Length (mm)	
1	0.00	-	unfertilized ovum
2	0.16	-	recently fertilized ovum
3	0.66	-	1-celled blastodisc
4	1.00	-	2-celled blastodisc
5	1.33	-	4-celled blastodisc
6	1.58	-	8-celled blastodisc
7	2.25	-	16-celled blastodisc
8	2.83	-	32-celled blastodisc
9	3.50	-	late cleavage
10	4.50	-	high blastula
11	5.25	-	flat blastula
12	6.00	-	early gastrula
13	7.33	-	one quarter epiboly
14	9.50	-	one half epiboly
15	12.00	-	three quarters epiboly
16	15.00	-	closure of the germ ring
17	16.50	-	neurula stage, 4-5 somite pairs
18	17.75	-	optic vesicles, 9-10 somite pairs
19	20.00	-	neuromeres, 14 somite pairs
20	22.00	-	otic vesicle, 16 somite pairs
21	24.00	-	tailbud stage, 18-20 somite pairs
22	26.00	-	first movements, lens formation
23	30.00	2.19	heartbeat without circulation
24	35.33	2.83	onset of circulation
25	40.00	3.35	retinal pigmentation
26	50.00	3.56	blood in intersegmental arteries
27	60.00	3.89	horizontal duct in otic capsule
28	74.00	4.53	blood flow in pectoral fins
29	85.00	4.90	formation of yellow bile
30	95.00	5.10	dorsally pigmented swim bladder
31	105.00	5.12	large operculum, limited hatching
32	120.00	5.14	hatching, gill anlagen

VII. Effects of Toluene on the Prehatching Development
of the Fathead Minnow (Pimephales promelas Raf.)

INTRODUCTION

Many classes of stressors have been used to elicit resp. .es in fish embryos. These include wide variations in environmental conditions such as temperature, salinity, and dissolved oxygen concentration, as well as different chemical pollutants including heavy metals, herbicides, pesticides, and petroleum derived compounds.

Fish embryos incubated under elevated or sub-normal temperature conditions have shown edema of the yolk sac, yolk sac malformations, and spinal deformities (Alderdice and Velson, 1971; Coombs and Hiby, 1979; Emadi, 1973; Hokanson and Kleiner, 1974; Kokurewicz, 1969; Kwain, 1975; McCormick et al., 1977; Peterson et al., 1977).

Embryos reared under conditions of high salinity have exhibited enlargement of the pericardial region, hydration of the anterior yolk sac, spinal flexures, and blood clots (Dushkina, 1973; Karpenko, 1974; Mossier, 1971). Reduced oxygen conditions have resulted in embryos with slower development rates, hemorrhages, and enlargement of the pericardial cavity (Gulidov, 1974; Kamaldeep and Toor, 1978).

Embryos exposed to water soluble fractions of a variety of different petroleum fuels have exhibited abnormal spinal columns, enlargement of the yolk sac in the region surrounding the heart, disruption of early cleavage patterns, premature hatch and an alteration of lipid droplets of the yolk sac (Ernst et al., 1977; Kuhnhold and Busch, 1978; Leung and Bulkley, 1979; Linden, 1978; Sharp et al., 1979). Similar abnormalities have been reported for some of the individual aromatic hydrocarbons found in petroleum fuels (Eldridge et al., 1977; Rosenthal and Stelzer,

1970; Stoss and Haines, 1979). Spinal flexures have also be   orted in teleostean embryos exposed to chlorobenzene, the mollusc   Bayer 73, and aflotoxin B (Birge et al., 1979; Llewellyn et   ., 1977; Paflitschek, 1976).

The studies cited above, like most others, have concentrated on the acute effects of various pollutants or environmental conditions. Relatively little work has been done on chronic, sublethal responses of teleost embryos to toxicants or fluctuating environmental conditions.

Contamination of the aquatic environment by petroleum fuels has resulted in increased interest in the biological effects of these contaminants. One category of highly refined petroleum products which represent a potential source of contamination is jet fuels. JP-4, one such fuel used almost exclusively by the United States Air Force, contains toluene as its major aromatic water soluble component (Puyear et al., 1931).

The fathead minnow, Pimephales promelas, has been used extensively as an indicator species in toxicity testing. Acute toxicity of toluene (96-hour LC50) on adult fathead minnows was initially determined using a static exposure system by Pickering and Henderson (1956). A flow-through system was later ulitized by Devlin et al. (1982) to determine the acute levels (96-hour LC50's) of toluene on three age groups of fathead minnows. The present study was designed to investigate the sublethal effects of toluene on the pre-hatching development of the fathead minnow.

- 143 -

METHODS

Breeding facilities consisted of 28 ten liter tanks, each containing a U-shaped tile, one mature male and two mature females. Tanks were individually supplied with air and water (24 C +/- 0.5 C). The breeding system was enclosed in a light tight, insulated room with a photoperiod of 16 hours light (100 lux at the water surface) and 8 hours dark. Mature fish were fed frozen brine shrimp and Glenco No. 2 enriched trout food twice daily. Larval fish were fed live young brine shrimp twice daily. Fathead minnow stock cultures for our breeding facility were obtained from the U.S. Enviornmental Research Laboratory, Duluth, Minnesota.

Embryos to be exposed to toluene were removed from tiles, staged under a dissecting microscope, placed in egg cups, and then placed into a minidiluter system (Benoit et al. 1982). In the minidiluter a series of tanks are supplied with control water and a graded series of toluene-control water mixtures. Fargo city water (pH 8.3, hardness 80 mg/l $CaCO_3$) was passed through activated carbon and maintained at 25 C +/- 0.2 C for use as dilution water. Toluene concentrations in the exposure tanks were determined with a gas chromatograph as described by Puyear et al. (1981).

A series of ten experiments were performed in which 1-2 hour old fathead minnow embryos were continuously exposed to toluene concentrations of 5-120 mg/l and the time required until hatching was recorded. Embryos were dissected out of their chorion, photographed under a compound microscope, fixed in FAA (formalin acetic acid-alcohol)

- 144 -

(Humason, 1979), embedded in paraffin, serially sectioned at 6 microns, and stained with Harris hematoxylin and eosin. Stained slides were photographed under a compound microscope.

RESULTS

Toluene concentrations of 30-50 mg/l produced a premature hatch which occurred up to 30 hours before the controls (normal hatching at 25 C takes 120 hours). At higher toluene concentrations (60-80 mg/l) a delayed hatch of up to 20 hours longer than the control embryos was recorded.

The chorion of toluene treated embryos was often cloudy, fragile, and covered with a white material. This was especially noticeable in older embryos and at higher concentrations. The yolk mass of toluene treated embryos fixed in FAA was much less prone to mechanical damage when the chorion was removed than was the yolk mass of control embryos.

Typical morphological abnormalities noted in live embryos include curved notochord, abnormal heart and circulatory system development, hydration and swelling of the pericardial coelom, hemorrhaging, enlarged yolk sac, overall stunted appearence, and reduced eye size. At higher toluene concentrations, little activity or body movement of the embryos was observed.

Toluene's widespread effects on young embryos were clearly visible in serial sections. Toluene generally had little effect on early cleavage stages up to the high blastula. The exception to this was seen at very high toluene concentrations (75-100 mg/l), where cleavages were slower and more irregular when compared with controls. Toluene concentrations

necessary to cause abnormal cleavage patterns normally resulted in death of the embryo before the high blastula stage.

Embryos exposed to toluene exhibit retarded development and possess distorted tissues compared to controls of the same age. Virtually all tissues of exposed embryos are abnormal, but mesodermal derivates such as the heart and circulatory system, somites, and notochord appear especially sensitive. At 25 hours post-fertilization exposed embryos were smaller and markedly under-developed. Compared with controls exposed embryos had shorter tailbuds, (Plate 1, figures A and D) and reduced otic vesicles and optic cups (Plate 1, figures C and F). The undifferentiated mesoderm of the heart anlage appeared distorted and disorganized (Plate 1, figures B and E).

A unique movement of the ventrally located periblast layer was observed in in serial sections of exposed embryos (Plate 1-3). This periblast layer containing large primordal germ cells is found on the surface of the yolk mass in the tailbud region in control embryos. In toluene treated embryos as early as 25 hours post-fertilization, this periblast layer has migrated anteriorly to lie ventral to the head region (Plate 1, figure B). Throughout subsequent development the periblast layer is found ventral to the heart in embryos exposed to toluene concentrations greater than 50 mg/l (Plate 3, figures C and D).

At 50 hours post-fertilization the enlarged pericardial coelom and the reduced otic vesicle are visible in live exposed embryos (Plate 2, figures A and B). Serial sections of exposed embryos reveal spaces in the optic cup separating the pigmented tapetum nigrum layer from the layer of presumptive cone cells (Plate 2, figure B). The absence of

white matter and reduced olfactory grooves are also seen in serial sections of toluene treated embryos (Plate 2, figures B and E) and is indicative of their retarded growth.

At 75 hours post-fertilization distorted cells of the notochord of exposed embryos result in the commonly reported curved embryonic axis (Plate 3, figure A). The pericardial coelom and periblast layer of exposed embryos have enlarged while the rest of the embryo is reduced in size (Plate 3, figures A-C). One 75 hour old embryo exposed to 65 mg/l toluene had a deformed lens that extended well out of the optic cup.

At 125 hours exposed embryos are under-developed with a curved notochord, an enlarged yolk sac and pericardial coelom (Plate 4, figures A and D), and possess a reduced swim bladder, stomach, otic capsule, otoliths, and optic cups (Plate 4, figures B-F). There is an obvious overall distorted appearance of the exposed embryos.

DISCUSSION

Stunted size, hydration of the pericardial coelom, and curvature of the notochord were common responses seen in this study. Similar morphological abnormalities have been reported in other teleost embryos exposed to various environmental stresses (Wilson, 1976). Hickey (1973) reviewed common abnormalities in fish populations and proposed environmental changes during embryonic development may be a factor producing these abnormalities. It appears that toluene exposure results in a generalized stress response in fathead minnow embryos.

A major response of embryos to toluene was an overall retardation in growth and development. The tissues of the optic cup, otic capsule,

brain and other regions of exposed embryos were not only distorted, but were also less differentiated than the controls. These effects may result from the narcotizing effect of toluene (Struhsaker et al., 1974), which also may explain the reduced level of activity observed in treated embryos. According to Rosenthal and Alderdice (1976) decreased embryonic activity reduces the mixing of the perivitilline fluid and therefore the rate of respiration and development. It should be noted that the toluene concentrations necessary to elicit these morphological responses were very high, and may be approached in the environment only under extreme conditions, such as a major spill in a relatively confined area.

No reports have been found in the literature concerning the movement of the periblast layer under stress conditions. The developmental consequences of the migration of the periblast layer is of interest and could be determined by examining later stages of toluene exposed minnows. Further histologocal studies of embryos exposed to a variety of different environmental stressors would also be helpful in determining if the movenent of the periblast layer described here is unique to toluene exposure.

Plate 1. 25-Hour Old Embryo

Figure A. Toluene treated embryo, 60 mg/1 (80X)

In this figure the tailbud (tb) is markedly shorter than in the controls (figure D). ys-yolk sac, n-notochord, s-somites

Figure B. Toluene treated embryo, 60 mg/1 (200X)

This sagittal section through the head region shows the thick periblast layer (p) containing the primordial germ cells (pgc). The heart anlage (ha) is visible as two disorganized layers of mesoderm under the mesencephalon (m). ys-yolk sac, pr-prosencephalon

Figure C. Toluene treated embryo, 60 mg/1 (800X)

This sagittal section shows the otic vesicle (ov). Note its smaller size compared with the control (figure F). d-dorsal, v-ventral, ee-epidermal ectoderm.

Figure D. Control embryo (80X)

This figure shows the normal tailbud (tb), somites (s), and yolk sac (ys) of a live embryo.

Figure E. Control embryo (200X)

This sagittal section through the head region shows the two ventrally located sheets of mesoderm that make up the heart anlage (ha). Note the lack of a periblast layer and primordial germ cells as seen in figure B. m-mesencephalon pr-prosencephalon, ys-yolk sac

Figure F. Control embryo (800X)

This sagittal section shows the large otic vesicle (ov). d-dorsal, v-ventral, ee-epidermal ectoderm
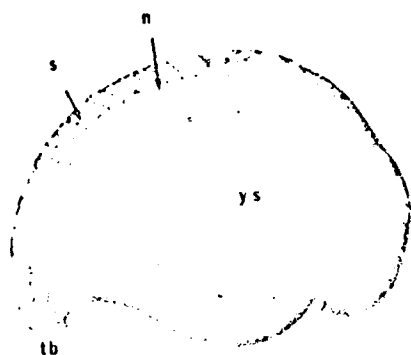
A
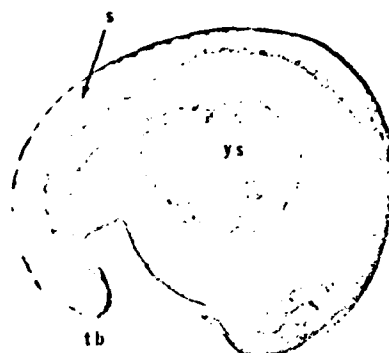
D
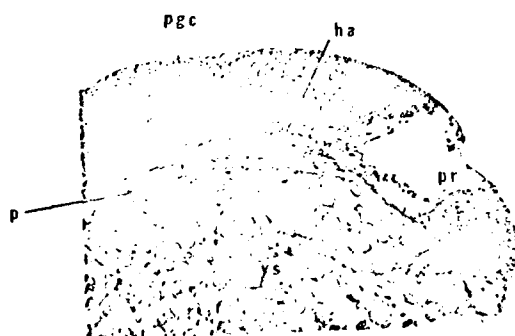
B

E

C
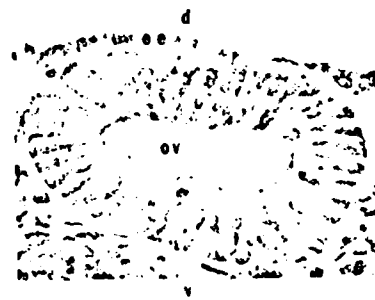
F

Plate 2. 50-Hour Old Embryo

Figure A. Toluene treated embryo, 60 mg/l (80X)

The enlarged pericardal coelom (pc) is visible in this live
embryo. Note the reduced size of the head region and the lack of
otoliths in the otic vesicle (ov) (see figure D). ys-yolk sac,
oc-optic cup

Figure B. Toluene treated embryo, 60 mg/l (200X)

This transverse section shows the spaces (sp) separating the
presumptive cone cells (cc) from the pigmented tapetum nigrum
layer (tn) in the optic cups. The dorsal-ventrally compressed
heart (h) and the periblast layer (p) containing the primordial
germ cells are also visible. Note the lack of white matter on the
lateral aspects of the diencephalon (d). l-lens

Figure C. Toluene treated embryo, 60 mg/l (200X)

This sagittal section shows the spaces (sp) in the optic cup (oc),
the otic vesicle (ov), periblast layer (p) on the yolk mass (ym),
and the reduced olfactory grooves (og).

Figure D. Control embryo (80X)

This figure shows the otoliths (o) in the otic vesicle, the yolk
sac (ys), and the small pericardial coelom (pc).

Figure E. Control embryo (200X)

This transverse section shows the optic cup (oc), lens (l), heart
(h), pituitary anlage (pa), and white matter (wm) consisting of
axons on the lateral aspects of the diencephalon (d).
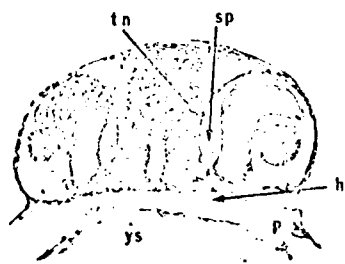
Figure F. Control embryo (200X)

This sagittal section shows the otic vesicle (ov), optic cup (oc),
olfactory groove (og), third (3v) and fourth ventricle (4v) of the
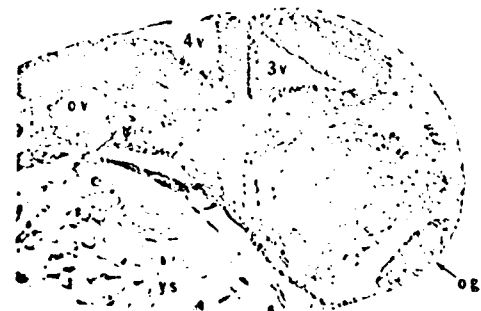brain.

- 151 -
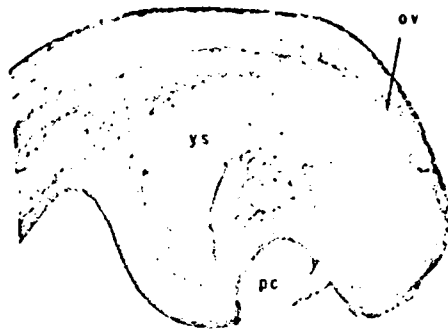
A
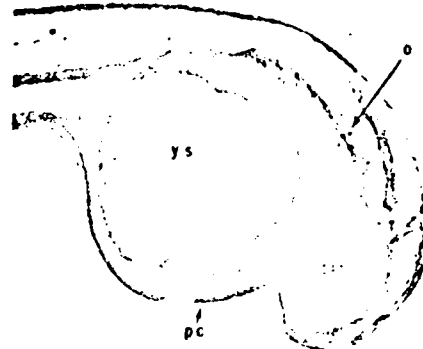
D

B

E

C

F

Plate 3. 75-Hour Old Embryo

Figure A. Toluene treated embryo, 60 mg/l (80X)

This figure shows the enlarged pericardial coelom (pc) and yolk
sac (ys) and the distorted heart (h), optic cup (oc), and pectoral
fin (pf).

Figure B. Toluene treated embryo, 60 mg/l (200X)

This sagittal section shows a space (sp) in the optic cup (oc),
the reduced otic capsule (otc), the heart (h), and the periblast
layer (p) containing the primordial germ cells (pgc).

Figure C. Toluene treated embryo, 60 mg/l (200X)

This sagittal section shows the liver (li) in a depression in the
yolk sac, spaces (s) in the optic cup, and the highly vacuolated
cells of the notochord (n). ys-yolk sac, pc-pericardial coelom,
wm-white matter

Figure D. Control embryo (200X)

This figure shows the heart (h), yolk sac (ys), optic cup (oc),
notochord (n), pectoral fins (pf), and two otoliths in the otic
capsule.

Figure E. Control embryo (200X)

This sagittal section shows the optic cup (oc), and otic capsule
(otc). The fourth ventricle (4v) is visible in the dorsal
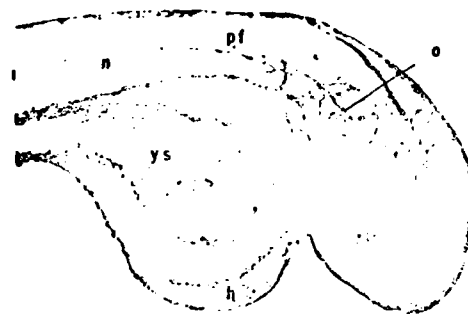rhombencephalon.

Figure F. Control embryo (200X)

This sagittal section shows the foregut (f), liver (li), aortic
arches (aa), and large cells of the notochord (n). White matter
(wm) is visible on the lateral aspect of the rhombencephalon (r).
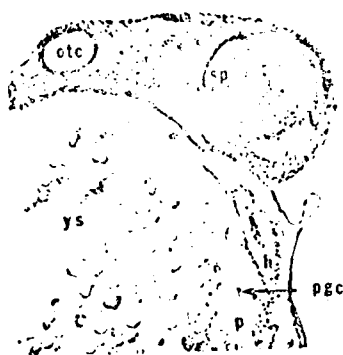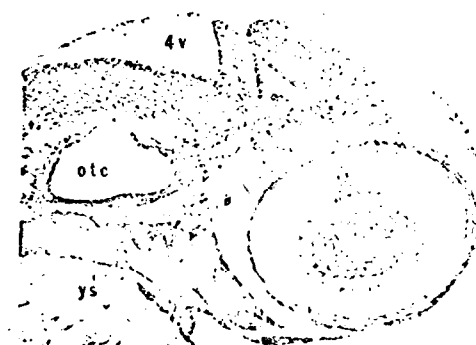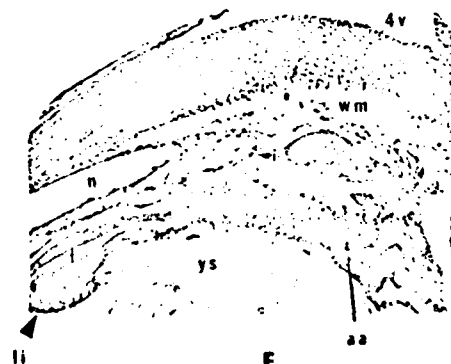4v-fourth ventricle

A

D

B

E

C

F

Plate 4. 125-Hour Old Embryo

Figure A. Toluene treated embryo, 60 mg/1 (80X)

This figure of a live embryo shows the characteristic curvature of the notochord, the reduced heart (h) and optic cup (oc), and the enlarged pericardial coelom (pc). Note the reduced size of the otoliths (o) compared to a control embryo in figure D.

Figure B. Toluene treated embryo, 60 mg/1 (200X)

This transverse section shows distortion in the notochord (n), lateral somites (s) and the spinal cord (sc). White matter (wm) is present on the lateral aspects of the spinal cord.The stomach (st) and swim bladder (sb) are reduced in size compared to the controls (figure E).

Figure C. Toluene treated embryo, 60 mg/1 (80X)

This sagittal section shows the distorted cells of the notochord (n) which result in the charactertistic curvature of the embryonic axis. otc-otic capsule

Figure D. Control embryo (80X)

This figure shows the heart (h), yolk sac (ys), swim bladder (sb), otoliths (o), and notochord (n). lj-lower jaw

Figure E. Control embryo (200X)

This transverse section shows the notochord (n), spinal cord (sc), stomach (st), swim bladder (sb), yolk sac (ys), and white matter (wm) of a control embryo.

Figure F. Control embryo (80X)

This sagittal section illustrates the normal spinal flexure of a control embryo. ga-gill arches, otc-otic capsule, n-notochord, ys-yolk sac
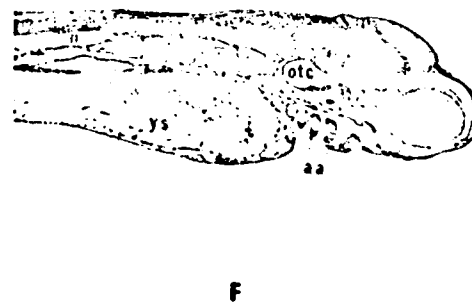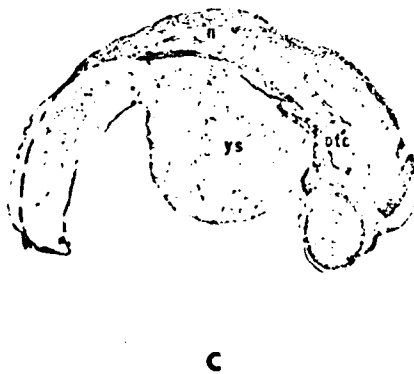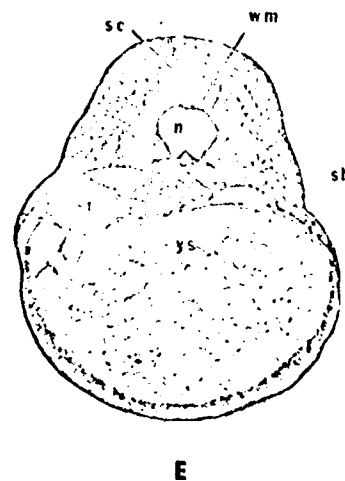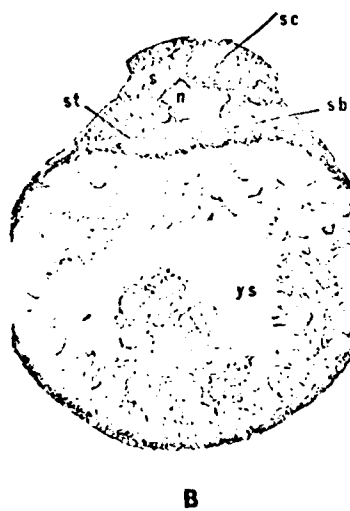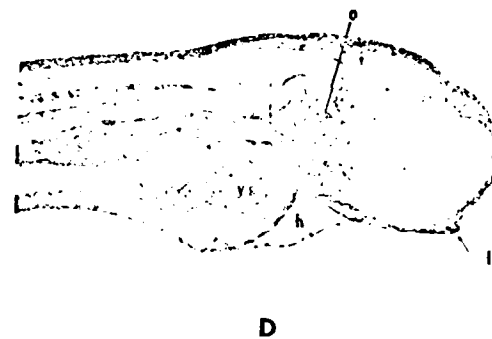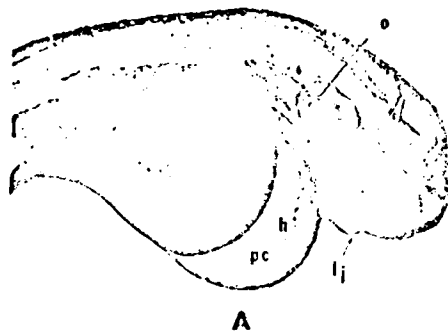
A

D

B

E

C

F

ACKNOWLEDGEMENTS

LITERATURE CITED

Alderdice, D.F., and F.P.S. Velson. 1971. Some effects of salinity and temperature on early development of pacific herring Clupea pallas. J. Fish. Res. Board Can., 28:1545-1552.

Benoit, D.A., V.R. Mattson, and D.L. Olson. 1982. A continuous-flow mini-diluter system for toxicity testing. Water Res. 16:451-457.

Birge, W.J., J.A. Black, and D.M. Bruser. 1979. Toxicity of organic chemicals to embryo larval stages of fish. EPA final report EPA-560/11-79-007. Contract No. 68-01-4321.

Coombs, H.S. and A.R. Hiby. 1979. The development of the eggs and early larvae of blue whiting, Micromesistius poutassou and the effect of temperature on development. J. Fish. Biol. 14:111-123.

Devlin, E.W., J.D. Brammer, and R.L. Puyear. 1982. Acute toxicity of toluene to three age groups of fathead minnows. Bull. Environ. Contam. Toxicol., (In Press).

Dushkina, L.A. 1973. Influence of salinity on eggs, sperm and larvae of low-vertebral herring reproducing in costal waters of the Soviet Union. Mar. Biol., 19:210-223.

Eldridge, M.B., T. Echeverria, and J.A. Whipple. 1977. Energetics of Pacific herring embryos exposed to concentrations of benzene, a monoaromatic component of crude oil. Trans. Am. Fish. Soc., 106(5):452-461.

Emadi, H. 1973. Yolk-sac malformation in Pacific salmon in relation to substrate, temperature, and water velocity. J. Fish. Res. Board Can., 30(8):1249-1250.

Ernst, V.V., J.M. Neff, and J.W. Anderson. 1977. The effects of the water-soluble fractions of No. 2 fuel oil in the early development of the estuarine fish Fundulus grandis. Environ, Pollut., 14(1):25-35.

Gulidov, U.M.. 1974. The effect of different oxygen conditions during incubation on the survival and some of the developmental characteristics of the Leucaspius delineatus in the embryonic period. J. Ichthyol., 14(6):993-995.

Hickey, C.R.. 1973. Common abnormalities in fishes, their causes and effects. Trans. Northeast Fish and Wild, Conf. May 14-17, Ellenville, N.Y., pp 71-83.

Hokanson, K.E.F. and C.F. Kleiner. 1974. Effects of constant and rising temperature on survival and developmental rates of embryonic larvae Yellow Perch, Perca flavescens. The early Life of Fish, J.H.S. Baxter, (Ed) Springer-Verlag, Berlin pp 437-448.

Humason, G.L.. 1979. Animal Tissue Techniques. 1979. W.H. Freeman and Co. San Francisco, p 21.

Kamaldeep, K. and H.S. Toor. 1978. Effect of dissolved oxygen on the survival and hatching of eggs of the Scale Carp. Progress. Fish. Cult., 40(1):35-37.

Karpenko, I.G.. 1974. The effect of salinity on the eggs and embryos of the "Shemaya" Chalcalburnus chalcoides schischkovi J. Ichthyol., 14(6):993-995.

Kokurewicz B.. 1969. The influence of temperature on the embryonic development of the perches· Perca fluviatilis and Lecioperca lucioperca. Zool. Poloniae., 19:47-67.

Kunhold, W.W., and F. Busch. 1973. On the uptake of 3 different types of hydrocarbons by salmon eggs. Meeresforsch, 26:50-59.

Kwain, W.. 1975. Embryonic development, early growth, and meristic variation in rainbow trout exposed to combinations of light intensity and temperature. J. Fish. Res. Board. Can., 32(3):397-402.

Leung, T.S., and R.V. Bulkley. 1979. Effects of petroleum hydrocarbons on length of incubation and hatching success in the Japanese Medaka. Bull. Environm. Contam. Toxicol., 23:236-243.

Linden, O.. 1978. Biological effects of oil on early development of the baltic herring. Mar. Biol., 45(3):273-283.

Llewellyn, C.G., G.A. Stephenson, and J.W. Hofman. 1977. Aflotoxin B, induced toxicity and teratogenicity in Japanese medaka eggs. Toxicon., 15:582-587.

McCormick, J.H., B.R. Jones, K.E. Hokanson. 1977. White sucker Catostomus commersoni embryo development and early growth and survival at different temperatures. J. Fish. Res. Board Can., 34:1019-1025.

Mossier, J.N.. 1971. The effect of salinity on the eggs and sac fry of the fathead minnow, Pimephales promelas, northern pike Esox lucius, and walleye Stizostedion vitreum vitreum. Masters thesis. North Dakota State Uni., Fargo, N.D..

Paflitschek, R.. 1975. Investigations on the toxic effects of Bayer 73 on eggs and yolk-sac larvae of Tilapia leucosticta cichildae. Specialia Experientia, 32(12):1537-1533.

Peterson, R. H., H.C.E. Spinney, and A. Sreedhran. 1977. Development of atlantic salmon eggs and alevins under varied temperature regime. J. Fish. Res. Board Can., 34(1):31-43.

Pickering, Q. H., and C. Henderson. 1965. Acute toxicity of some important petrochemicals to fish. J. Water Pollut. Cont. Fed., 38(9):1419-1429.

Puyear, R.L., K. J. Fleckenstien, W.E. Montz, and J.D. Brammer. 1981. Use of reverse phase C-18 mini-columns for concentrating water-soluble hydrocarbons. Bull. Environ. Contam. Toxicol., 27:790-797.

Rosenthal, H. and D. F. Alderdice. 1976. Sublethal effects of environmental stressors, natural and pollutional on marine fish and larvae. J. Fish. Res. Bd. Can., 33:2047-2055. Rosenthal, H., and R. Stelzer. 1970. Wirkungen von 2, 4-und 2, 5-dinitrophenol auf die embryohalentwicklung des herrings _Clupea_ _harengus_. Mar. Biol., 5:325-336.

Sharp, J.R., K.W. Fucik, and J.M. Neff. 1979. Physiological basis of differential sensitivity of fish embryonic stages to oil pollution. In: Marine pollution, functional responses, Academic Press, New York. pp 85-103.

Stoss, F.W., and T.A. Haines. 1979. The effects of toluene on embryo and fry of the Japanese medaka with a proposal for rapid determination of maximum acceptable toxicant concentration. Environ. Pollut., 20:139-148.

Struhsaker, J.W., M.B. Eldridge, and T.E. Echeverria. 1974. Effects of benzene (a water soluble component of crude oil) on eggs and larvae of pacific herring and northern anchovy. In: Pollution and physiology of marine organisms, J. Vernberg and W. Vernberg (Eds), Academic Press. New York, pp 252-284.

Wilson, K.W.. 1976. Effects of oil dispersants on the developing embryos of marine fish. Mar. Biol., 36:259-268.

DATE
ILME